

# **Discovery and Characterization of Small-Molecule Inhibitors of CRISPR/Cas13a**

by

Filip Marek Reformat

A thesis submitted in partial fulfillment of the requirements for the degree of

Master of Science

Department of Pharmacology

University of Alberta

© Filip Marek Reformat, 2021

# Abstract

**Background:** Clustered Regularly Interspaced Palindromic Repeats, or CRISPR, is an array of DNA sequences found in bacteria that confer immunity against phage. Sequences within the CRISPR array are transcribed into CRISPR RNA (crRNA), which hybridize with CRISPR associated proteins (Cas) to search for and cleave nucleic acids of the invading phage. A variety of CRISPR systems have been discovered and characterized, one member of this family, the DNA targeting enzyme Cas9, has had a significant impact in the field of biology and medicine after being adapted into a robust and intuitive gene-editing tool. Another recently discovered member of the CRISPR family called Cas13 is unique in its ability to target and cleave RNA rather than DNA. CRISPR/Cas13 has been used to knock down RNA transcripts in a variety of organisms and has been adapted into a diverse range of tools. Despite its wide range of applications, Cas13 has its limitations: toxicity due to prolonged RNA knockdown, and potential for off-target effects. Inhibitory small-molecule compounds could address these issues by imparting temporal control over Cas13. This dissertation presents my main research project: discovery and characterization of small-molecule inhibitors of Cas13a.

**Methods:** We adapted and employed a FAM (6-Carboxyfluorescein) cleavage assay, which utilizes a fluorophore/quencher reporter RNA molecule, to screen for Cas13a inhibitors. In this assay, cleavage of the reporter RNA

removes the quencher leading to a fluorescent signal. If a compound inhibits Cas13a then there will be no detectable fluorescent signal. Over 13000 compounds were screened using this assay. The most effective inhibitors were identified and validated with the FAM assay. Furthermore, they were subjected to a quenching assay, a redox cycling test via the Amplex® Red assay, and a non-fluorophore based gel cleavage assay to confirm genuine inhibition. The compounds that passed these tests had their IC50s and mechanism of inhibition determined.

**Results:** Using the aforementioned approach, we found nine compounds that were able to inhibit Cas13a. The IC50 of these compounds ranged from 1  $\mu$ M to 3  $\mu$ M. Most of the compounds were either non-competitive or competitive inhibitors, and initial cell data showed that most compounds were non-toxic.

**Conclusion:** We have demonstrated the ability to use a fluorescent assay in a high-throughput approach to find small molecule inhibitors of Cas13a. A total of nine chemical compounds have been validated and characterized. Additional experiments need to be performed to examine the compounds' effect on RNA binding and their ability to inhibit Cas13a in cells. If successful, these compounds could prove to be useful in laboratory work and clinical trials to limit the duration of Cas13a activity.

## Preface

The central project of the thesis includes collaborations with research labs from the University of Alberta and the University of British Columbia. The high-throughput screening of 1280 compounds was carried out with the help of Dr. Joaquin Lopez-Orozco at the High Content Analysis Core Facility, University of Alberta. The high-throughput screening of 11840 compounds was carried out with the help of Dr. Tom Pfeifer at the Biofactorial Facility, University of British Columbia. Graphic summary and statistics of the main screen in **Figure 5C** were provided by Dr. Tom Pfeifer. Dr. Basil Hubbard and myself conceived and designed the experiments. The experiments and assays were carried out and conducted by myself. My colleague and MSc student Jerry Chen assisted me in the high-throughput screening of 1280 compounds and data analysis.

**Appendix A:** In this project, a Ph.D. student Hyeong Jin Kim, supervised by Dr. Mark Glover, assisted me in the purification of Cas9-eGFP. Dr. Basil Hubbard and myself conceived and designed the experiments. I performed the following experiments: cloning of the aptamer/gRNA hybrids, production of Cas9, and testing of these sequences *in vitro*.

**Appendix B:** In this project I collaborated with a postdoctoral fellow Dr. Benjamin Brigant and Ph.D. student Christopher Cromwell, supervised by Dr. Basil Hubbard. Dr. Benjamin Brigant, Christopher Cromwell, Dr. Basil Hubbard, and myself conceived and designed the experiments. Christopher Cromwell assisted me in Cas13-PE3 design, assay development, and cloning of Cas13-PE3 plasmids. Dr. Benjamin Brigant helped me in the production of dCas13-PE3 proteins, performing the ribosylation assays, and provided general assistance in data analysis. Dr. Gary Eitzen, from the Department of Cell Biology, assisted me in the optimization of initial eEF2 expression and purification. My contributions included: assistance in Cas13-PE3 design, *in vitro* production of all target and crRNAs, production of eEF2, assistance in the production of dCas13-PE3

proteins, testing cleavage capabilities of dCas13-PE3 proteins, and assistance in performing ribosylation assays.

**Appendix C:** This project was led by my colleague Jerry Chen and supervised by Dr. Basil Hubbard. Jerry Chen provided the data in **Figures C1B, C2C, and C2D**. The screening was carried out with the help of Dr. Joaquin Lopez-Orozco at the High Content Analysis Core Facility, University of Alberta, Canada, and Dr. Tom Pfeifer at the Biofactorial facility, University of British Columbia, Canada. I contributed to the following experiments: cloning of Nsp15 proteins, assistance in assay design, and development of the secondary Nsp15 screen.

## **Dedication**

*To my grandparents.*

## **Acknowledgments**

I would like to start first and foremost by thanking my supervisor Dr. Basil Hubbard. I would like to thank him for giving me the great opportunity to do a graduate program in his lab. He provided me with constant support and mentorship throughout these three years. I also would like to thank my committee members Dr. Elena Posse de Chaves and Dr. Andrew MacMillan, for their continued encouragement and assistance in guiding me throughout my MSc program. Next, I would like to thank my fellow lab members: starting with Dr. Benjamin Brigant, whose assistance and support was invaluable throughout his stay in the lab. I also would like to thank Jerry Chen for his assistance and support, as well as Christopher Cromwell, Evan Kerek, and Amanda Krysler for their help and encouragement. Lastly, I would like to thank my fellow Department of Pharmacology lab mates, particularly the Pharmacology Graduate Students Association members. All of them made my time in the lab enjoyable and rewarding. Special thanks go to my parents for their continuous kindness, love, and devotion over all these years. Thank you all!

# Table of Contents

<b>Abstract</b>	<b>ii</b>
<b>Preface</b>	<b>iv</b>
<b>Dedication</b>	<b>vi</b>
<b>Acknowledgments</b>	<b>vii</b>
<b>List of Tables</b>	<b>xiii</b>
<b>List of Figures</b>	<b>xiv</b>
<b>List of Abbreviations</b>	<b>xvi</b>
<b>Scope of Thesis</b>	<b>xviii</b>
<b>Chapter 1: Introduction</b>	<b>1</b>
1.1 Background	1
1.1.1 Discovery and Characterization of CRISPR	1
1.1.2 The CRISPR Family	1
1.1.3 CRISPR/Cas9	4
1.1.4 Discovery of CRISPR/Cas13	5
1.1.5 Cas13 Protein Structure	7
1.1.6 Cas13 crRNA Structure	9
1.1.7 Cas13 Applications	10
1.1.8 Cas13 Inhibitors	13
1.2 Rationale	14
1.3 Hypothesis	15

<b>Chapter 2: Materials and Methods</b>	<b>17</b>
2.1 Techniques for FAM Cleavage Assay Optimization	17
2.1.1 Cas13a and dCas13a Expression and Purification	17
2.1.2 crRNA and Target RNA Synthesis	18
2.1.3 Cas13a $K_M$ Determination	18
2.1.4 Target RNA Optimization	19
2.1.5 Cas13a RNP Optimization	20
2.1.6 DMSO Optimization	20
2.2 High Throughput Screening Protocol	21
2.2.1 FAM Cleavage Assay for 13120 Compound Screen	21
2.3 Techniques for Validating Cas13a Inhibitors	22
2.3.1 FAM Cleavage Validation Assay	22
2.3.2 Quenching Assay	22
2.3.3 Redox Cycling Determination via Amplex® Red Assay	23
2.3.4 Gel Cleavage Assay	24
2.4 Techniques for Characterization of Cas13a Inhibitors	25
2.4.1 IC50 Determination	25
2.4.2 Mechanism of Inhibition Determination	25
2.4.3 CC50 Determination	26
2.5 Additional Techniques for Testing Cas13a Inhibitors in Cells	27
2.5.1 Generation of Cas13a HEK293T Cell Line	27
2.5.2 Cloning of crRNA Mammalian Expression Plasmids	27

<b>Chapter 3: Experiments and Results</b>	<b>28</b>
3.1 FAM Cleavage Assay Optimization	28
3.1.1 Selection of Assay	28
3.1.2 Cas13a $K_M$ Determination and RNA Optimization	28
3.1.3 Cas13a RNP Determination and DMSO Tolerance	31
3.1.4 Selection of Positive and Negative Controls	31
3.2 Screening of 13120 Compounds	33
3.3 Compound Validation	33
3.3.1 FAM Cleavage and Quenching Assay	33
3.3.2 Redox Cycling Determination	34
3.3.3 Gel Cleavage Assay	34
3.4 Compound Characterization	36
3.4.1 IC50 Determination	36
3.4.2 Mechanism of Inhibition Determination	36
3.4.3 Compound Cytotoxicity	40
<b>Chapter 4: Discussion and Future Directions</b>	<b>41</b>
4.1 Discussion	41
4.2 Contributions	42
4.3 Limitations	44
4.4 Future Directions	45
<b>References</b>	<b>47</b>
<b>Supplementary Figures</b>	<b>56</b>

<b>Tables</b>	<b>60</b>
<b>Appendix A: Delivery of Cas9 Ribonucleoprotein Complex via a Hybrid Aptamer/gRNA</b>	<b>66</b>
Background	66
Methodology	67
Results	69
Discussion	71
Limitations	72
Future Directions	73
References	73
Tables	75
<b>Appendix B: Targeting and Eliminating Specific Cells via RNA Identification using Tandem dCas13-PE3 Toxin System</b>	<b>79</b>
Background	79
Methodology	80
Results	87
Discussion	93
Limitations	94
Future Directions	94
References	95
Tables	97

<b>Appendix C: Identification and Characterizations of Compounds that Inhibit Nsp15 of SARS-CoV-2</b>	<b>105</b>
Background	105
Methodology	106
Results	109
Discussion	112
Limitations	112
Future Directions	113
References	113
Tables	115

## List of Tables

Table 1: Compounds' Mechanisms of Inhibition Summary	39
Table 2: Compounds' CC50s Summary	40
Table 3: Summary of Compounds' Characteristics	43
Table S1: DNA Sequences of 6xHis-Cas13a and 6xHis-dCas13a	60
Table S2: RNA Sequences used in Cas13a Inhibitor Project	63
Table S3: DNA Oligonucleotides used to produce RNA for Cas13a Inhibitor Project	64
Table S4: Double-stranded DNA Oligonucleotides used to clone crRNA Expression Plasmids	64
Table S5: Full Compound Names	65
Table A1: Hybrid Aptamer/gRNA Sequences	75
Table A2: DNA Oligonucleotides to produce Hybrid Sequences	77
Table B1: Cas13-PE3 Hybrids cloned and produced	97
Table B2: Primers used to clone dLwaCas13a-PE3 Plasmids	98
Table B3: crRNA Sequences for Cas13- PE3 Tandem Project	100
Table B4: DNA Oligonucleotides to produce crRNA	101
Table B5: Target RNA Sequences for Cas13- PE3 Tandem Project	102
Table B6: DNA Oligonucleotides to produce Target RNAs	103
Table C1: Primers used to clone Nsp15 & Inactive Mutants	115
Table C2: RNA Sequences used in Nsp15 Inhibitor Project	116

## List of Figures

Figure 1: CRISPR Immune Response and CRISPR Systems	2
Figure 2: Class 2 CRISPR Systems	3
Figure 3: Cas13 Subtypes	7
Figure 4: Schematic of Assay, Validation of Assay, and Enzyme/Substrate Optimization	30
Figure 5: Additional Optimization Experiments, Screening Result, and Compound Validation Workflow	32
Figure 6: Compound Validation Assays and Compound Structures	35
Figure 7: Characterization of Compounds- IC50s	37
Figure 8: Characterization of Compounds- Mechanisms of Inhibition	38
Figure S1: Additional Michaelis-Menten Curve Replicates and Summary of Results	56
Figure S2: Additional IC50 Replicates and Gel Cleavage IC50s	57
Figure S3: Additional Mechanism of Inhibition Replicates	58
Figure S4: CC50 Curves and Summary of Results	59
Figure A1: Selected Cell- Internalizing Aptamers and Locations for Attachment	70
Figure A2: 16 Aptamer/gRNA Sequences and <i>In Vitro</i> Cleavage Assay	71
Figure B1: Diagram of dCas13d-PE3 System and Protein Permutations	88
Figure B2: <i>In Vitro</i> ADP-Ribosylation Assay	89
Figure B3: Schematics, Ribosylation, and Cleavage Data for dCas13d-PE3 Hybrids	90

Figure B4: Schematics, Ribosylation, and Cleavage Data for dCas13a-PE3 Hybrids	92
Figure C1: Nsp15 and Non-Catalytically Active Mutants	110
Figure C2: Nsp15 Cleavage Assay, Nsp15 Secondary Screening Workflow, and Screening Results	111

## List of Abbreviations

<b>Acr</b>	Anti-CRISPR proteins
<b>ADAR2</b>	Adenosine deaminase acting on RNA
<b>AFU</b>	Arbitrary Fluorescence Units
<b>APS</b>	Ammonium persulfate
<b>BHQ1</b>	Black Hole Quencher®-1
<b>Cas</b>	CRISPR-associated protein
<b>CC50</b>	50% Cytotoxic Concentration
<b>CCAR2</b>	Cell Cycle and Apoptosis Regulator 2
<b>Covid-19</b>	Coronavirus disease 2019
<b>CRISPR</b>	Clustered Regularly Interspaced Palindromic Repeats
<b>crRNA</b>	CRISPR RNA
<b>CRUIS</b>	CRISPR-based-RNA-United Interacting System
<b>Cy5</b>	Cyanine 5
<b>DMSO</b>	Dimethylsulfoxide
<b>DR region</b>	Direct Repeat region
<b>eEF2</b>	Eukaryotic Elongation Factor 2
<b>FAM (or 6-FAM)</b>	6-Carboxyfluorescein
<b>gRNA</b>	guide RNA
<b>HEPN</b>	Higher Eukaryotes and Prokaryotes Nucleotide-Binding
<b>His-Tag</b>	Polyhistidine-tag (6xHis)
<b>IBFQ</b>	Iowa Black® FQ Quencher
<b>IC50</b>	50% Inhibitory Concentration
<b>IEX</b>	Ion Exchange
<b><math>k_{cat}</math></b>	Catalytic rate constant
<b><math>k_{off}</math></b>	Enzyme-substrate dissociation rate constant
<b><math>K_M</math></b>	Michaelis constant
<b>LwaCas13a</b>	<i>Leptotrichia wadeii</i> Cas13a
<b>Nsp15</b>	Nonstructural protein 15

<b>PAM</b>	Protospacer Adjacent Motif
<b>PE3</b>	<i>Pseudomonas aeruginosa</i> exotoxin A domain III
<b>PFS</b>	Protospacer Flanking Site
<b>RfxCas13d</b>	<i>Ruminococcus flavefaciens</i> Cas13d
<b>RNP</b>	Ribonucleoprotein
<b>SARS-CoV-2</b>	Severe Acute Respiratory Syndrome Coronavirus 2
<b>SHERLOCK</b>	Specific High Sensitivity Enzymatic Reporter Unlocking
<b>SIRT1</b>	Sirtuin 1
<b>TALEN</b>	Transcription activator-like effector nucleases
<b>TBE</b>	Tris/Borate/EDTA
<b>tracrRNA</b>	Trans-activating crRNA

## Scope of Thesis

During my MSc program, I have contributed to four projects. For my main thesis project, I discovered and characterized chemical compounds that inhibit Cas13a to have more control in using Cas13a *in vitro*, cell culture, and in animal models. **Chapter 1** describes background information. I illustrate the discovery of CRISPR; describe the CRISPR family and CRISPR/Cas9; portray the discovery of CRISPR/Cas13; detail the protein and crRNA organization of several Cas13 subtypes; describe Cas13 applications; and present current methods of inhibiting this Cas endonuclease. Furthermore, I state the rationale and hypothesis of the project. **Chapter 2** presents the materials and techniques used in the project. This chapter is divided into subsections: assay optimization, high throughput screening, validation of inhibitors, characterization of inhibitors, and additional cell culture techniques. **Chapter 3** describes the process, the acquired data, and data analysis of the main thesis project. **Chapter 4** is the concluding section where I discuss the project, and state the contributions, limitations, and future directions that can be pursued.

The three additional projects, I was involved in, are described in the appendices. **Appendix A** presents an independent project to address the difficulty of delivering CRISPR/Cas9 into cells through the usage of cell penetrating aptamers. The cell-permeable RNA aptamers were fused to portions of the gRNA protruding from the RNP complex. The background, methods, results, discussion, limitations, and future directions of this project are described.

**Appendix B** includes details about a collaborative project with a postdoctoral researcher and Ph.D. student to develop our own Cas13 tool. The idea was to fuse two catalytically dead Cas13s with portions of a PE3 toxin, where tandem binding to a specific cancer RNA transcript would result in the hybridization of the PE3 toxin. This would lead to the cessation of protein production and eventual

cell death. The background, methods, results, discussion, limitations, and future directions of this project are presented.

**Appendix C** describes a collaborative project with an MSc student. The project's aim was to find a way to combat the COVID-19 pandemic. This involved discovering and characterizing chemical compounds that inhibit an RNA endonuclease of SARS-CoV-2 called Nsp15. The background, methods, results, discussion, limitations, and future directions of this project are included.

# Chapter 1: Introduction

## 1.1 Background

### **1.1.1 Discovery and Characterization of CRISPR**

In 1987, Japanese researchers discovered a peculiar array of repeating DNA sequences while studying the IAP gene of *E. coli* (Ishino et al., 1987). Mojica and collaborators initially designated this clustered sequence with the name **Short Regularly Spaced Repeats (SRSR)** (Mojica et al., 2000). However, Jansen and collaborators, a different group studying this array, referred to it as **SPacers Interspersed Direct Repeats (SPIDR)** (Jansen et al., 2002a). To avoid confusion, the two groups came to a consensus to designate this array as **Clustered Regularly Interspaced Palindromic Repeats** or **CRISPR** (Jansen et al., 2002b; Mojica and Rodriguez-Valera, 2016). It was found that this array contained sequences complementary to phage DNA, and has subsequently been shown to function as a bacterial immune defense system (**Figure 1**) (Mojica et al., 2005). The CRISPR immune response can be described as follows: *Adaptation* – if a bacteria survives a phage attack, it will incorporate part of the phage DNA into the bacteria's CRISPR array; *Processing* – the CRISPR array is transcribed into pre CRISPR RNA (crRNA), processed into mature crRNA, and hybridized with multiple or a single CRISPR associated protein (Cas); and *Interference* – the Cas/crRNA RNP (ribonucleoprotein) seeks the invading phage, binds to its nucleic acids, and degrades it: stopping the phage infection (Yosef et al., 2012; Wright et al., 2016).

### **1.1.2 The CRISPR Family**

During the last two decades a multitude of CRISPR systems have been discovered and characterized through both laboratory and bioinformatics approaches. CRISPR systems are found both in bacteria and archaea and are organized into Type I through Type VI systems (**Figure 1**) (Wright et al., 2016;

Makarova et al., 2018). Class 1 systems (Type I, Type III, and Type IV) involve multiple Cas proteins interacting with a specific crRNA. Class 2 systems (Type II, Type V, and Type VI) involve only one Cas protein interacting with a crRNA (Makarova et al., 2018). With only one protein being involved, Class II systems are much easier to modify and work with, making them viable for genetic engineering applications.

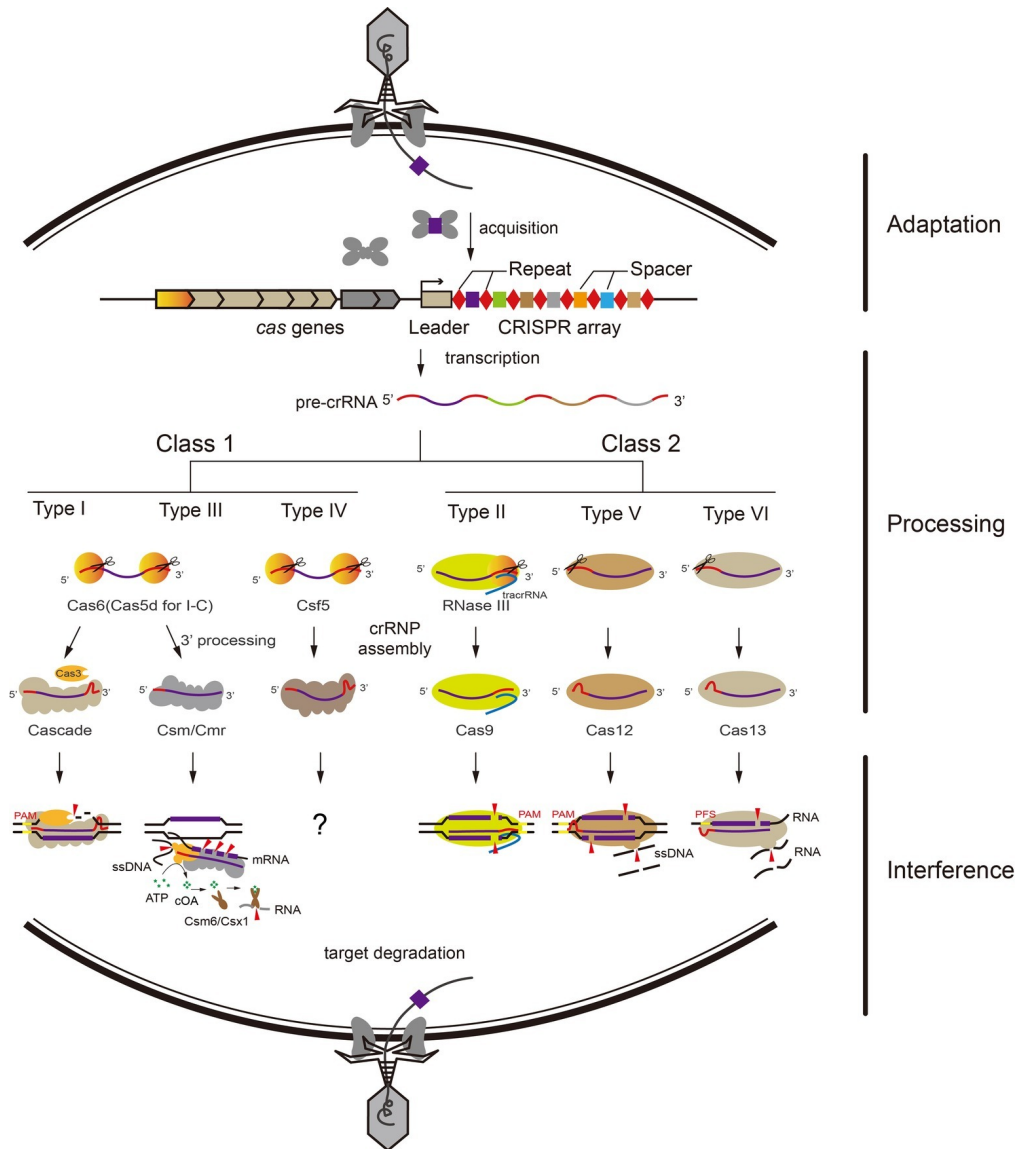


**Figure 1: CRISPR Immune Response and CRISPR Systems.** An overview of the steps involved in the CRISPR immune response and all the types of CRISPR systems. The CRISPR immune response involves three stages: Adaptation, Processing, and Interference. The two types of CRISPR classes are: Class 1 and Class 2. Class 1 involves many proteins interacting with one crRNA, while Class 2 involves one Cas protein interacting with one crRNA. **Figure taken from Li and Peng (2019)**

Type II systems encompass the Cas9 enzymes that hybridize with a crRNA and trans-activating crRNA (tracrRNA) to cleave double-stranded DNA with a blunt end cut upon PAM site identification (Jinek et al., 2012). Type V systems include Cas12 proteins that hybridize with a crRNA and cleave double-stranded DNA with a staggered cut upon PAM site recognition (Zetsche et al., 2015). The non-complementary strand dissociates from the active site, and the Cas12 RNP complex can conduct collateral cleavage of single-stranded DNA (Chen et al., 2017). Other subtypes, such as Cas12b, require a tracrRNA for RNP formation (Shamkov et al., 2015). Type VI systems encompass Cas13 proteins. Cas13 hybridizes to a crRNA and binds to single-stranded RNA. The system cleaves the targeted single-stranded RNA and then can conduct collateral cleavage of other single-stranded RNA (Abudayyeh et al., 2016). Unlike the previous systems, it does not require a PAM site but rather a PFS (protospacer flanking site) (Abudayyeh et al., 2016) (**Figure 2**).

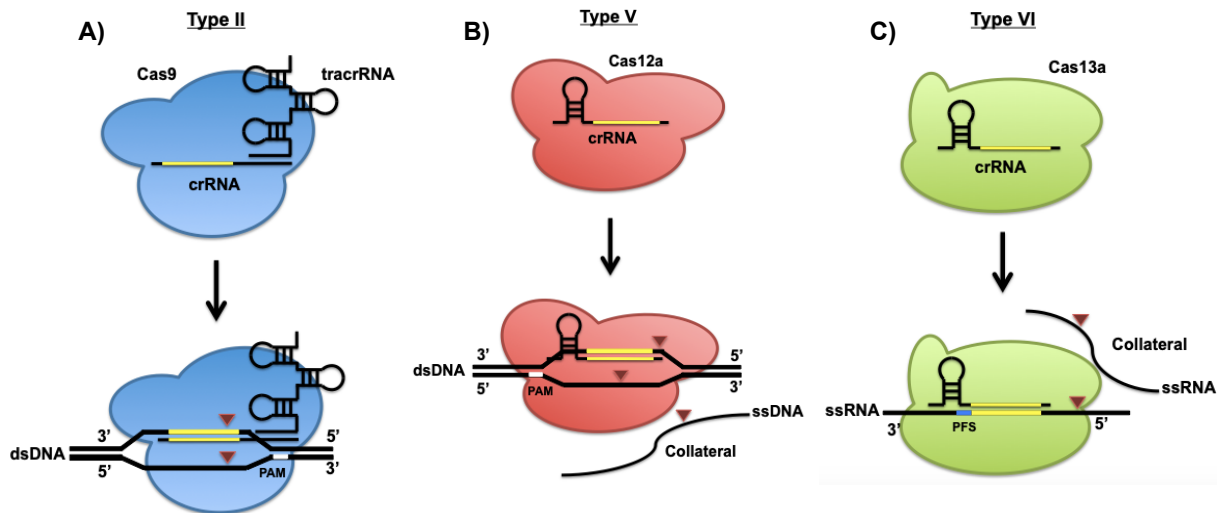


**Figure 2: Class 2 CRISPR Systems.** An overview of the three Class 2 CRISPR systems. **A)** Type II systems encompass the Cas9 enzymes that cleave dsDNA with a blunt end cut. **B)** Type V systems encompass the Cas12 enzymes that cleave dsDNA with a 5' overhang and can conduct collateral cleavage of single stranded DNA. **C)** Type VI systems encompass Cas13 proteins that cleave ssRNA, followed by collateral cleavage of ssRNA. The small red triangles denote cleavage location.

### 1.1.3 CRISPR/Cas9

The first characterized Class 2 system, as well as the best known and utilized, is CRISPR/Cas9 (Tang & Fu, 2018). The CRISPR/Cas9 system is comprised of multiple parts: the Cas9 nuclease that performs double-stranded cleavage, the crRNA that defines and binds to a specific genomic target, and the tracrRNA that binds to Cas9 and crRNA, stabilizing the entire complex (Jinek et al., 2012). Additionally, the tracrRNA and crRNA are fused into one RNA that is referred to as a single guide RNA (sgRNA) or guide RNA (gRNA) (Mali et al., 2013; Jiang et al., 2015). For Cas9 to cleave a DNA sequence, it needs to identify a short upstream sequence on the non-complementary strand of the DNA called the protospacer adjacent motif or PAM sequence (5' NGG 3' for *S. pyogenes* Cas9) (Jinek et al., 2012). The PAM site distinguishes bacterial DNA from phage DNA and prevents the Cas9 RNP from self-cleaving its genome (Marraffini and Sontheimer, 2010). The DNA cleavage process is preceded by recognition of the PAM sequence (Jiang et al., 2015); followed by DNA melting and hybridization of the first 10-12 bp (base pairs) of the 3' end of crRNA sequence (seed pairing) (Jiang et al., 2015); and, lastly, a complete hybridization between the gRNA and the DNA target. Cleavage of the double-stranded DNA occurs through the HNH and RuvC domains of Cas9 that cleaves the complementary and non-complementary strands, respectively (Gasiunas et al., 2012).

In 2012, it was discovered that CRISPR/Cas9 complexes of *Streptococcus pyogenes* and *Streptococcus thermophilus* could be modified to cleave any desired DNA sequence (Jinek et al., 2012). Consequently, in 2013, two research labs adapted the CRISPR/Cas9 system to cleave dsDNA in eukaryotic cells (Cong et al., 2013; Mali et al., 2013). This provided researchers with a powerful and robust tool for gene modification. By only understanding Watson-Crick base pairing rules, one can manipulate the 20bp nucleotide sequence of the crRNA's spacer region to target and cleave any gene of interest (Cong et al., 2013; Mali et al., 2013). This discovery allowed gene editing to evolve from a difficult

process that only specialized labs could perform to a relatively simple method that most labs could implement. The CRISPR/Cas9 system has rapidly replaced other gene editing tools, such as the more cumbersome zinc finger nuclease and TALENs, and is used increasingly in many disciplines of research (Ledford, 2015). The double-stranded cleavage of DNA by CRISPR/Cas9 in eukaryotic cells elicits the response of one of two repair mechanisms: non-homologous end-joining (NHEJ), an imprecise method of repair resulting in insertion/deletion (indel) formation and subsequent gene inactivation, which is used for generating gene knockouts (Ablain and Zon, 2016); or homology-directed repair (HDR), a high fidelity method that utilizes a DNA template to repair the double-stranded DNA break, this method is used for gene editing (Cheng et al., 2014).

CRISPR/Cas9 has been used to induce gene knockouts and knock-ins in cells and several organisms, including insects (Gratz et al., 2013), fish (Ablain and Zon, 2016), and mice (Cheng et al., 2014). It has also been used to perform screens for genes involved in cancer (Toledo et al., 2015) and immune function (Manguso et al., 2017), and to treat diseases such as sickle cell anemia (Dever et al., 2016), haemophilia (Guan et al., 2016), and muscular dystrophy (Himeda et al., 2016) in preclinical mouse models. Currently, there are 46 pending clinical trials involving CRISPR technology<sup>1</sup>.

### **1.1.3 Discovery of CRISPR/ Cas13**

Cas13 was discovered *in silico*. Shamkov and collaborators designed a computational pipeline that searched the entire NCBI WGS database to find new Class 2 CRISPR systems (Shamkov et al., 2015). To perform this task, they searched for sequences associated with the *cas1* gene. Cas1 is highly conserved in all Class 2 CRISPR systems (Takeuchi et al., 2012) and, along with Cas2, is responsible for integrating phage DNA into the CRISPR array (Yosef et

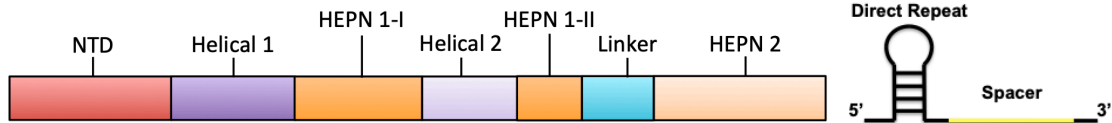
---

<sup>1</sup> [www.ClinicalTrials.gov](http://www.ClinicalTrials.gov)

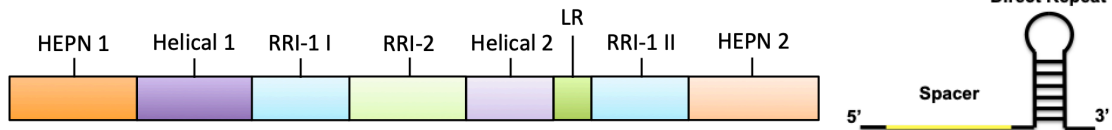
al., 2012). The criteria for the search was further refined by focusing only on loci that contained genes that encode for proteins that are more than 500 amino acids long: that is an attribute of Class 2 systems, i.e., Cas9 and Cpf1 (now called Cas12a) (Shamkov et al., 2015). This approach resulted in the discovery of several Cas proteins (Shamkov et al., 2017). One of the discovered proteins, C2c2, demonstrated unique characteristics and appeared to have no sequence similarity to other known proteins (Shamkov et al., 2015). However, upon further examination, two conserved HEPN (higher eukaryotes and prokaryotes nucleotide-binding) domains were found in the sequence (Shamkov et al., 2015). The presence of these domains indicated that C2c2 has RNase activity rather than DNase activity. Abudayyeh, Gootenberg, and collaborators subsequently confirmed the RNase activity of C2c2 (Abudayyeh et al., 2016). The research team expressed the endonuclease from the bacterial species *Leptotrichia shahii* and found that it not only was able to confer immunity against MS2 phage, but it also was able to be engineered to knockdown any mRNA of interest, and underwent collateral cleavage after binding/cleaving its target RNA (Abudayyeh et al., 2016). Furthermore, Cas13a requires only a crRNA and possesses crRNA processing activity (Abudayyeh et al., 2016). As this protein is part of the CRISPR system, it was designated as Cas13a (Shamkov et al., 2017).

Further work has identified multiple subtypes of Cas13. Along with the original Cas13a, computational studies have discovered Cas13b (Cox et al., 2017; Smargon et al., 2017), Cas13c, and Cas13d (Konermann et al., 2018; Yan et al., 2018) (**Figure 3**). The Cas13 subtypes are quite different: with only 11-16% sequence identity between subtypes (O'Connell, 2019). They, however, all share the same catalytic domain, HEPN, which is found in duplicate. As of writing this dissertation, two more compact Cas13 subtypes have been discovered: Cas13X and Cas13Y (Xu et al., 2021).

**Cas13a: average size 1250aa**



**Cas13b: average size 1150aa**



**Cas13d: average size 930aa**



**Figure 3: Cas13 Subtypes.** A schematic of Type VI CRISPR/Cas13 subtypes: Cas13a, Cas13b, and Cas13d. The Cas13 subtypes are quite different. However, all share the same active HEPN (Higher Eukaryotic Prokaryotic Nuclease) domain where they are found in duplicate. The average sizes of the Cas13 were taken from O'Connell 2019.

### 1.1.4 Cas13 Protein Structure

Cas13a is organized in a bi-lobed structure consisting of REC lobe or 'recognition lobe' and NUC lobe or 'nuclease lobe' (Liu, L., et al., 2017a; Liu, L., et al., 2017b). The REC lobe consists of NTD (N-terminal domain) and Helical-1 domain. The primary function of these domains is to interact and stabilize the crRNA by interacting with the direct repeat (DR) region of the crRNA (Liu, L., et al., 2017a). Additionally, residues in the Helical-1 domain are responsible for crRNA processing (Liu, L., et al., 2017a). However, further work found that for some bacterial species residues in the HEPN-2 domain are also involved with crRNA processing (East-Seletsky et al., 2016). The NUC lobe consists of the HEPN-1, Helical-2, Linker, and HEPN-2 domains. The Helical-2 and Linker domains further stabilize the RNP complex by binding to the crRNA: target RNA duplex (Liu, L., et al., 2017b). The HEPN domains are responsible for the cleavage of the target RNA. These domains have an RX4-6H motif, and two of them are required for catalytic function (Anantharaman et al., 2013). Upon binding the target RNA, Cas13a undergoes a conformational change where the

Helical-2 domain shifts away from the HEPN-2 domain bringing the two HEPN domains together, forming the mature active site (Liu, L., et al., 2017b). This catalytic site is solvent-exposed allowing Cas13 to cut not only in cis but in trans as well (Liu, L., et al., 2017b). This means that once Cas13 binds the intended target and adopts its active form, it can cut ssRNA non-specifically – this is called collateral cleavage.

The other Cas13 subtypes differ in domain organization (**Figure 3**). Cas13d structure is similarly arranged to Cas13a, but there are key differences: Cas13d lacks a domain that corresponds to Cas13a's Helical-1 domain and instead uses the NTD domain and both HEPN domains to interact with the DR region of the crRNA (Zhang B., et al., 2019). Interestingly, Mg<sup>2+</sup> plays a more active role in Cas13d by helping to stabilize the crRNA: Cas13d complex (Zhang B., et al., 2019). crRNA processing is performed solely by the HEPN-2 domain, but by different residues than those responsible for target RNA cleavage (Zhang B., et al., 2019). Similar to Cas13a, both HEPN and Helical domains recognize and bind to the crRNA: target RNA duplex (Zhang, C., et al., 2018).

Cas13b is the most unique out of all the Type VI systems. It possesses many differences when compared to the other Cas13 subtypes. Cas13b contains repeat region interacting domains (RRI) and, unlike the previously described subtypes, has its HEPN domains located at the beginning of the N-terminal and the end of the C-terminal (Zhang, B., et al., 2018). The Helical-2, two RRI domains, and the linker domain form a pocket that stabilizes the DR region of the crRNA (Zhang, B., et al., 2018). In particular, the RRI-2 domain maintains heavy contact with the crRNA and performs crRNA processing (Zhang, B., et al., 2018). Cas13b accommodates the crRNA-target duplex within the pocket formed by Helical-1, Helical-2, RRI-1, and HEPN-1 domains (Zhang, B., et al., 2018; Zhang, B., et al., 2019). Another critical and fascinating difference between the Cas13b and other subtypes is its recognition of the crRNA. Most of the interactions are with the sugar-phosphate backbone of the crRNA, which most likely indicates a

preference for structure-specific recognition rather than sequence-specific recognition (Zhang, B., et al., 2018; Zhang, B., et al., 2019). In contrast, both forms of recognition are important for Cas13a and Cas13d (Zhang, B., et al., 2019). Finally, there is not much known about Cas13c. However, due to its similarity to Cas13a, Cas13c is believed to be organized in much the same way as Cas13a (O'Connell, 2019).

### **1.1.5 Cas13 crRNA structure**

Cas13's crRNA is organized into two distinct regions: a direct repeat region (DR) and a spacer region (**Figure 3**). The DR region is a stem-loop that interacts with the Cas13 protein by forming bonds with various residues of the Cas13 protein, stabilizing the entire complex (O'Connell 2019). The spacer region, as with other CRISPR systems, defines the target of the Cas13 RNP. Cas13a and Cas13d have their DR region on the 5' end (Abudayyeh et al., 2016; Konermann et al., 2018; Yan et al., 2018), while Cas13b has its DR region in the 3' end (Smargon et al., 2017; Cox et al., 2017): yet another example of the differences between Cas13b and other subtypes. Additionally, the crRNA does not require a PAM site for binding. Unlike Cas9 or Cas12, it requires a PFS site (protospacer flanking site) (Abudayyeh et al., 2016). The PFS site varies by subtype and even by ortholog. For example, Cas13a ortholog from *Leptotrichia shahii* (LshCas13a) prefers H nucleotides (A, U, C, and not G) flanking the 3' end on the target RNA (Abudayyeh et al., 2016). Conversely, Cas13a ortholog from *Leptotrichia wadeii* (LwaCas13a) did show slight H preference in *in vitro* assays (Gootenberg et al., 2017) but no such PFS preference is seen in bacteria and mammalian cells (Abudayyeh et al., 2017; Cox et al., 2017). Meanwhile, some species of Cas13b have both 5' and 3' PFS requirements (Smargon et al., 2017; Cox et al., 2017), while Cas13d appears to have none (Konermann et al., 2018; Yan et al., 2018).

The reason for the existence of a PFS preference might be that it disrupts the interactions between the Cas13 protein and crRNA (O'Connell 2019). In LbuCas13a, a conserved cytosine in the crRNA at position -1 forms hydrogen

bonds with several amino acids in the HEPN-2 domain and is crucial for proper HEPN activation (Liu, L., et al., 2017b; O'Connell 2019). Guanine in the target RNA at position -1 disrupts this interaction by binding with the conserved cytosine, preventing proper LbuCas13a activation (Liu, L., et al., 2017b; O'Connell 2019). Interestingly in EsCas13d, the cytosine in the crRNA at position -1 is flipped away from the target RNA, preventing any interactions between the target RNA and this nucleotide (Zhang, B., et al., 2019; O'Connell 2019). This is the most likely reason there is no PFS preference for EsCas13d (Zhang, B., et al., 2019; O'Connell 2019). For Cas13b, PFS preferences exist on both 5' end and 3' end (Cox et al., 2017). Analogously to Cas13a, there is much variation for PFS preferences, with some species only having a 5' end preference. There is still more work that needs to be performed to elucidate the nature of the PFS site (O'Connell 2019).

### **1.1.6 Cas13 Applications**

Cas13a, b, and d subtypes have been used in eukaryotic cells to knockdown both mRNAs and long noncoding RNAs (Abudayyeh et al., 2017; Cox et al., 2017; Konermann et al., 2018). Cas13 has shown incredible specificity with only a few, and sometimes even zero, off-target sites (Abudayyeh et al., 2017; Konermann et al., 2018). This makes Cas13 the most specific RNA targeting tool to date. Curiously, initial data showed that collateral cleavage could not be replicated in eukaryotic cells (Abudayyeh et al., 2017; Cox et al., 2017). However, recent research showed that when Cas13a was applied to glioblastoma cells, it conducted collateral cleavage killing the glioma cells (Wang et al., 2019). It is not known why collateral cleavage occurred in these cells and not in HEK293T. Cas13 has been applied to numerous organisms with great success (Palaz et al., 2021) including yeast (Jing et al., 2018), plants (Aman et al., 2018), insects (Buchman et al., 2020; Kulkarni et al., 2020), fish (Ma et al., 2019; Kushawah et al., 2020), and mice (Kushawah et al., 2020; Zhou, H., et al., 2020). Additionally, Cas13 has been used for a multitude of applications (Palaz et al., 2021) including, but not limited to: disease therapy (Zhou, C., et al., 2020; Zhou, H., et

al., 2020), cancer therapy (Fan et al., 2019; Wang et al., 2019), small molecule detection (Iwasaki and Batey, 2020), alternative mRNA splicing (Koneremann et al., 2018), RNA base editing (Cox et al., 2017; Abudayyeh et al., 2019), RNA methylation (Li et al., 2020), live-cell RNA imaging (Yang et al., 2019), and mapping of RNA-protein interactions (Zhang, Z., et al., 2020). The ability of this endonuclease to target RNA rather than DNA has prompted the development of several Cas13 based genetic tools. Two notable examples are a diagnostic tool dubbed SHERLOCK (Gootenberg et al., 2017) and an RNA editing tool that relies on ADAR2 to perform point mutations in RNA (Cox et al., 2017).

SHERLOCK (**S**pecific **H**igh **S**ensitivity **E**nzymatic **R**eporter **U**n**L**OCKing) uses Cas13 to detect small amounts of RNA (Gootenberg et al., 2017). This method combines recombinase polymerase amplification (RPA) and Cas13's unique ability to perform collateral cleavage to amplify and generate a detectable fluorescent signal (Gootenberg et al., 2017). This signal comes from the cleavage of a reporter RNA that separates the fluorophore on the 5' end from the quencher on the 3' end. This tool was adapted to detect viral RNA, and could detect viral particles at concentrations as low as 2 aM (Gootenberg et al., 2017). Additionally, it has been applied to cancer cells. In this specific instance, SHERLOCK detected oncogenic mutations EGFR-L858R and BRAF-V600E mutations in DNA samples containing as low as 0.1% mutant alleles (Gootenberg et al., 2017). An improved version of SHERLOCK, called SHERLOCKv2, was able to distinguish between ZIKA viral RNA, Dengue viral RNA, synthetic RNA, and synthetic DNA through the usage of four different Cas13s and reporter RNAs pairs (Gootenberg et al., 2018).

Another interesting example of a Cas13 application is the production of an RNA editing tool (Cox et al., 2017). Researchers fused catalytically dead Cas13b to ADAR2 (adenosine deaminases acting on RNA 2). Here, Cas13b binds to a transcript of interest allowing ADAR2 to perform a single pinpoint mutation by converting adenosine to inosine, which functions as a guanosine in the cell

(Nishikura, 2010). The system is called RNA Editing for Programmable A to I Replacement (REPAIR) and was able to perform point mutations in several transcripts (Cox et al., 2017). This tool has been adapted to Cas13a and Cas13d, and has inspired analogous systems such as the RNA Editing for Specific C-to-U Exchange or (RESCUE) (Abudayyeh et al., 2019). RESCUE was developed via taking the ADAR2 protein and directly evolving it into a protein that is capable of cytidine deamination. RESCUE was used to alter activation of the STAT and Wnt/ $\beta$ -catenin pathways. This resulted in increased cell proliferation of HEK293FT and human umbilical vein endothelial cells (HUVECs) (Abudayyeh et al., 2019).

There are a few other exciting and innovative applications that further illustrate Cas13's robustness. Cas13 was used to convert glial cells into neurons to alleviate symptoms of Parkinson's disease in mice (Zhou, H., et al., 2020). RfxCas13d (CasRx) targeted a single RNA-binding protein called polypyrimidine tract-binding protein 1 (Ptbp1) in Müller glial cells (Zhou, H., et al., 2020). The protein's downregulation led to the conversion of the glial cells into retinal ganglion cells, alleviating the motor defects in a Parkinson's disease mouse model (Zhou, H., et al., 2020). Cas13 has been used to study protein-RNA interactions by combining Cas13 with a proximity-labeling system called pupylation-based interaction tagging or PUP-IT (Liu, Q., et al., 2018; Zhang, Z., et al., 2020). This tool, named CRUIS, fused dLwaCas13a with the ligase PafA that mediated the ligation of a small protein PupE to any surrounding lysines (Zhang, Z., et al., 2020). CRUIS could label any protein that interacted with an RNA strand that CRUIS was bound to (Zhang, Z., et al., 2020).

At the moment, no clinical trials are being conducted with Cas13. However, there is a tremendous clinical potential to use Cas13 due to its ability to target RNA rather than DNA. Treatments using this technology have the advantage of being transient and reversible, and address one of the more significant concerns of using CRISPR/Cas9 in humans. Though off-target effects of Cas9 cleavage

have been known for some time (Fu et al., 2013), a recent study using Cas9 in cells found large unforeseen consequences of Cas9 cleavage where an entire chromosome was truncated (Cullot et al., 2019). This resulted in the loss of 43 genes (7.5 Mb) and highlighted the danger of directly altering DNA (Cullot et al., 2019). This further emphasizes the importance of having a tool that can alter RNA rather than DNA.

### **1.1.7 Cas13 Inhibitors**

The effectiveness and widespread usage of CRISPR/Cas13 has created the need for more precise control of Cas13. Having an effective way to inhibit Cas13 would limit the effects of prolonged RNA disruption and prevent off-target cleavage (Lin et al., 2020). Currently, there are two ways in which Cas13 activity can be inhibited: anti CRISPR proteins, and anti-tag RNAs. Anti CRISPR proteins, or Acr for short, are phage proteins that have evolved to counteract prokaryotic CRISPR/Cas systems to prevent genome degradation (Lin et al., 2020). Two families of Acr proteins, AcrIIA and AcrVA, that inhibit Cas9 and Cas12 respectively, have been discovered (Rauch et al., 2017; Watters et al., 2018). However, Anti CRISPR proteins that target Cas13 were still unknown (Marino et al., 2020). Using a bioinformatic pipeline, Lin and researchers identified and characterized a series of AcrVIA proteins that inhibited LwaCas13a (Lin et al., 2020). Six proteins were identified, AcrVIA1 to AcrVIA6, that reliably and specifically inhibited Cas13a, but not Cas13b and Cas13d. AcrVIA5 was remarkably effective and even prevented binding by the aforementioned dCas13a-ADAR2 RNA editing tool (Lin et al., 2020). Interestingly, these proteins varied mechanistically, with AcrVIA1, 4, 5, and 6 binding only to the LwaCas13a protein, while AcrVIA2 and 3 could bind only to the LwaCas13-crRNA complex (Lin et al., 2020). How these proteins work is still not known, and identification of new Acr proteins is slow due to high sequence heterogeneity (Lin et al., 2020).

Meeske and Marraffini speculated how Type VI systems prevent autoimmune cleavage. Observing the inhibitory methods of Type III Cas systems led to the hypothesis that 'anti-tag' RNAs may fulfill the role of preventing self-cleavage in Type VI systems (Meeske & Marraffini, 2018). Anti-tag RNAs are target RNAs that have extended complementation with the DR loop region of the crRNA (Meeske & Marraffini, 2018). These researchers found that such RNAs fully inhibit cleavage *in vitro* and *in vivo*, and discovered this method of inhibition in two different Cas13a orthologs: indicating high conservation of anti-tag RNAs among Cas13 orthologs (Meeske & Marraffini, 2018). The binding of Cas13 RNP to the anti-tag RNAs prevents the activation of the Cas13 complex, and in turn, prevents cleavage (Meeske & Marraffini, 2018). 5-7 complementary nucleotides are sufficient to disrupt Cas13 activation (Meeske & Marraffini, 2018).

## 1.2 Rationale

With the adaptation of CRISPR/Cas9 as a gene editing tool, and the subsequent discovery of CRISPR/Cas12, manipulation of DNA has become accessible to most research labs. There has been an exponential increase in publications that utilize this gene editing technology (Idnurm & Meyer 2018). Despite the ease in which DNA could be manipulated with these CRISPR systems, ways to target RNA efficiently remained limited. At the time, small interfering RNAs (siRNAs) were used to knockdown RNA by inducing RNA interference in eukaryotic cells (Fire et al., 1998). However, this method often yielded many off-targets and was not ideal for therapeutic usage in cells (Jackson et al., 2003; Jackson, 2006). Another approach was tried by adapting CRISPR/Cas9. This system called CRISPR interference, or CRISPRi, used a catalytically dead Cas9 (dCas9) to bind to a specific DNA sequence and block RNA transcription (Qi et al., 2015). This tool was quite effective at silencing RNA (Larson et al., 2015). However the requirement of a PAM site (Larson et al., 2015), the influence that CRISPRi had on nearby genes (Goyal et al., 2016), and CRISPRi's cytotoxic effects in eukaryotes all limited its usage (Cui et al., 2018).

The discovery of Cas13 introduced a new method to target RNA. Cas13 has proven to be both robust and accurate: being able to target RNA in a variety of organisms (Aman et al., 2018; Jing et al., 2018; Buchman et al., 2020; Kushawah et al., 2020) and being readily adapted into a wide range of tools (Cox et al., 2017; Gootenberg et al., 2017). The additional advantage of targeting RNA rather than DNA, thus overcoming the drawbacks of Cas9 usage (Fu et al., 2013; Cullot et al., 2019), gives Cas13 tremendous potential. Despite being effective and widely used, there are very few ways of inhibiting CRISPR/Cas13. Currently, there are two methods for inhibiting Cas13 – as described in the previous section. Unfortunately, both these methods have drawbacks: a recent paper refuted the claims that AcrVIA proteins can inhibit Cas13a (Meeske et al., 2021); and when Cas13 is bound to its target RNA then anti-tag RNAs can no longer bind and impart inhibition on Cas13. Furthermore, introducing another protein or RNA may cause unforeseen cytotoxic effects in cell culture and clinical studies; and delivery of these larger macromolecules into cells is still a major hurdle that needs to be addressed (Stewart et al., 2018). The effects of prolonged RNA knockdown in humans could have toxic effects, thus, in order for clinical trials to occur, it is crucial to have an easy way to induce temporal control of Cas13, i.e., either to stop unwanted side effects or to permit Cas13 cleavage for a limited time only. In this project, the aim was to find another way of inhibiting Cas13 that was more effective and easier to use.

### **1.3 Hypothesis**

We decided to pursue a project to find small molecule inhibitors (i.e. chemicals) that could reliably inhibit Cas13a on the basis that small molecules would provide a more accessible way to inhibit Cas13. To date, there are no small-molecule inhibitors of Cas13 that have been documented. However, a recent paper used a high-throughput approach to find chemical inhibitors of Cas9 (Maji et al., 2019). A 15000 compound screen led to the identification and

characterization of one compound (BRD0539). This compound is a potent inhibitor of SpCas9 and it is cell-permeable, reversible, and stable under physiological conditions (Maji et al., 2019).

Our ultimate objective was to find and characterize compounds that can inhibit Cas13a. To accomplish such a task we turned to high-throughput screening. We hypothesized that high-throughput screening is an effective way of discovering small molecules that could inhibit Cas13a. Initially, we focused on finding and optimizing a reliable assay to test Cas13a cleavage capabilities. Once this was completed, this assay was screened against libraries of compounds. The most effective inhibitors were validated through a series of experiments; and the genuine inhibitors were characterized *in vitro*. Following that, we performed some preliminary experiments in cells to test the compounds cytotoxicity.

## CHAPTER 2: Materials and Methods

### 2.1 Techniques for FAM Cleavage Assay Optimization

#### **2.1.1 Cas13a and dCas13a Expression and Purification**

To express and purify His-Tag Cas13a and dCas13, custom pC013-Cas13a and pC013-dCas13a bacterial expression plasmids (designed for other projects conducted in our lab) were transfected into BL21 DE3 competent *E. coli* cells (NEB) and plated on carbenicillin plates (100 µg/mL). Cells were grown in lysogeny broth (LB) at 37°C, induced at an OD of 0.6 with 1 mM of IPTG, and incubated at 18°C at 200rpm overnight. The bacteria were pelleted and resuspended with Lysis Buffer (50 mM HEPES, 500 mM NaCl, 20 mM Imidazole, 1% Triton X100, 1 mM DTT, and cOmplete™, Mini, EDTA-free Protease Inhibitor Cocktail (Roche)). The suspension was incubated for 20 minutes at 4°C and lysed via sonication. The lysate was ultracentrifuged at 18 000 g for 1 hour. The supernatant was applied to 1 mL HisTrap HP affinity column (Cytiva). The column was washed with wash buffer (50 mM Tris-HCl pH 7.5, 500 mM NaCl, 35 mM Imidazole, 10% Glycerol, and 1 mM DTT) and eluted with elution buffer (50 mM Tris-HCl pH 7.5, 500 mM NaCl, 300 mM Imidazole, 10% Glycerol, and 1 mM DTT). Specific fractions were pooled, concentrated with 50 kDa concentrator (Pierce), and buffer exchanged into storage buffer (50 mM Tris pH 8.0, 10% glycerol, 1M NaCl, and 1mM DTT). Protein was analyzed on an SDS-page gel. The final concentration was determined with a BCA assay (Pierce). Protein was aliquoted and stored in the -80°C. The complete nucleotide sequence for both Cas13a and dCas13a can be found in **Table S1**. Bolded nucleotides denote RXXXH or AXXXH motifs in Cas13a and dCas13a, respectively.

### 2.1.2 crRNA and Target RNA Synthesis

We selected crRNA and target RNA used in the literature, specifically, the crRNA that targets the B4GALNT1 transcript (Konermann et al., 2018). To produce the crRNAs and target RNAs, the same technique was used as was performed by Konermann and collaborators. The sequences were ordered as DNA oligonucleotide primers: the 5' sequence for the T7 promoter and the 3' sequence for the T7 promoter and the respective RNA sequence. These two oligonucleotide sequences were annealed and then *in vitro* transcribed (IVT) using the HiScribe™ T7 Quick High Yield RNA Synthesis Kit from NEB. The mixture was incubated at 37°C for 14 hours to transcribe the template into RNA. The final transcribed RNA was treated with DNaseI (Invitrogen) for 10 minutes at 37°C to remove the DNA template and purified using the Guide-it™ IVT RNA Clean-Up Kit (Takara). Final RNAs were denatured for 10 minutes at 70°C with 2x RNA loading dye and run on 5% TBE Urea Gels (Biorad) for visualization. For all RNA sequences used in the project, and all DNA oligonucleotides templates used to make RNA see **Table S2** and **Table S3**, respectively.

### 2.1.3 Cas13a $K_M$ Determination

The amount of reagents and protocol used for  $K_M$  determination was the same as previously described in the paper by Shan 2019. The Cas13a Cleavage Buffer 10x is composed of the following: (200 mM HEPES, 600 mM NaCl, 60 mM MgCl<sub>2</sub>, pH 6.8) (Gootenberg et al., 2018).

**Mixture 1:** 12.5 µl

Cas13a: 20 nM

crRNA: 10 nM

Cas13a cleavage buffer 10x: 2.5 µl

Water: to 12.5 µl

**Mixture 2:** 12.5 µl

Reporter RNA: variable (0.001 µM to 10 µM)

Target RNA: 0.01 nM

Water: to 12.5 µl

Mixture 1 was incubated at 37°C for 10 minutes to hybridize the Cas13a and crRNA. Next, mixture 1 was added to a 384 well plate, followed by the addition of mixture 2. To begin the reaction the plate was incubated at 37°C and read at 30 second intervals for a total of 15 minutes with the SpectraMax® i3x spectrophotometer at an excitation of 490 nm and an emission of 510 nm. The amount of cut RNA substrate was determined using a standard curve equation that converts the fluorescence generated by cleaved reporter RNA substrate into the concentration of cleaved reporter RNA substrate:  $y = 9011943 \cdot x$  where  $y$  = fluorescence (AFU) and  $x$  = product ( $\mu$ M). The reaction rate at the 5-minute interval was determined by dividing the amount of cut RNA substrate by 5. The rate was plotted against substrate concentration and was normalized and fitted to a Michaelis-Menten curve using PRISM software to find the  $K_M$  and  $V_{max}$ .

#### **2.1.4 Target RNA Optimization**

The amount of reagents and protocol used to optimize the amount of target RNA.

**Mixture 1:** 12.5  $\mu$ l

Cas13a: 20 nM

crRNA: 10 nM

Cas13a cleavage buffer 10x: 2.5  $\mu$ l

Water: to 12.5  $\mu$ l

**Mixture 2:** 12.5  $\mu$ l

Reporter RNA: 1000 nM

Target RNA: variable (0.01 nM to 10 nM)

Water: to 12.5  $\mu$ l

A reaction with scrambled crRNA was used as a negative control. Mixture 1 was incubated at 37°C for 10 minutes to hybridize the Cas13a and crRNA. Mixture 1 was added to a 384 well plate, followed by the addition of mixture 2. To begin the reaction the plate was incubated at 37°C and read at the 15-minute time point with the SpectraMax® i3x spectrophotometer at an excitation of 490 nm and an emission of 510 nm. The fluorescence values were uploaded into the PRISM program for analysis.

### **2.1.5 RNP Optimization**

The amount of reagents and protocol used for RNP optimization.

#### **Mixture 1:** 12.5 $\mu$ l

Cas13a: variable (0.0 nM to 5 nM)

crRNA: variable (0.0 nM to 5 nM)

Cas13a cleavage buffer 10x: 2.5  $\mu$ l

Water: to 12.5  $\mu$ l

#### **Mixture 2:** 12.5 $\mu$ l

Reporter RNA: 1000 nM

Target RNA: 1 nM

Water: to 12.5  $\mu$ l

Reaction prepared as described in the Cas13a target RNA optimization experiment (**2.1.4**). To begin the reaction the plate was incubated at 37°C and read at 5 minute intervals for a total of 30 minutes with the SpectraMax® i3x spectrophotometer at an excitation of 490 nm and an emission of 510 nm. The fluorescence values were uploaded into the PRISM program for analysis.

### **2.1.6 DMSO Optimization**

The amount of reagents and protocol used for DMSO optimization

#### **Mixture 1:** 12.5 $\mu$ l

Cas13a: 2.5 nM

crRNA: 1.25 nM

Cas13a cleavage buffer 10x: 2.5  $\mu$ l

Water: to 12.5  $\mu$ l

#### **DMSO:** Variable (0.5 $\mu$ l to 2 $\mu$ l)

#### **Mixture 2:** 12.5 $\mu$ l

Reporter RNA: 1000 nM

Target RNA: 1.0 nM

Water: to 12.5  $\mu$ l

The experimental procedure was performed as described for target RNA optimization experiment (**2.1.4**).

## **2.2 High Throughput Screening Protocol**

### ***2.2.1 FAM Cleavage Assay for 13120 Compound Screen***

The amount of reagents and protocol used for the 11840 compound screen at the University of British Columbia and for the 1280 compound screen at the University of Alberta. The Cas13a Cleavage Buffer 10x is composed of the following: (200 mM HEPES, 600 mM NaCl, 60 mM MgCl<sub>2</sub>, pH 6.8).

**Mixture 1:** 12.5 µl

Cas13a: 2.5 nM

crRNA: 1.25 nM

Cas13a cleavage buffer 10x: 2.5 µl

Water: to 12.5 µl

**Compound:** 10 µM

**Mixture 2:** 12.5 µl

Reporter RNA: 1000 nM

Target RNA: 1.0 nM

Water: to 12.5 µl

DMSO in place of chemical compound was added to the reaction for the positive control. 10 µM of Benzopurpurin (BPP) was added to the reaction for the negative control. Mixture 1 was incubated at 37°C for 10 minutes to hybridize the Cas13a and crRNA. Next, mixture 1 was added to a 384 well plate containing the compounds. After, mixture 2 was added, mixed, and incubated at 37°C for 15 minutes. A final concentration of 10 mM of EDTA was added to stop the reaction. A spectrophotometer performed a fluorescence reading at an excitation of 490 nm and an emission of 525 nm. Lastly, FAM+ RNA was added to each well for a final concentration of 200nM. Another reading was performed at the same excitation and emission to determine if quenching was present and to eliminate any compounds that were false positives. Dr. Tom Pfeifer at the University of British Columbia and Dr. Joaquin Lopez-Orozco at the University of Alberta analyzed the results.

## **2.3 Techniques for Validating Cas13a Inhibitors**

### ***2.3.1 FAM Cleavage Validation Assay***

The amount of reagents and protocol used for FAM validation assays.

**Mixture 1:** 37  $\mu$ l

Cas13a: 2.5 nM

crRNA: 1.25 nM

Cas13a cleavage buffer 10x: 5.0  $\mu$ l

Water: to 37  $\mu$ l

**Compound:** 1  $\mu$ l

**Mixture 2:** 12  $\mu$ l

Reporter RNA: 500 nM

Target RNA: 1.0 nM

Water: to 12  $\mu$ l

DMSO in place of a chemical compound was added to the reaction for the positive control, and scrambled crRNA was added to the reaction for the negative control. First, mixture 1 was incubated at 37°C for 10 minutes to hybridize the Cas13a and crRNA. Next, mixture 1 was added to a 96 well plate followed by the addition of 1  $\mu$ l of compound. After that, mixture 2 was added and mixed. To begin the reaction, the plate was incubated at 37°C and read at the 15-minute time point with the SpectraMax® i3x spectrophotometer at an excitation of 490 nm and an emission of 510 nm. The fluorescence values were uploaded into the PRISM program for analysis.

### ***2.3.2 Quenching Assay***

Assay conditions were replicated as closely to the FAM validation assay as possible. 100 nM of FAM+ RNA was used, as it was comparable to the maximum signal achieved in the FAM assay.

**Mixture:** 49  $\mu$ l

Cas13a: 2.5 nM

Cas13a cleavage buffer 10x: 5.0  $\mu$ l

FAM+ RNA: 100 nM

Target RNA: 1.0 nM

Water: to 49  $\mu$ l

**Compound:** 1  $\mu$ l

All components were mixed, incubated at 37°C, and read at the 5-minute time point with the SpectraMax<sup>®</sup> i3x spectrophotometer at an excitation of 490 nm and an emission of 510 nm. The fluorescence values were uploaded into the PRISM program for analysis.

### **2.3.3 Redox Cycling Determination via Amplex<sup>®</sup> Red Assay**

This was performed as per the Amplex<sup>®</sup> Red Hydrogen Peroxide/Peroxidase Assay Kit (Invitrogen) instructions. For the positive control, H<sub>2</sub>O<sub>2</sub> was added to the reaction. For the negative control, only DMSO was added. For the chemical compounds, 2  $\mu$ L of 2.5 mM stock concentration was added for a final concentration of 100  $\mu$ M. For justification of performing this assay see Section

#### **3.3.2.**

**Mixture 1:** 50  $\mu$ l

Reaction Buffer 1X: 48  $\mu$ l

2.5 mM of Compound (or DMSO): 2  $\mu$ l

**Mixture 1 (Positive Control):** 50  $\mu$ l

Reaction Buffer 1X: 47  $\mu$ l

DMSO: 2  $\mu$ l

0.5 mM of H<sub>2</sub>O<sub>2</sub>: 1  $\mu$ l

**Mixture 2:** 50  $\mu$ l

Reaction Buffer 1X: 48.5  $\mu$ l

10 U/mL of HRP: 1  $\mu$ l

10 mM of Amplex Red: 0.5  $\mu$ l

All components were mixed and incubated at room temperature for 30 minutes. Readings were taken every 10 minutes with the SpectraMax<sup>®</sup> i3x spectrophotometer at an excitation of 560 nm and an emission of 590 nm. The fluorescence values were uploaded into the PRISM program for analysis.

### **2.3.4 Gel Cleavage Assay**

The amount of reagents and protocol used for the gel cleavage assay:

**Mixture 1:** 19.5  $\mu$ l

Cas13a: 25 nM

crRNA: 12.5 nM

Cas13a cleavage buffer 10x: 2.5  $\mu$ l

Water: to 19.5  $\mu$ l

**Compound:** 0.5  $\mu$ l

**Mixture 2:** 5  $\mu$ l

Target RNA: 100 nM

Water: to 5  $\mu$ l

DMSO in place of a chemical compound was added to the reaction for the positive control, and scrambled crRNA was added to the reaction for the negative control. Mixture 1 was incubated at 37°C for 10 minutes to hybridize the Cas13a and crRNA. 0.5  $\mu$ l of compound was added and mixed with mixture 1. After, mixture 2 was added, mixed, and incubated at 37°C for 25 minutes. After, 10  $\mu$ l of 2x RNA Loading Dye was added and boiled at 95°C for 5 minutes. 15% Criterion™ TBE-Urea Precast Gel 18-well (30  $\mu$ l) (Biorad) was pre-ran at 175 V for 10 minutes, followed by flushing the wells with 1x TBE buffer to remove residual urea and APS. 20  $\mu$ l of samples were loaded, and the gel was run at 175 V for 45 minutes. SYBR gold (Invitrogen) staining solution was prepared by adding 5  $\mu$ l of 10000x stock to 50 mL of TBE buffer. Staining was conducted for 15 minutes, followed by visualization using the Fluorescence Cy5 channel of the Amersham Imager 600.

## **2.4 Techniques for Characterization of Cas13a Inhibitors**

### **2.4.1 IC<sub>50</sub> Determination**

The amount of reagents and protocol used for IC<sub>50</sub> determination assays.

**Mixture 1:** 37  $\mu$ l

Cas13a: 2.5 nM

crRNA: 1.25 nM

Cas13a cleavage buffer 10x: 5.0  $\mu$ l

Water: to 37  $\mu$ l

**Compound:** 1  $\mu$ l

**Mixture 2:** 12  $\mu$ l

Reporter RNA: 500 nM

Target RNA: 1.0 nM

Water: to 12  $\mu$ l

The experiment was performed as described in the Cas13a FAM validation assay (**2.3.1**). Eight different drug concentrations were tested for each IC<sub>50</sub> curve. Data was analyzed using the PRISM software. All data points were normalized and fit to an [Inhibitor] vs. normalized response – variable slope curve.

### **2.4.2 Mechanism of Inhibition Determination**

The amount of reagents and protocol used for mechanism of inhibition assays:

**Mixture 1:** 36  $\mu$ l

Cas13a: 2.5 nM

crRNA: 1.25 nM

Cas13a cleavage buffer 10x: 5.0  $\mu$ l

Water: to 36  $\mu$ l

**Compound (or DMSO):** 1  $\mu$ l

**Mixture 2:** 12  $\mu$ l

Reporter RNA: variable (0  $\mu$ M to 24  $\mu$ M)

Target RNA: 1.0 nM

Water: to 12  $\mu$ l

The experiment was performed as described in the Cas13a FAM validation assay (**2.3.1**). Data was analyzed using the PRISM software. To determine the mechanism of inhibition, Michaelis-Menten curves were generated. The amount of cut RNA substrate was determined as described in the Cas13a  $K_M$  determination experiment (**2.1.3**). The reaction rate at the 15-minute interval was determined by dividing the amount of cut RNA substrate by 15. The rate was plotted against substrate concentration and was normalized and fitted to a Michaelis-Menten curve using PRISM software to find the  $K_M$  and  $V_{max}$ .

### **2.4.3 CC50 Determination**

MTT assay was used to determine cytotoxic concentration 50% (CC50) of the compounds. HEK293T cells were cultured in Dulbecco's Modified Eagle Medium high glucose, sodium pyruvate (Gibco) supplemented with 10% FBS (Gibco) and 1x Penicillin-Streptomycin-Glutamine (Gibco) at 37°C, 5% CO<sub>2</sub>. Cells were plated in a 96 well plate with 8000 cells per well with 150  $\mu$ l of media. 24 hours later, compounds were added to the wells at 8 different concentrations with a final DMSO concentration of 1% per well. 48 hours later, media was aspirated and replaced with 100  $\mu$ l 1x MTT reagent with serum-free media per well. Plates were incubated at 37°C for 90 minutes. After, reagent was carefully aspirated and 100  $\mu$ l of DMSO was added to dissolve the crystals. Plates were incubated 20 minutes at room temperature on an orbital shaker. Plates were read using a SpectraMax® i3x spectrophotometer at absorbance of 570 nM. Data was analyzed using the PRISM software. All data points were normalized and fit to an [Inhibitor] vs. normalized response – variable slope curve.

## **2.5 Additional Techniques for Testing Cas13a Inhibitors in Cells**

### **2.5.1 Generation of Cas13 HEK293T Cell Line**

Stably expressing Cas13a cell lines were made via lentiviral transduction. HEK293T cells were transfected with the plasmids psPAX2 (Addgene- item #12260), PMD2.G (Addgene- item #12259), and pC034 - LwCas13a-msfGFP-2A-Blast (Addgene- item #91924) at a ratio of 1:3:4 using FuGENE® HD Transfection Reagent (Promega). After 48 hours, the virus was harvested. The viral supernatant was filtered with a 0.45 µM PES filter and diluted with fresh media at a 1:1 ratio. Polybrene (Sigma) was added to the mixture for a final concentration of 8.0 µg/mL and added to cells in a 6 well plate. 24 hours later, the media was replaced with blasticidin selection media (10 µg/mL) to select for the LwCas13a-msfGFP expressing cells.

### **2.5.2 Cloning of crRNA Mammalian Expression Plasmids**

To generate crRNA mammalian expression plasmids for the Cas13 cell line, the transcripts for SIRT1 and CCAR2 were found on the Ensembl genome browser. The sequence of the most prevalent transcript for each gene was entered into the CRISPR-RT web application tool, and the top hit for both targets was selected. Additionally, the transcript ID of these two transcripts was entered into another online tool called Cas13design tool. The top hit for both targets was found. Since this is a tool for Cas13d, an additional 5 nucleotides were added to the 3' end of the spacer sequence. The sequences were ordered as gBlocks (IDT) with BbsI cut sites on each end. The gBlocks were restriction digested at 37°C for 3 hours with restriction enzymes BbsI (NEB) and ligated into the plasmid pC016 - LwCas13a guide expression backbone U6 promoter (Addgene- item #91906) using Quick Ligase from NEB. Ligated plasmids were transformed into Subcloning Efficiency™ DH5α cells (Invitrogen), and the plasmids were isolated and purified using Miniprep kit (Qiagen). The plasmids were Sanger sequenced and verified using the SnapGene alignment tool. The gBlock sequences can be found in **Table S4**.

## CHAPTER 3: Experiments and Results

### 3.1 FAM Cleavage Assay Optimization

#### **3.1.1 Selection of Assay**

To identify chemical compounds that inhibit LwaCas13a, we adapted the Cas13 biochemical assay from the SHERLOCK system (Gootenberg et al., 2017; Gootenberg et al., 2018). This assay relies on an RNA oligonucleotide referred to as a reporter RNA. This RNA comprises of a penta-uracil sequence with a 6-Carboxyfluorescein (6-FAM) fluorophore on the 5' end, and an Iowa Black® FQ quencher (IBFQ) on the 3' end (6-FAM-UUUUU-IBFQ): this particular sequence was shown to be very well suited for LwaCas13a (Gootenberg et al., 2018). The biochemical assay depends on the collateral cleavage of Cas13, where upon binding to a target RNA, Cas13 becomes activated and begins to collaterally cleave the reporter RNA. This separates the quencher from the fluorophore and results in fluorescent signal (**Figure 4A**). Thus, if a drug inhibits LwaCas13a then there will be no fluorescent signal. This assay will be referred to as the FAM assay throughout the dissertation. Once all the components were made (LwaCas13a, crRNA, target RNA, and cleavage buffer) and bought (reporter RNA), control experiments were performed to verify the assay. Scrambled crRNA, scrambled target RNA, and dCas13a resulted in no increase in fluorescence in the FAM assay. An increase in fluorescent signal was observed only when all on-target components were present (**Figure 4B**). Further verification was performed using a gel-based cleavage assay. As with the FAM assay, only on-target active components led to cleavage (**Figure 4C**).

#### **3.1.2 Cas13a $K_M$ Determination and RNA Optimization**

Experiments were then performed to determine the  $K_M$  of Cas13 and to optimize the amount of RNP and target RNA per reaction for the FAM assay.  $K_M$ , or Michaelis constant, is the substrate concentration level for which the reaction is at 50%  $V_{max}$  (maximum velocity) at a given enzyme concentration (Nath, 2007).

It was crucial to know the  $K_M$  value as we would like to screen for all inhibitors regardless of their mode of action; to ensure this, a substrate concentration that was lower than the  $K_M$  was required (Strelow et al., 2004). Furthermore, by having the substrate concentration below the  $K_M$ , we can ensure that the product formation is linear in time. This satisfies one of the assumptions of the Michaelis-Menten equation: the steady-state approximation where there is no change in enzyme-substrate complex concentration (Nath, 2007). The other two assumptions are the free-ligand assumption (total enzyme concentration is far smaller than  $K_M$ ) and rapid equilibrium approximation (substrate binding and dissociation occur much more rapidly than product formation i.e.  $k_{cat} \ll k_{off}$ ) both of which were satisfied in our assay (Nath, 2007).

A literature search showed that the  $K_M$  of Cas13a with the PolyU reporter RNA is 4.45  $\mu\text{M}$  (Shan et al., 2019). In another paper, the  $K_M$  was presented as a range from 1.0  $\mu\text{M}$  to 3.0  $\mu\text{M}$  (Fozouni et al., 2021). The  $K_M$  determination experiments in the literature were replicated as in Shan, 2019. We titrated different amounts of reporter RNA substrate from 0  $\mu\text{M}$  to 10  $\mu\text{M}$  at a fixed Cas13/crRNA RNP amount (10 nM) (**Figure 4D**). The amount of cut RNA substrate was determined using a standard curve equation that converts the fluorescence generated by cleaved reporter RNA substrate into the concentration of cleaved reporter RNA substrate:  $y = 9011943 \cdot x$  where  $y$  = fluorescence (AFU) and  $x$  = product ( $\mu\text{M}$ ). The reaction rate at the 5-minute interval was determined by dividing the amount of cut RNA substrate by 5. The rate was plotted against substrate concentration, and then fitted to a Michaelis-Menten curve using the PRISM software. We received a final  $K_M$  of 8.04  $\mu\text{M}$  and a  $V_{max}$  of 0.095  $\mu\text{M}/\text{min}$  (**Figure 4E**). This experiment was repeated multiple times with final  $K_M$ 's ranging from 2  $\mu\text{M}$  to 8  $\mu\text{M}$  and  $V_{max}$ 's ranging from 0.02  $\mu\text{M}/\text{min}$  to 0.13  $\mu\text{M}/\text{min}$  for the PolyU reporter RNA substrate (**Figure S1**). We chose 1  $\mu\text{M}$  for our final reporter RNA concentration as it was below the  $K_M$  and balanced good signal/noise ratio and cost-efficiency.

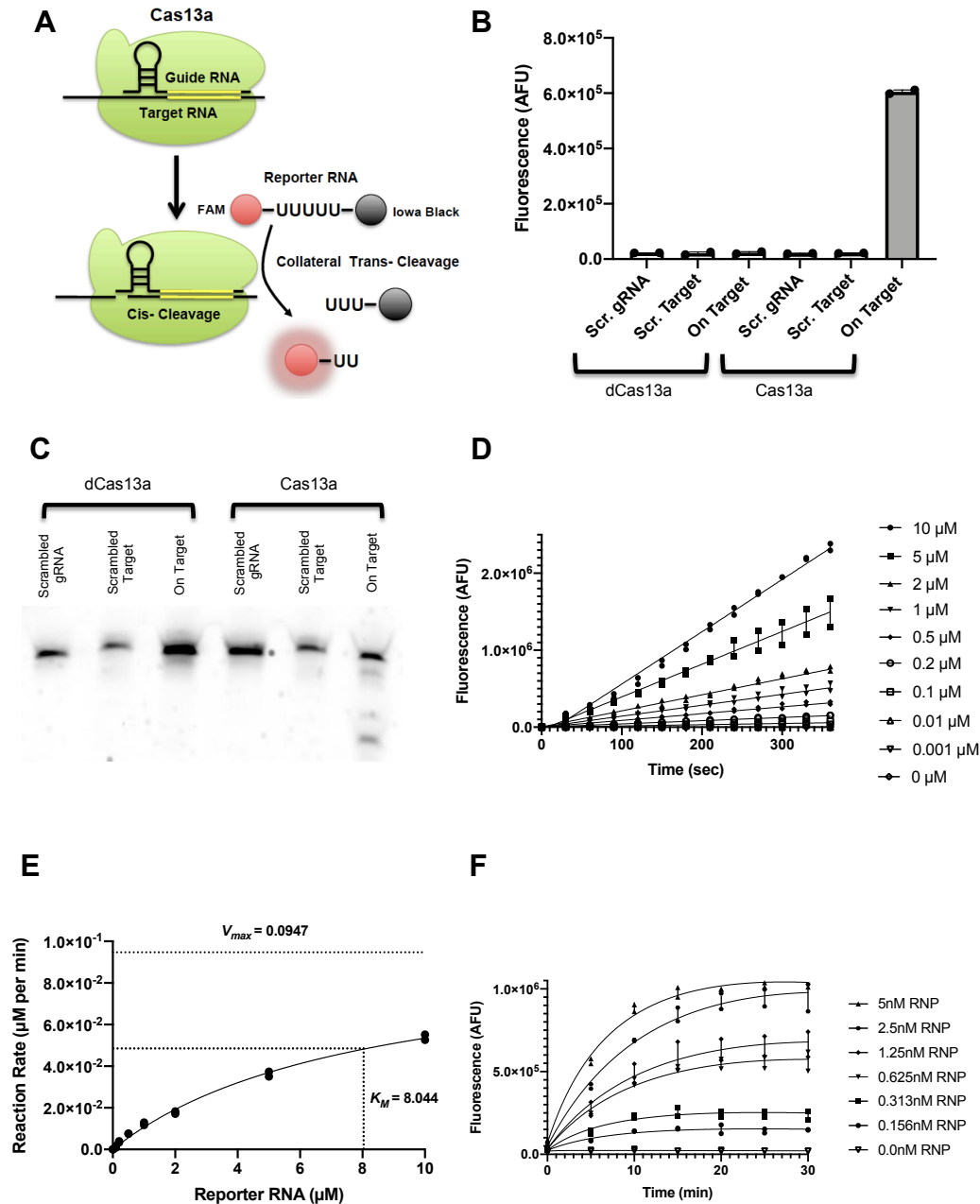


**Figure 4: Schematic of Assay, Verification of Assay, and Enzyme/Substrate Optimization.**

**A)** A schematic diagram for the collateral cleavage FAM assay is shown. **B)** Control assay. Only non-scrambled RNA with active Cas13a was able to yield fluorescent signal. Both technical replicates are shown on the graph. **C)** Control gel cleavage assay further verified that only non-scrambled RNA with active Cas13a could cleave. **D)** Constant RNP (10 nM) and target RNA (0.01 nM) concentration with various reporter RNA concentrations measured over time. Both technical replicates are shown on the curve. **E)** Determination of  $K_M$  of Cas13a.  $K_M$  of Cas13a was found to be 8.04  $\mu\text{M}$  with a  $V_{max}$  of 0.0947  $\mu\text{M}/\text{min}$ . Both technical replicates are shown on the curve. **F)** Constant Reporter RNA concentration at different RNP concentrations. Reactions were performed with 1  $\mu\text{M}$  of reporter RNA. 1.25 nM of RNP was selected as the concentration for all subsequent assays as the enzyme activity was linear at the 10-15 minute range. Both technical replicates are shown on the curve. Future students will perform additional replicates for all optimization experiments.

Additionally, the assays target RNA concentration was determined by comparing the signal/noise (S/N) ratio at varying target RNA concentrations. 1.0 nM of target RNA was selected as it showed an excellent S/N ratio. The original concentration of 0.01 nM yielded a very low signal to noise ratio (**Figure 5A**).

### **3.1.3 Cas13a RNP Determination and DMSO Tolerance**

An experiment was conducted to determine the ideal amount of RNP (Cas13/crRNA) and the ideal time to read the fluorescence of the reaction. The amount of reporter RNA and target RNA was kept constant while the amount of RNP was changed. 1.25 nM of RNP was selected, as the enzyme activity was linear at the 10-15 minute range and still maintained a strong signal (**Figure 4F**). Lastly, a DMSO titration was performed to determine how sensitive Cas13 is to DMSO. The enzyme worked up to a final concentration of 2% DMSO. However, there was no Cas13 activity at a concentration of 4% DMSO (**Figure 5B**). To summarize, we used the following reagent concentrations for our downstream biochemical assays: Cas13 2.5 nM, crRNA 1.25 nM, target RNA 1 nM, reporter RNA 1000 nM, and 2% DMSO.

### **3.1.4 Selection of Positive and Negative Controls**

For the positive control, DMSO in place of a chemical compound was added to the reaction. For the negative control, we used a chemical compound known as benzopurpurin B (BPP). This compound was initially discovered to be a potent inhibitor of an RNase called Nsp15 of SARS-CoV-2 (Ortiz-Alcantra et al., 2004). Related work in the lab showed that benzopurpurin B was also a potent inhibitor of Cas13a. We selected this compound, as we wanted to use an inhibitory chemical compound as a negative control instead of a scrambled RNA.

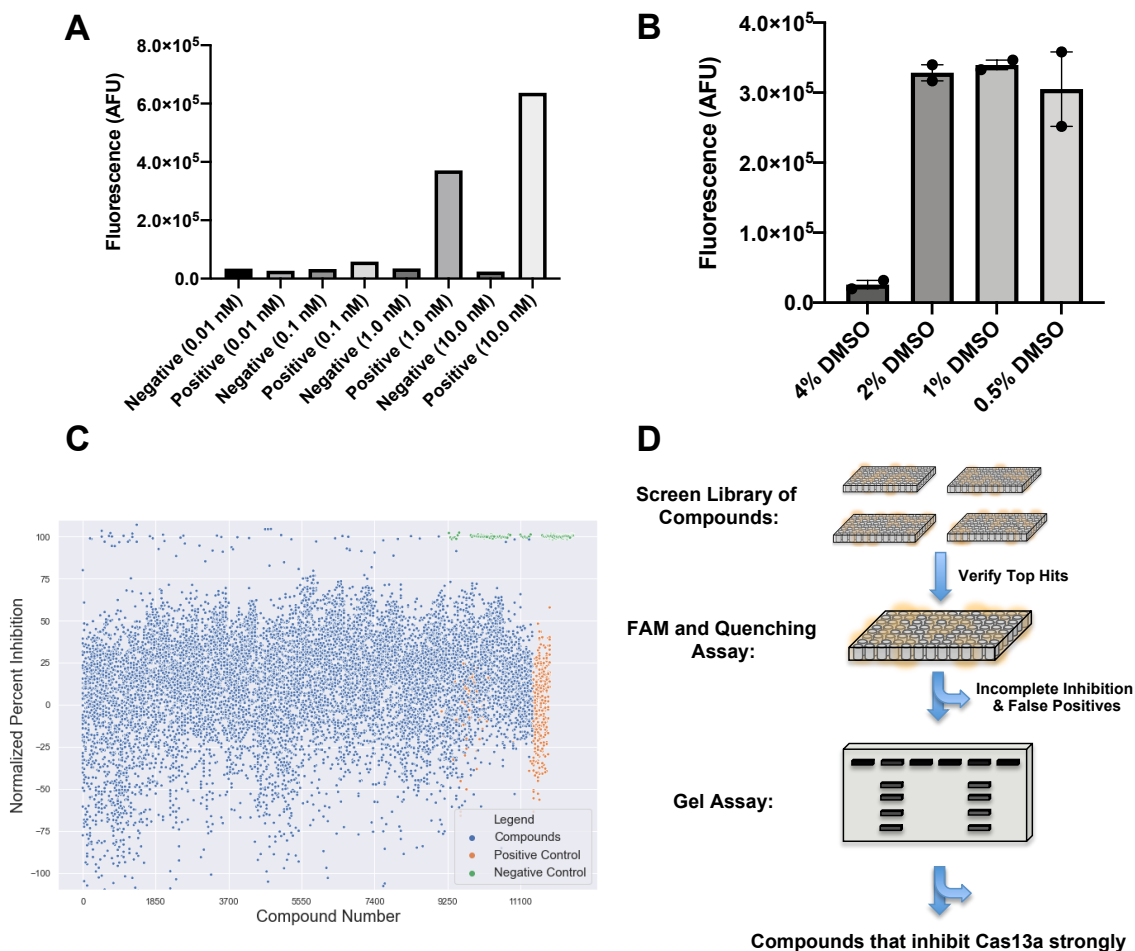


**Figure 5: Additional Optimization Experiments, Screening Result, and Compound Validation Workflow.** **A)** The amount of target RNA was determined by comparing the signal/noise ratio at varying target RNA concentrations. 1.0 nM of target RNA was selected. **B)** DMSO titration was conducted to determine the sensitivity of Cas13a to DMSO. 2% had no effect, while 4% abolished activity. Both technical replicates are shown on the graph. Future students will perform additional replicates for all optimization experiments. **C)** The final screening result with all 13120 compounds tested. In total 99 compounds had a standard deviation of 2.0 or higher of normalized percent inhibition. The top 20 compounds were bought and tested. **D)** Compound Validation Workflow. The top hits from the library screen were validated with FAM assay, followed by quenching assay, and Amplex<sup>®</sup> Red assay. Compounds that were not eliminated were subjected to a gel cleavage assay for final verification. The final remaining compounds were characterized.

## **3.2 Screening of 13120 Compounds**

The assay was utilized to screen a total of 13120 compounds at a 10  $\mu\text{M}$  concentration. 1280 compounds were screened at the University of Alberta. It was an assortment of compounds from various libraries and collections: Chembridge, Maybridge, Prestwick, Microsource Spectrum compounds, LOPAC compounds, TimTec, Chembridge DIVERSet collection, and Chembridge GlycoNet collections. Additional 11840 compounds, 10240 (32 plates) compounds from Chembridge, and 1600 (5 plates) compounds from Maybridge, were screened at the University of British Columbia. All of these compounds were from the Canadian Chemical Biology Network (CCBN) collection. Out of these 13120 compounds, 99 chemical compounds inhibited Cas13a strongly at a standard deviation of 2.0 or higher of normalized percent inhibition (**Figure 5C**). The top 20 inhibitors that demonstrated greater than 60% inhibition were selected and verified in downstream assays. An overview of these downstream assays is found in (**Figure 5D**). For the full chemical names of all 20 compounds, see **Table S5**.

## **3.3 Compound Validation**

### ***3.3.1 FAM Cleavage and Quenching Assay***

Initially, the 20 selected compounds were tested at 25  $\mu\text{M}$  and 50  $\mu\text{M}$  concentrations with the FAM assay to test their inhibition. 11 out of the 20 inhibited Cas13a strongly at 25  $\mu\text{M}$  concentrations. The other 9 compounds C1, C4, C6, C8, and C16-C20 failed to fully inhibit Cas13a at either 25  $\mu\text{M}$  or 50  $\mu\text{M}$  reproducibly (**Figure 6A**). The 11 effective compounds were further subjected to a quenching assay. This quenching test showed around 20-30% quenching for most compounds; the exception was C14, with 75% quenching at 25  $\mu\text{M}$  (**Figure 6B**). C14 was tested at lower doses (5 $\mu\text{M}$  and 10 $\mu\text{M}$ ) and showed reduced quenching while still exhibiting 100% Cas13a inhibition. From these results we deduced that C14 is still an inhibitor and decided to continue to test it.

### **3.3.2 Redox Cycling Determination**

Another property that we wanted to test was to see if these compounds exhibited redox cycling. Redox cycling is the process where a chemical compound shuttles electrons from a reductase, usually NADH, to oxygen (Gutierrez, 2000). The reduced oxygen is called superoxide, which leads to the formation of reactive oxygen species such as hydrogen peroxide (Gutierrez, 2000). The formation of these reactive oxygen species leads to cytotoxicity and is detrimental to future cell work. Dithiothreitol (DTT) is present in the Cas13a storage buffer, which may lead to redox cycling in the presence of compounds and may result in non-specific inhibition (Johnston, 2011). To perform this experiment, we utilized the Amplex® Red Hydrogen Peroxide/Peroxidase Assay Kit. This kit relies on the reagent Amplex™ Red that is converted into resorufin by hydrogen peroxidase in the presence of hydrogen peroxide (Zhou, M., et al., 1997). Resorufin has an excitation of 560 nm and an emission of 590 nm that can be detected (Zhou, M., et al., 1997). None of the compounds showed this effect (**Figure 6C**).

### **3.3.3 Gel Cleavage Assay**

For final confirmation, a gel cleavage assay with a non-fluorophore based RNA substrate was performed to determine if the inhibition was genuine. Quenching was present in all compounds, and we wanted to see how well or if the compounds could inhibit the enzyme when using a natural substrate. 9 out of the 11 compounds strongly inhibited Cas13 activity at 50  $\mu$ M concentration or lower (**Figure 6D**); their structures are shown in (**Figure 6E**). These 9 inhibitors were then subjected to a series of tests to determine their IC<sub>50</sub>s, mechanism of inhibition, and cytotoxicity.

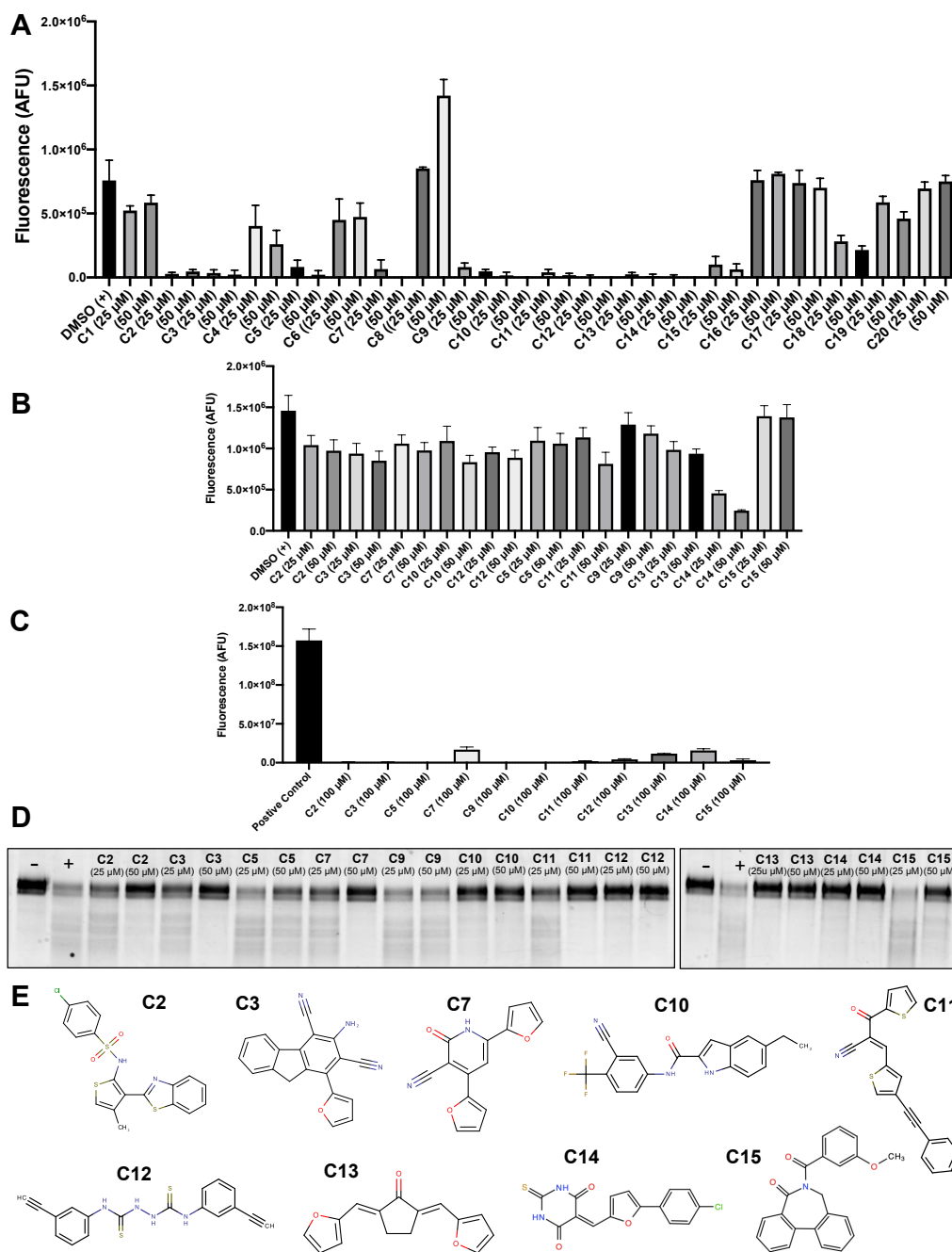


**Figure 6: Compound Validation Assays and Compound Structures. A)** Top 20 compounds tested at 25  $\mu\text{M}$  and 50  $\mu\text{M}$  final concentrations. 11 out of the 20 inhibited Cas13a strongly at 25  $\mu\text{M}$  concentrations. Results expressed as the mean  $\pm$  SD  $n=3$ . **B)** Quenching test showed a low-moderate amount of quenching for most compounds. The only exception is C14, where quenching was at around 75% at 25  $\mu\text{M}$ . Results expressed as the mean  $\pm$  SD  $n=3$ . **C)** An Amplex<sup>®</sup> Red assay was performed to determine if the compounds partake in redox cycling. No appreciable redox cycling was seen with any of the compounds. Results expressed as the mean  $\pm$  SD  $n=3$ . **D)** For a final verification, the compounds were tested with an RNA substrate with no fluorophore. 9 out of the 11 compounds fully inhibited Cas13a at 50  $\mu\text{M}$  concentration. **E)** The chemical structures of the 9 compounds.

## **3.4 Compound Characterization**

### **3.4.1 IC50 Determination**

Inhibitory concentration 50%, or IC50, is the concentration of compounds where enzymatic activity is reduced to half. This is an efficient way of gauging the fidelity of a drug. Initially, the IC50s of these compounds were determined with the FAM assay. The FAM-based IC50s showed that most of the compounds had an IC50 between 1.0  $\mu\text{M}$  to 3.0  $\mu\text{M}$ : exceptions being C12 at 0.3  $\mu\text{M}$ , C7 at 15.2  $\mu\text{M}$ , and C15 at 24.3  $\mu\text{M}$  (**Figure 7**). All curves were repeated at least twice to make sure IC50s were close to the obtained values (**Figure S2A**). As quenching remains a problem with the FAM-based assay, gel cleavage-based IC50s were also tried. Although only one round of IC50 gel cleavage assays was performed, partly due to time and material constraints, the results showed that the IC50s for all compounds were higher than IC50s found using the FAM assays (**Figure S2B**). More experiments are required to replicate these results.

### **3.4.2 Mechanism of Inhibition Determination**

Michaelis-Menten curves with and without compounds were plotted to determine the mechanism of inhibition of the compounds. The reaction rate was plotted against substrate concentration, and the changes in  $K_M$  and  $V_{max}$  were analysed. There are three main modes of inhibition that could occur: competitive inhibition- an increase in  $K_M$  with no change in  $V_{max}$ ; non-competitive inhibition- no change in  $K_M$  with a decrease in  $V_{max}$ ; and uncompetitive inhibition- a decrease in both  $K_M$  and  $V_{max}$  (Strelow et al., 2004). Additionally, a combination of competitive and non-competitive inhibition results in the fourth type of inhibition called mixed inhibition, characterized by an increase in  $K_M$  and a decrease in  $V_{max}$  (Strelow et al., 2004). For these reactions, a compound concentration was selected to ensure there is no quenching to ensure genuine inhibition: for most compounds, it was the IC50 concentration.

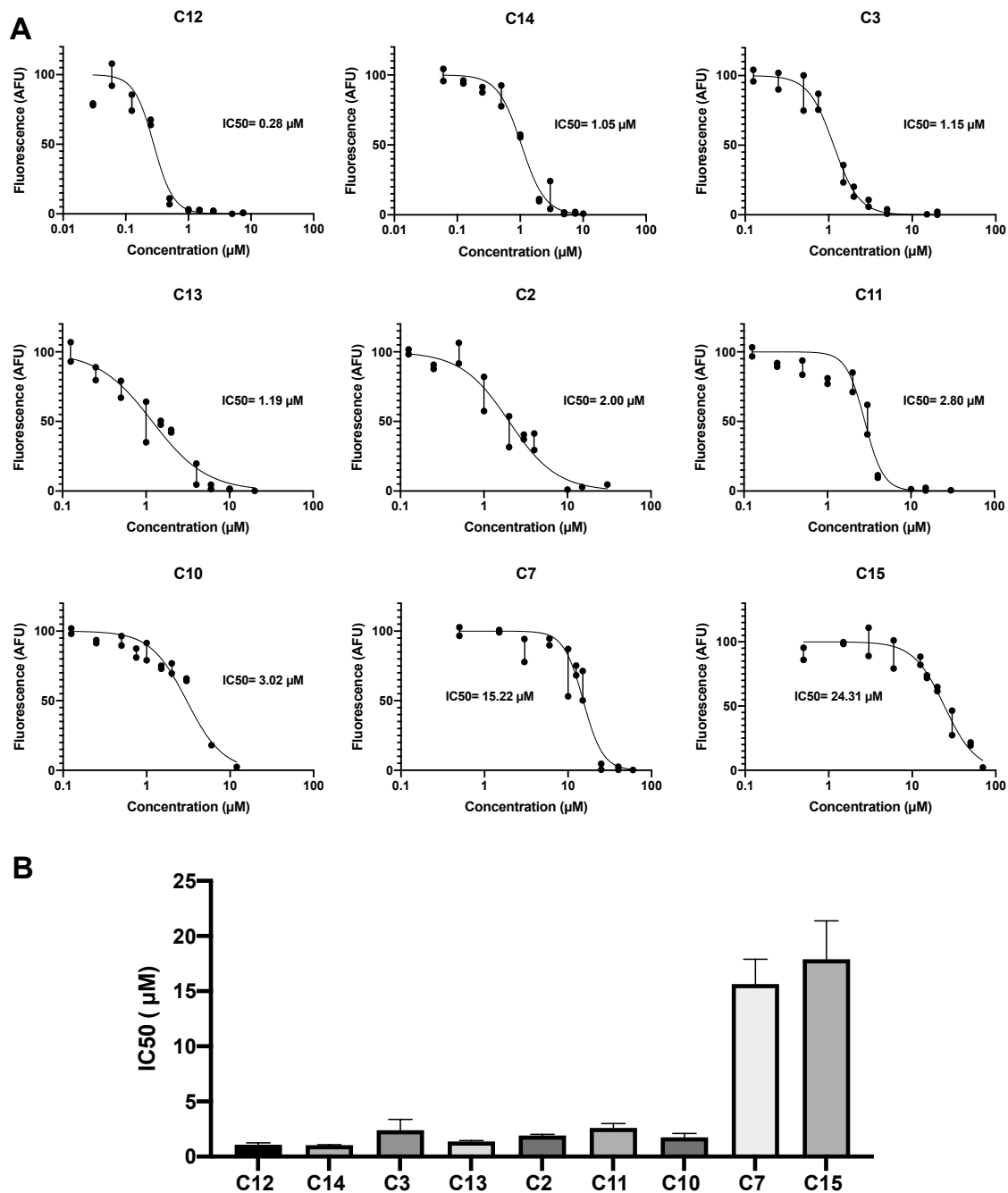


**Figure 7: Characterization of Compounds- IC50s. A)** IC50s of the 9 compounds as determined using the FAM assay: graphs are ordered by most effective to least effective. C12 had the lowest IC50 of 0.28 µM. The majority of the compounds had IC50s ranging from 1.0 µM to 3.0 µM. Compounds C7 and C15 were less effective and had higher IC50s of 15.22 µM and 24.31 µM, respectively. Both technical replicates are shown on the curve. **B)** Summary of IC50 values for the Cas13a inhibitors. Results represented as mean with ± SEM (Standard Error of the Mean) n=3.

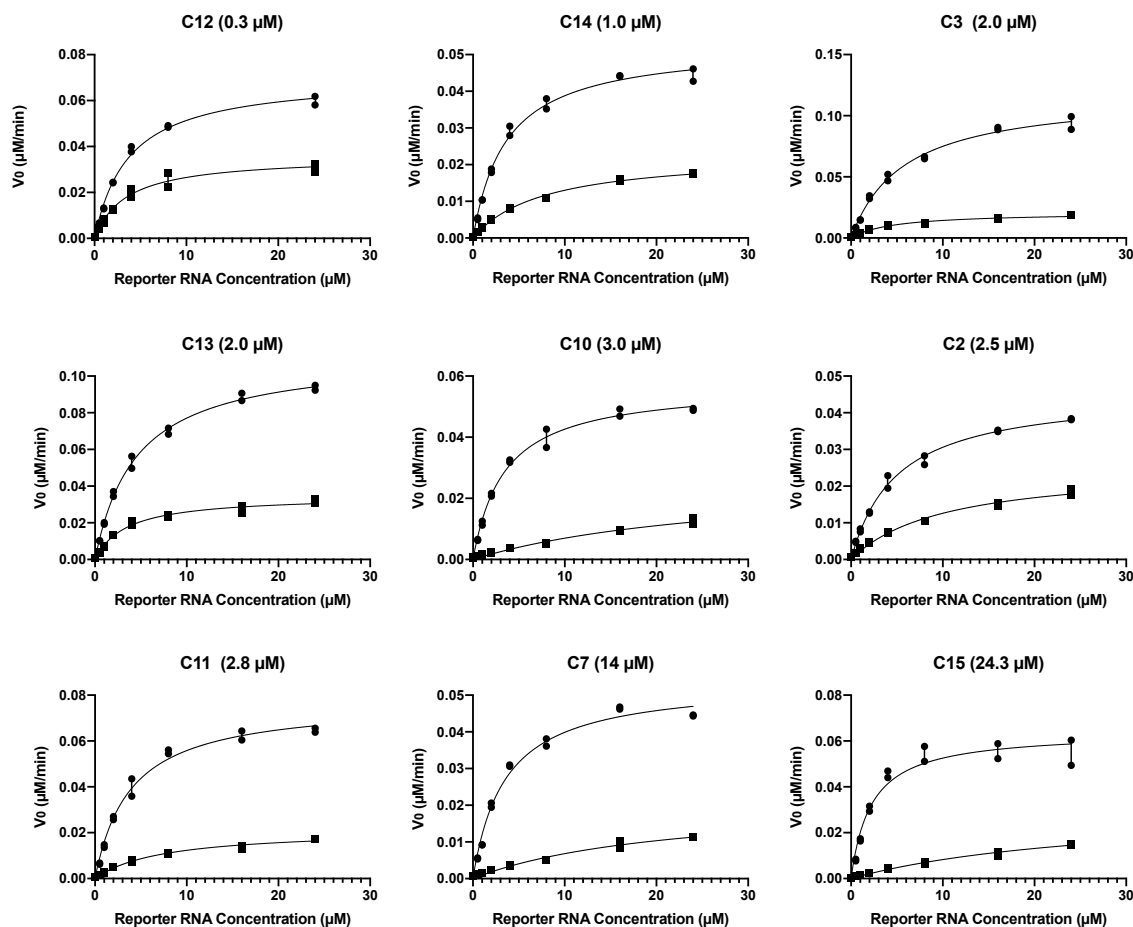


**Figure 8: Characterization of Compounds- Mechanism of Inhibition.** Michaelis-Menten curves were generated to find the mechanism of inhibition: compounds are ordered by most effective to least effective. Comparing the  $K_M$  and  $V_{max}$  of the curves with and without compounds revealed that the compounds C12, C14, C3, C13, and C11 are non-competitive inhibitors, and compounds C10, C2, C7, and C15 are competitive inhibitors. However, some compounds may exhibit mixed inhibition. Both technical replicates are shown on the curve. Future students will perform additional replicates.

The curves were generated by varying concentrations of reporter RNA from 0.25  $\mu\text{M}$  to 24  $\mu\text{M}$  with and without compound. The rate of the reaction was found by taking the fluorescent value at the 15 minute interval and using the previously described equation to find the concentration of substrate: (fluorescence (AFU))= 9011943\*x(product ( $\mu\text{M}$ )). The concentration was divided by 15 minutes to acquire the rate. Analyzing the changes in  $K_M$  and  $V_{max}$  revealed (**Figure 8**) that most compounds are non-competitive or competitive inhibitors with several

compounds that might exhibit mixed inhibition. A summary of the results is found in (Table 1). Additional curves can be found in (Figure S3).

**Table 1. Compounds' Mechanisms of Inhibition Summary**

Compounds ordered from most effective to least effective

Name	DMSO $V_{max}$ ( $V_0$ /min) [95CI]	Compound $V_{max}$ ( $V_0$ /min) [95CI]	DMSO $K_M$ ( $\mu$ M) [95CI]	Compound $K_M$ ( $\mu$ M) [95CI]	Predicated Type of Inhibition
<b>C12</b>	0.071 (0.067 to 0.075)	0.036 (0.032 to 0.040)	3.74 (3.18 to 4.39)	3.44 (2.56 to 4.60)	Non-competitive
<b>C14</b>	0.053 (0.050 to 0.056)	0.023 (0.022 to 0.024)	3.62 (3.09 to 4.23)	7.70 (6.73 to 8.84)	Non-competitive
<b>C3</b>	0.118 (0.110 to 0.127)	0.021 (0.019 to 0.023)	5.75 (4.76 to 6.98)	4.59 (3.65 to 5.81)	Non-competitive
<b>C13</b>	0.112 (0.108 to 0.116)	0.035 (0.032 to 0.038)	4.51 (4.02 to 5.06)	3.43 (2.72 to 4.34)	Non-competitive (Uncompetitive)
<b>C10</b>	0.057 (0.055 to 0.060)	0.02688 (0.019 to 0.048)	3.42 (2.93 to 3.99)	28.57 (15.92 to 66.01)	Competitive (Mixed)
<b>C2</b>	0.046 (0.043 to 0.048)	0.025 (0.023 to 0.029)	4.97 (4.27 to 5.79)	10.18 (7.77 to 13.59)	Competitive (Mixed)
<b>C11</b>	0.077 (0.073 to 0.082)	0.021 (0.019 to 0.024)	3.86 (3.21 to 4.64)	7.43 (5.69 to 9.85)	Non-competitive
<b>C7</b>	0.054 (0.050 to 0.057)	0.021 (0.016 to 0.033)	3.49 (2.85 to 4.28)	21.53 (12.78 to 42.11)	Competitive (Mixed)
<b>C15</b>	0.064 (0.059 to 0.070)	0.032 (0.025 to 0.045)	2.20 (1.59 to 3.03)	28.31 (18.73 to 47.86)	Competitive (Mixed)

### 3.4.3 Compound Cytotoxicity

To determine the cytotoxic concentration 50% (CC50) of the compounds preliminary trials were conducted in cells. The CC50 is the amount of compound that kills half the cells. The compounds were placed on HEK293T cells at 1% DMSO for 48 hours. An MTT assay revealed that most of the compounds were not toxic to the cell: CC50 greater than 60  $\mu\text{M}$ . However, several compounds appear to be toxic: C14 9.19  $\mu\text{M}$ , C2 9.30  $\mu\text{M}$ , and C15 16.47  $\mu\text{M}$  (**Table 2**). CC50 curves can be found in (**Figure S4**). Furthermore, we generated HEK293T cells that stably expressed Cas13a-eGFP, and cloned plasmids that encode for crRNAs that target SIRT1 and CCAR2 transcripts. Unfortunately, there was not enough time to test these cells and plasmids with the compounds.

**Table 2. Compounds' CC50s Summary**

Compounds ordered from most effective to least effective

Name	Predicted CC50s
C12	>100 $\mu\text{M}$
C14	9.19 $\mu\text{M}$
C3	>100 $\mu\text{M}$
C13	75.29 $\mu\text{M}$
C10	>100 $\mu\text{M}$
C2	9.30 $\mu\text{M}$
C11	64.71 $\mu\text{M}$
C7	64.93 $\mu\text{M}$
C15	16.47 $\mu\text{M}$

## CHAPTER 4: Discussion and Future Directions

### 4.1 Discussion

The initial inspiration for the project came from performing a literature search to find methods to prevent Cas13 cleavage. We were surprised to discover that there were so few ways to inhibit this enzyme. The two existing methods are anti-CRISPR proteins, i.e., AcrVIA, (Lin et al., 2020), and anti-tag RNAs (Meeske and Marraffini, 2018). We believe that neither of these two methods is ideal for controlling Cas13 cleavage and that small-molecules would provide researchers a more accessible way to inhibit Cas13. Such molecules could provide temporal control of the Cas13 protein and further assist in the development of various Cas13 techniques and tools. Furthermore, the possession of compound inhibitors is crucial for clinical trials. Patients may develop side effects from prolonged Cas13 cleavage, and small molecule inhibitors could halt this adverse event. With Cas13a chemical inhibitors unknown to science, the project was pursued.

In order to accomplish this task we adapted the SHERLOCK assay (Gootenberg et al., 2018). This assay relies on the robust collateral cleavage of a fluorophore/quencher reporter RNA to generate a fluorescent signal. Two screenings were performed: a 1280 compound screen at the University of Alberta, and a larger 11840 compound screen at the University of British Columbia. These compounds were from various libraries originating from the Canadian Chemical Biology Network (CCBN) collection. Of the total 13120 compounds screened, 99 compounds had a standard deviation of 2.0 or higher of normalized percent inhibition. The top 20 compounds that demonstrated greater than 60% inhibition were tested. 9 out of these 20 compounds were able to completely inhibit Cas13a at 25  $\mu$ M or lower using the FAM assay. These 9 compounds did not have 100% quenching and did not participate in redox recycling. Finally, these compounds were able to completely inhibit Cas13a at 50  $\mu$ M using a non-fluorescently labeled RNA substrate.

The characterization of the 9 compounds revealed that most of them were quite effective, with an IC<sub>50</sub> of around 1.0 μM to 3.0 μM. Due to quenching concerns, a series of non-fluorophore based gel cleavage IC<sub>50</sub>s assays were undertaken. Initial results show that many of the compounds have a higher IC<sub>50</sub> than the values found using the FAM assay. Only one replicate has been performed so far, and another replicate will be conducted to confirm these findings. Mechanistic studies found that the majority of the compounds inhibit Cas13a either competitively or non-competitively. Despite the drugs being tested around their IC<sub>50</sub> concentrations, some of the compounds exhibited very strong inhibition at that concentration: in particular the compounds C10, C11, C7, and C15. These compounds could benefit from another replicate at a lower drug concentration to confirm the respective type of inhibition. Lastly, the cytotoxicity of the cells seems to be relatively low, with 6 compounds having a CC<sub>50</sub> of greater than 60 μM. However, several compounds appear to be more toxic (C14, C2, and C15) and may not be appropriate for cell usage. Several experiments were performed only in duplicate; to increase confidence in our results, a future student will perform another replicate. A summation of the characteristics of these 9 compounds can be found in **Table 3**.

## **4.2 Contributions**

Throughout this project, we have made a number of contributions to the field of CRISPR. We have adapted the SHERLOCK assay and further optimized it to use less materials and reagents. This was accomplished without sacrificing the signal/noise ratio and reproducibility. Such optimization was especially important for screening a large number of compounds and sequences.

**Table 3. Summary of Compounds' Characteristics**  
Compounds ordered from most effective to least effective

Name	IC50 using FAM Assay	Predicated Type of Inhibition	CC50 HEK293T cells
<b>C12</b>	0.3 $\mu$ M	Non-competitive	>100 $\mu$ M
<b>C14</b>	1.1 $\mu$ M	Non-competitive	9.19 $\mu$ M
<b>C3</b>	1.2 $\mu$ M	Non-competitive	>100 $\mu$ M
<b>C13</b>	1.2 $\mu$ M	Non-competitive (uncompetitive)	75.29 $\mu$ M
<b>C10</b>	3.0 $\mu$ M	Competitive (Mixed)	>100 $\mu$ M
<b>C2</b>	2.0 $\mu$ M	Competitive (Mixed)	9.30 $\mu$ M
<b>C11</b>	2.8 $\mu$ M	Non-competitive	64.71 $\mu$ M
<b>C7</b>	15.2 $\mu$ M	Competitive (Mixed)	64.93 $\mu$ M
<b>C15</b>	24.3 $\mu$ M	Competitive (Mixed)	16.47 $\mu$ M

We developed an effective workflow to discover and characterize chemical compounds that inhibit Cas13. This workflow was comprised of the following steps.

- Screening a number of desired compounds
- Selecting the most effective compounds from the screen
- Repeating the assay for the most effective compounds
- Conducting experiments to determine if the compounds are true inhibitors, i.e., 1) a quenching assay to see if any compounds quench or fluoresce; 2) an Amplex<sup>TM</sup> Red peroxidase assay to see if the compounds partake in redox cycling in the presence of reducing agents; and 3) a non-fluorophore based gel cleavage assay for a final and definitive test.
- Characterizing the true inhibitors. These experiments include: 1) IC50 determination; 2) mechanism of inhibition determination; and 3) cytotoxicity determination.

This workflow can be applied to any Cas13 orthologs and subtypes, and with a few adjustments can be also applied to any CRISPR Class 2 endonucleases.

We discovered and characterized nine chemical compounds that were able to prevent Cas13a cleavage *in vitro*. They constitute a new way of inhibiting Cas13. Though further work is required, we are optimistic that several of these small molecules will be used to control Cas13. This will provide researchers with another method to inhibit Cas13 that is both easier to use and more reliable. It can further help with the development of various Cas13 tools and can open the doors for Cas13 clinical usage.

### **4.3 Limitations**

The first limitation is the efficacy of fluorescence-based assays. Chemical compounds either quench (absorption of the emitted photon) or fluoresce (compounds with identical/similar excitation/emission profiles). In the case of quenching, this leads to an increased chance of false positives. This problem was alleviated with the usage of non-fluorophore based substrates, as was conducted with the utilization of the gel cleavage assay. For compounds that have similar excitation/emission profiles, the screen cannot distinguish between compounds that do not inhibit Cas13a and ones that fluoresce naturally. Therefore, a high-throughput screening method that does not rely on fluorescent substrates would have to be used to avoid this issue.

Additional issues are the permeability of compounds and their toxicity. If the compounds are unable to penetrate the cell membrane, they will not be able to inhibit Cas13a cleavage in the cell. Similarly, if the compounds are toxic, they will kill the cell and be ineffective. CC50s curves were generated for the compounds in HEK239T cells. Most of the compounds appear to be non-toxic (CC50 > 60 $\mu$ M), but this could be due to an inability to enter the cell and, thus, the compounds do not impact cell functions. Additional cell work will need to be performed to clarify these questions.

It is still unknown whether these compounds exclusively inhibit Cas13a or are broad-range RNase inhibitors. A second screening with another endonuclease could be implemented to test the top inhibitory compounds of Cas13a. Any compounds that inhibit both proteins would be discarded. Lastly, it is unknown how stable these compounds are. Compounds that degrade quickly will not be effective Cas13a inhibitors for general usage.

#### **4.4 Future Directions**

There are three more directions where the project can be expanded on. The first direction is to test the compounds' ability to inhibit LwaCas13a in cells. We hope that this would lead to the adoption of one or two different chemical inhibitors. As seen in the methodology section, we made a Cas13a-eGFP stably expressing cell line and we cloned several plasmids that encode for crRNA that targets SIRT1 and CCAR2 transcripts (these transcripts were chosen as our lab has suitable antibodies for both these proteins). Unfortunately, due to time constraints, we could not use this system to test the drug efficacy in cells. However, the plan would be to adapt an existing Cas13 transfection protocol in cells and add the compounds sometime after the initial transfection. A western blot would be conducted to see a reduction in SIRT1 and CCAR2 expression in cells with and without the chemical compounds. Another, more direct method of determination would be via quantitative PCR. It is unknown how long these compounds are effective for. A process of optimization is needed to determine the time frame in which these compounds can be used. This work would take several months and could be conducted by another student.

A second direction is to see if these nine compounds can also inhibit Cas13 binding. So far, we have only explored the inhibitors' effect on cleavage, but we do not know if the compounds could affect binding. Isothermal titration calorimetry or surface plasmon resonance could be performed to elucidate this question. Isothermal titration calorimetry functions by measuring the temperature change when a biochemical interaction occurs. The instrument contains two

cells: a reference cell and a sample cell (Srivastava and Yadav, 2019). Titrations of the ligand into the sample cell result in changes in temperature. The instrument responds to these changes by adjusting the temperature back to original value (Srivastava and Yadav, 2019). From this information, the binding constants ( $K_d$ ), reaction stoichiometry ( $n$ ), enthalpy ( $\Delta H$ ), and entropy ( $\Delta S$ ) can be determined (Srivastava and Yadav, 2019). Surface plasmon resonance (SPR) is another method of detecting biochemical interactions. SPR occurs when polarized light strikes an electrically conducting surface at the interface between two mediums<sup>1</sup>. This generates electron charge density waves called plasmons<sup>1</sup>. These plasmons reduce the intensity of reflected light at a specific angle known as the resonance angle in proportion to the mass on a sensor surface<sup>1</sup>. The surface is coated with the sample of interest, and if a ligand binds to the sample, the resonance angle will change. Bonding, specificity, kinetics, and affinity can be determined using this device<sup>1</sup>. Additionally, it would also be interesting to see if these compounds inhibit Cas13a reversibly or irreversibly.

The third direction is to see if the compounds can inhibit other Cas13s. It would be interesting to see if these compounds could inhibit Cas13d and Cas13b subtypes. Cas13d shares more similarities with Cas13a, both in protein and crRNA structure, and we suspect that the compounds could inhibit Cas13d as well. Cas13b, on the other hand, is quite different in both protein and crRNA structure, and we do not know if these nine inhibitors would function in the same way.

In conclusion, using a fluorescent based assay we high throughput screened 13120 chemical compounds. From these compounds we identified nine compounds that reliably inhibit LwaCas13a *in vitro*.

---

<sup>1</sup> <https://www.cytivalifesciences.com/en/us/solutions/protein-research/knowledge-center/surface-plasmon-resonance/surface-plasmon-resonance>

## References

- Ablain, J., & Zon, L. I. (2016). Tissue-specific gene targeting using CRISPR/Cas9. *Methods in Cell Biology*, 189–202. <https://doi.org/10.1016/bs.mcb.2016.03.004>
- Abudayyeh, O. O., Gootenberg, J. S., Konermann, S., Joung, J., Slaymaker, I. M., Cox, D. B. T., Shmakov, S., Makarova, K. S., Semenova, E., Minakhin, L., Severinov, K., Regev, A., Lander, E. S., Koonin, E. V., & Zhang, F. (2016). C2C2 is a single-component programmable RNA-guided RNA-targeting CRISPR effector. <https://doi.org/10.1101/054742>
- Abudayyeh, O. O., Gootenberg, J. S., Essletzbichler, P., Han, S., Joung, J., Belanto, J. J., Verdine, V., Cox, D. B., Kellner, M. J., Regev, A., Lander, E. S., Voytas, D. F., Ting, A. Y., & Zhang, F. (2017). RNA targeting with CRISPR–Cas13. *Nature*, 550(7675), 280–284. <https://doi.org/10.1038/nature24049>
- Abudayyeh, O. O., Gootenberg, J. S., Franklin, B., Koob, J., Kellner, M. J., Ladha, A., Joung, J., Kirchgatterer, P., Cox, D. B., & Zhang, F. (2019). A cytosine deaminase for programmable single-base RNA editing. *Science*, 365(6451), 382–386. <https://doi.org/10.1126/science.aax7063>
- Aman, R., Ali, Z., Butt, H., Mahas, A., Aljedaani, F., Khan, M. Z., Ding, S., & Mahfouz, M. (2018). RNA virus interference via CRISPR/Cas13a system in plants. *Genome Biology*, 19(1). <https://doi.org/10.1186/s13059-017-1381-1>
- Anantharaman, V., Makarova, K. S., Burroughs, A. M., Koonin, E. V., & Aravind, L. (2013). Comprehensive analysis of the HEPN superfamily: identification of novel roles in intra-genomic conflicts, defense, pathogenesis and RNA processing. *Biology Direct*, 8(1). <https://doi.org/10.1186/1745-6150-8-15>
- Buchman, A. B., Brogan, D. J., Sun, R., Yang, T., Hsu, P. D., & Akbari, O. S. (2020). Programmable RNA targeting using CasRx in flies. *The CRISPR Journal*, 3(3), 164–176. <https://doi.org/10.1089/crispr.2020.0018>
- Chen, J. S., Ma, E., Harrington, L. B., Tian, X., & Doudna, J. A. (2017). CRISPR-Cas12a target binding unleashes single-stranded DNase activity. <https://doi.org/10.1101/226993>
- Cheng, R., Peng, J., Yan, Y., Cao, P., Wang, J., Qiu, C., Tang, L., Liu, D., Tang, L., Jin, J., Huang, X., He, F., & Zhang, P. (2014). Efficient gene editing in adult mouse livers via adenoviral delivery of CRISPR/Cas9. *FEBS Letters*, 588(21), 3954–3958. <https://doi.org/10.1016/j.febslet.2014.09.008>
- Cong, L., Ran, F. A., Cox, D., Lin, S., Barretto, R., Habib, N., Hsu, P. D., Wu, X., Jiang, W., Marraffini, L. A., & Zhang, F. (2013). Multiplex Genome Engineering using CRISPR/Cas Systems. *Science*, 339(6121), 819–823. <https://doi.org/10.1126/science.1231143>
- Cox, D. B., Gootenberg, J. S., Abudayyeh, O. O., Franklin, B., Kellner, M. J., Joung, J., & Zhang, F. (2017). RNA editing with CRISPR-Cas13. *Science*, 358(6366), 1019–1027. <https://doi.org/10.1126/science.aaq0180>

- Cui, L., Vigouroux, A., Rousset, F., Varet, H., Khanna, V., & Bikard, D. (2018). A CRISPRi screen in *E. coli* reveals sequence-specific toxicity of dCas9. *Nature Communications*, 9(1). <https://doi.org/10.1038/s41467-018-04209-5>
- Cullot, G., Boutin, J., Toutain, J., Prat, F., Pennamen, P., Rooryck, C., Teichmann, M., Rousseau, E., Lamrissi-Garcia, I., Guyonnet-Duperat, V., Bibeyran, A., Lalanne, M., Prouzet-Mauléon, V., Turcq, B., Ged, C., Blouin, J.-M., Richard, E., Dabernat, S., Moreau-Gaudry, F., & Bedel, A. (2019). CRISPR-Cas9 genome editing induces megabase-scale chromosomal truncations. *Nature Communications*, 10(1). <https://doi.org/10.1038/s41467-019-09006-2>
- Dever, D. P., Bak, R. O., Reinisch, A., Camarena, J., Washington, G., Nicolas, C. E., Pavel-Dinu, M., Saxena, N., Wilkens, A. B., Mantri, S., Uchida, N., Hendel, A., Narla, A., Majeti, R., Weinberg, K. I., & Porteus, M. H. (2016). CRISPR/Cas9  $\beta$ -globin gene targeting in human haematopoietic stem cells. *Nature*, 539(7629), 384–389. <https://doi.org/10.1038/nature20134>
- East-Seletsky, A., O'Connell, M. R., Knight, S. C., Burstein, D., Cate, J. H., Tjian, R., & Doudna, J. A. (2016). Two distinct RNase activities of CRISPR-C2c2 enable guide-RNA processing and RNA detection. *Nature*, 538(7624), 270–273. <https://doi.org/10.1038/nature19802>
- Fan, J., Liu, Y., Liu, L., Huang, Y., Li, X., & Huang, W. (2019). A multifunction lipid-based CRISPR-Cas13a genetic circuit delivery system for bladder cancer gene therapy. *ACS Synthetic Biology*, 9(2), 343–355. <https://doi.org/10.1021/acssynbio.9b00349>
- Fire, A., Xu, S. Q., Montgomery, M. K., Kostas, S. A., Driver, S. E., & Mello, C. C. (1998). Potent and specific genetic interference by double-stranded RNA in *Caenorhabditis elegans*. *Nature*, 391(6669), 806–811. <https://doi.org/10.1038/35888>
- Fozouni, P., Son, S., Díaz de León Derby, M., Knott, G. J., Gray, C. N., D'Ambrosio, M. V., Zhao, C., Switz, N. A., Kumar, G. R., Stephens, S. I., Boehm, D., Tsou, C.-L., Shu, J., Bhuiya, A., Armstrong, M., Harris, A. R., Chen, P.-Y., Osterloh, J. M., Meyer-Franke, A., ... Ott, M. (2021). Amplification-free detection of SARS-CoV-2 with CRISPR-Cas13a and mobile phone microscopy. *Cell*, 184(2). <https://doi.org/10.1016/j.cell.2020.12.001>
- Fu, Y., Foden, J. A., Khayter, C., Maeder, M. L., Reyon, D., Joung, J. K., & Sander, J. D. (2013). High-frequency off-target mutagenesis induced by CRISPR-Cas nucleases in human cells. *Nature Biotechnology*, 31(9), 822–826. <https://doi.org/10.1038/nbt.2623>
- Gasiunas, G., Barrangou, R., Horvath, P., & Siksnys, V. (2012). Cas9-crRNA ribonucleoprotein complex mediates specific DNA cleavage for adaptive immunity in bacteria. *Proceedings of the National Academy of Sciences*, 109(39). <https://doi.org/10.1073/pnas.1208507109>
- Gootenberg, J. S., Abudayyeh, O. O., Lee, J. W., Essletzbichler, P., Dy, A. J., Joung, J., Verdine, V., Donghia, N., Daringer, N. M., Freije, C. A., Myhrvold, C., Bhattacharyya, R. P., Livny, J., Regev, A., Koonin, E. V., Hung, D. T., Sabeti, P. C., Collins, J. J., & Zhang, F. (2017). Nucleic acid detection with CRISPR-Cas13a/C2c2. *Science*, 356(6336), 438–442. <https://doi.org/10.1126/science.aam9321>
- Gootenberg, J. S., Abudayyeh, O. O., Kellner, M. J., Joung, J., Collins, J. J., & Zhang, F. (2018). Multiplexed and portable nucleic acid detection platform with Cas13, Cas12a, and Csm6. *Science*, 360(6387), 439–444. <https://doi.org/10.1126/science.aaq0179>

- Goyal, A., Myacheva, K., Groß, M., Klingenberg, M., Duran Arqué, B., & Diederichs, S. (2016). Challenges of CRISPR/Cas9 applications for long non-coding RNA genes. *Nucleic Acids Research*. <https://doi.org/10.1093/nar/gkw883>
- Gratz, S. J., Cummings, A. M., Nguyen, J. N., Hamm, D. C., Donohue, L. K., Harrison, M. M., Wildonger, J., & O'Connor-Giles, K. M. (2013). Genome engineering of drosophila with the CRISPR RNA-guided Cas9 nuclease. *Genetics*, *194*(4), 1029–1035. <https://doi.org/10.1534/genetics.113.152710>
- Guan, Y., Ma, Y., Li, Q., Sun, Z., Ma, L., Wu, L., Wang, L., Zeng, L., Shao, Y., Chen, Y., Ma, N., Lu, W., Hu, K., Han, H., Yu, Y., Huang, Y., Liu, M., & Li, D. (2016). CRISPR /Cas9-mediated somatic correction of a novel coagulator factor IX gene mutation ameliorates hemophilia in mouse. *EMBO Molecular Medicine*, *8*(5), 477–488. <https://doi.org/10.15252/emmm.201506039>
- Gutierrez, P. L. (2000). The metabolism of quinone-containing alkylating agents: Free radical production and measurement. *Frontiers in Bioscience*, *5*(1), d629. <https://doi.org/10.2741/gutier>
- Himeda, C. L., Jones, T. I., & Jones, P. L. (2016). Scalpel or straitjacket: CRISPR/Cas9 approaches for muscular dystrophies. *Trends in Pharmacological Sciences*, *37*(4), 249–251. <https://doi.org/10.1016/j.tips.2016.02.001>
- Idnurm, A., & Meyer, V. (2018). The CRISPR revolution in fungal biology and biotechnology, and beyond. *Fungal Biology and Biotechnology*, *5*(1). <https://doi.org/10.1186/s40694-018-0064-3>
- Ishino, Y., Shinagawa, H., Makino, K., Amemura, M., & Nakata, A. (1987). Nucleotide sequence of the IAP gene, responsible for alkaline phosphatase isozyme conversion in *Escherichia coli*, and identification of the gene product. *Journal of Bacteriology*, *169*(12), 5429–5433. <https://doi.org/10.1128/jb.169.12.5429-5433.1987>
- Iwasaki, R. S., & Batey, R. T. (2020). Sprint: A Cas13a-based platform for detection of small molecules. *Nucleic Acids Research*, *48*(17). <https://doi.org/10.1093/nar/gkaa673>
- Jackson, A. L., Bartz, S. R., Schelter, J., Kobayashi, S. V., Burchard, J., Mao, M., Li, B., Cavet, G., & Linsley, P. S. (2003). Expression profiling reveals off-target gene regulation by RNAi. *Nature Biotechnology*, *21*(6), 635–637. <https://doi.org/10.1038/nbt831>
- Jackson, A. L. (2006). Widespread siRNA "off-target" transcript silencing mediated by seed region sequence complementarity. *RNA*, *12*(7), 1179–1187. <https://doi.org/10.1261/rna.25706>
- Jansen, R., van Embden, J. D. A., Gaastra, W., & Schouls, L. M. (2002a). Identification of a novel family of sequence repeats among prokaryotes. *OMICS: A Journal of Integrative Biology*, *6*(1), 23–33. <https://doi.org/10.1089/15362310252780816>
- Jansen, R., Embden, J. D., Gaastra, W., & Schouls, L. M. (2002b). Identification of genes that are associated with DNA repeats in prokaryotes. *Molecular Microbiology*, *43*(6), 1565–1575. <https://doi.org/10.1046/j.1365-2958.2002.02839.x>

- Jiang, F., Zhou, K., Ma, L., Gressel, S., & Doudna, J. A. (2015). A Cas9-guide RNA complex preorganized for target DNA recognition. *Science*, 348(6242), 1477–1481. <https://doi.org/10.1126/science.aab1452>
- Jinek, M., Chylinski, K., Fonfara, I., Hauer, M., Doudna, J. A., & Charpentier, E. (2012). A programmable dual-RNA-guided DNA endonuclease in adaptive bacterial immunity. *Science*, 337(6096), 816–821. <https://doi.org/10.1126/science.1225829>
- Jing, X., Xie, B., Chen, L., Zhang, N., Jiang, Y., Qin, H., Wang, H., Hao, P., Yang, S., & Li, X. (2018). Implementation of the CRISPR-Cas13a system in fission yeast and its repurposing for precise RNA editing. *Nucleic Acids Research*, 46(15). <https://doi.org/10.1093/nar/gky433>
- Johnston, P. A. (2011). Redox cycling compounds generate H<sub>2</sub>O<sub>2</sub> in HTS buffers containing strong reducing reagents—real hits or promiscuous artifacts? *Current Opinion in Chemical Biology*, 15(1), 174–182. <https://doi.org/10.1016/j.cbpa.2010.10.022>
- Konermann, S., Lotfy, P., Brideau, N. J., Oki, J., Shokhirev, M. N., & Hsu, P. D. (2018). Transcriptome engineering with RNA-targeting type VI-D CRISPR effectors. *Cell*, 173(3). <https://doi.org/10.1016/j.cell.2018.02.033>
- Kulkarni, A., Yu, W., Moon, A., Pandey, A., Hanley, K. A., & Xu, J. (2020). Programmable CRISPR interference for gene silencing using Cas13a in mosquitoes. *Journal of Genomics*, 8, 30–36. <https://doi.org/10.7150/jgen.43928>
- Kushawah, G., Abugattas-Nuñez del Prado, J., Martinez-Morales, J. R., DeVore, M., Guelfo, J. R., Brannan, E. O., Wang, W., Corbin, T. J., Moran, A. M., Alvarado, A. S., Málaga-Trillo, E., Takacs, C. M., Bazzini, A. A., & Moreno-Mateos, M. A. (2020). CRISPR-Cas13d induces efficient mRNA knock-down in animal embryos. <https://doi.org/10.1101/2020.01.13.904763>
- Larson, M. H., Gilbert, L. A., Wang, X., Lim, W. A., Weissman, J. S., & Qi, L. S. (2013). CRISPR interference (CRISPRi) for sequence-specific control of gene expression. *Nature Protocols*, 8(11), 2180–2196. <https://doi.org/10.1038/nprot.2013.132>
- Ledford, H. (2015). CRISPR, the disruptor. *Nature*, 522(7554), 20–24. <https://doi.org/10.1038/522020a>
- Li, J., Chen, Z., Chen, F., Xie, G., Ling, Y., Peng, Y., Lin, Y., Luo, N., Chiang, C.-M., & Wang, H. (2020). Targeted mRNA demethylation using an engineered dCas13b-ALKBH5 fusion protein. *Nucleic Acids Research*, 48(10), 5684–5694. <https://doi.org/10.1093/nar/gkaa269>
- Li, Y., & Peng, N. (2019). Endogenous CRISPR-Cas system-based genome editing and antimicrobials: Review and prospects. *Frontiers in Microbiology*, 10. <https://doi.org/10.3389/fmicb.2019.02471>
- Lin, P., Qin, S., Pu, Q., Wang, Z., Wu, Q., Gao, P., Schettler, J., Guo, K., Li, R., Li, G., Huang, C., Wei, Y., Gao, G. F., Jiang, J., & Wu, M. (2020). CRISPR-Cas13 inhibitors block RNA editing in bacteria and mammalian cells. *Molecular Cell*, 78(5). <https://doi.org/10.1016/j.molcel.2020.03.033>

- Liu, L., Li, X., Wang, J., Wang, M., Chen, P., Yin, M., Li, J., Sheng, G., & Wang, Y. (2017a). Two distant catalytic sites are responsible for C2c2 RNase activities. *Cell*, 168(1-2). <https://doi.org/10.1016/j.cell.2016.12.031>
- Liu, L., Li, X., Ma, J., Li, Z., You, L., Wang, J., Wang, M., Zhang, X., & Wang, Y. (2017b). The molecular architecture for RNA-guided RNA cleavage by Cas13a. *Cell*, 170(4). <https://doi.org/10.1016/j.cell.2017.06.050>
- Liu, Q., Zheng, J., Sun, W., Huo, Y., Zhang, L., Hao, P., Wang, H., & Zhuang, M. (2018). A proximity-tagging system to identify membrane protein–protein interactions. *Nature Methods*, 15(9), 715–722. <https://doi.org/10.1038/s41592-018-0100-5>
- Ma, Z., Zhu, P., Shi, H., Guo, L., Zhang, Q., Chen, Y., Chen, S., Zhang, Z., Peng, J., & Chen, J. (2019). PTC-bearing mRNA elicits a genetic compensation response via UPF3A and COMPASS components. *Nature*, 568(7751), 259–263. <https://doi.org/10.1038/s41586-019-1057-y>
- Maji, B., Gangopadhyay, S. A., Lee, M., Shi, M., Wu, P., Heler, R., Mok, B., Lim, D., Siriwardena, S. U., Paul, B., Dančík, V., Vetere, A., Mesleh, M. F., Marraffini, L. A., Liu, D. R., Clemons, P. A., Wagner, B. K., & Choudhary, A. (2019). A high-throughput platform to identify small-molecule inhibitors of CRISPR-Cas9. *Cell*, 177(4). <https://doi.org/10.1016/j.cell.2019.04.009>
- Makarova, K. S., Wolf, Y. I., & Koonin, E. V. (2018). Classification and nomenclature of CRISPR-Cas Systems: Where from here? *The CRISPR Journal*, 1(5), 325–336. <https://doi.org/10.1089/crispr.2018.0033>
- Mali, P., Yang, L., Esvelt, K. M., Aach, J., Guell, M., DiCarlo, J. E., Norville, J. E., & Church, G. M. (2013). RNA-guided human genome engineering via Cas9. *Science*, 339(6121), 823–826. <https://doi.org/10.1126/science.1232033>
- Manguso, R. T., Pope, H. W., Zimmer, M. D., Brown, F. D., Yates, K. B., Miller, B. C., Collins, N. B., Bi, K., LaFleur, M. W., Juneja, V. R., Weiss, S. A., Lo, J., Fisher, D. E., Miao, D., Van Allen, E., Root, D. E., Sharpe, A. H., Doench, J. G., & Haining, W. N. (2017). *In vivo* CRISPR screening identifies *Ptpn2* as a cancer immunotherapy target. *Nature*, 547(7664), 413–418. <https://doi.org/10.1038/nature23270>
- Marino, N. D., Zhang, J. Y., Borges, A. L., Sousa, A. A., Leon, L. M., Rauch, B. J., Walton, R. T., Berry, J. D., Joung, J. K., Kleinstiver, B. P., & Bondy-Denomy, J. (2018). Discovery of widespread type I and type V CRISPR-Cas inhibitors. *Science*, 362(6411), 240–242. <https://doi.org/10.1126/science.aau5174>
- Marraffini, L. A., & Sontheimer, E. J. (2010). Self versus non-self discrimination during CRISPR RNA-directed immunity. *Nature*, 463(7280), 568–571. <https://doi.org/10.1038/nature08703>
- Meeske, A. J., & Marraffini, L. A. (2018). RNA guide complementarity prevents self-targeting in type VI CRISPR systems. *Molecular Cell*, 71(5). <https://doi.org/10.1016/j.molcel.2018.07.013>
- Meeske, A. J., Johnson, M. C., Hille, L. T., Kleinstiver, B. P., & Bondy-Denomy, J. (2021). Lack of Cas13a inhibition by anti-CRISPR proteins from *Leptotrichia* prophages. <https://doi.org/10.1101/2021.05.27.445852>

- Mojica, F. J., Díez-Villasenor, C., Soria, E., & Juez, G. (2000). Biological significance of a family of regularly spaced repeats in the genomes of archaea, bacteria and mitochondria. *Molecular Microbiology*, 36(1), 244–246. <https://doi.org/10.1046/j.1365-2958.2000.01838.x>
- Mojica, F. J. M., Díez-Villaseñor, C., García-Martínez, J., & Soria, E. (2005). Intervening sequences of regularly spaced prokaryotic repeats derive from foreign genetic elements. *Journal of Molecular Evolution*, 60(2), 174–182. <https://doi.org/10.1007/s00239-004-0046-3>
- Mojica, F. J., & Rodríguez-Valera, F. (2016). The discovery of CRISPR in archaea and bacteria. *The FEBS Journal*, 283(17), 3162–3169. <https://doi.org/10.1111/febs.13766>
- Nath, A. (2007, December). *Michaelis-Menten kinetics and Briggs-Haldane Kinetics*. A Quick Guide to Enzyme Kinetics & Simulations. <https://depts.washington.edu/wmatkins/kinetics/michaelis-menten.html>.
- Nishikura, K. (2010). Functions and regulation of RNA editing by ADAR deaminases. *Annual Review of Biochemistry*, 79(1), 321–349. <https://doi.org/10.1146/annurev-biochem-060208-105251>
- O'Connell, M. R. (2019). Molecular mechanisms of RNA targeting by Cas13-containing type VI CRISPR–Cas Systems. *Journal of Molecular Biology*, 431(1), 66–87. <https://doi.org/10.1016/j.jmb.2018.06.029>
- Ortiz-Alcantara, J., Bhardwaj, K., Palaninathan, S., Frieman, M., Baric, R., & Kao, C. (2010). Small molecule inhibitors of the SARS-CoV Nsp15 endoribonuclease. *Virus Adaptation and Treatment*, 125–133. <https://doi.org/10.2147/vaat.s12733>
- Palaz, F., Kalkan, A. K., Can, Ö., Demir, A. N., Tozluyurt, A., Özcan, A., & Ozsoz, M. (2021). CRISPR-Cas13 system as a promising and versatile tool for cancer diagnosis, therapy, and research. *ACS Synthetic Biology*. <https://doi.org/10.1021/acssynbio.1c00107>
- Qi, L. S., Larson, M. H., Gilbert, L. A., Doudna, J. A., Weissman, J. S., Arkin, A. P., & Lim, W. A. (2013). Repurposing CRISPR as an RNA-guided platform for sequence-specific control of gene expression. *Cell*, 152(5), 1173–1183. <https://doi.org/10.1016/j.cell.2013.02.022>
- Rauch, B. J., Silvis, M. R., Hultquist, J. F., Waters, C. S., McGregor, M. J., Krogan, N. J., & Bondy-Denomy, J. (2017). Inhibition of CRISPR-Cas9 with bacteriophage proteins. *Cell*, 168(1-2). <https://doi.org/10.1016/j.cell.2016.12.009>
- Shan, Y., Zhou, X., Huang, R., & Xing, D. (2019). High-fidelity and rapid quantification of miRNA combining crRNA programmability and CRISPR/Cas13a trans-cleavage activity. *Analytical Chemistry*, 91(8), 5278–5285. <https://doi.org/10.1021/acs.analchem.9b00073>
- Shmakov, S., Abudayyeh, O. O., Makarova, K. S., Wolf, Y. I., Gootenberg, J. S., Semenova, E., Minakhin, L., Joung, J., Konermann, S., Severinov, K., Zhang, F., & Koonin, E. V. (2015). Discovery and functional characterization of diverse class 2 CRISPR-Cas Systems. *Molecular Cell*, 60(3), 385–397. <https://doi.org/10.1016/j.molcel.2015.10.008>

- Shmakov, S., Smargon, A., Scott, D., Cox, D., Pyzocha, N., Yan, W., Abudayyeh, O. O., Gootenberg, J. S., Makarova, K. S., Wolf, Y. I., Severinov, K., Zhang, F., & Koonin, E. V. (2017). Diversity and evolution of class 2 CRISPR–Cas Systems. *Nature Reviews Microbiology*, 15(3), 169–182. <https://doi.org/10.1038/nrmicro.2016.184>
- Smargon, A. A., Cox, D. B. T., Pyzocha, N. K., Zheng, K., Slaymaker, I. M., Gootenberg, J. S., Abudayyeh, O. A., Essletzbichler, P., Shmakov, S., Makarova, K. S., Koonin, E. V., & Zhang, F. (2017). Cas13b is a type VI-B CRISPR-associated RNA-guided RNase differentially regulated by accessory proteins Csx27 and Csx28. *Molecular Cell*, 65(4). <https://doi.org/10.1016/j.molcel.2016.12.023>
- Srivastava, V. K., & Yadav R. (2019). Chapter 9 – Isothermal titration calorimetry. In G. Misra (Eds.), *Data Processing Handbook for Complex Biological Data Sources* (pp. 125-137). Academic Press. doi: 10.1016/B978-0-12-816548-5.00009-5.
- Stewart, M. P., Langer, R., & Jensen, K. F. (2018). Intracellular delivery by membrane disruption: mechanisms, strategies, and concepts. *Chemical Reviews*, 118(16), 7409–7531. <https://doi.org/10.1021/acs.chemrev.7b00678>
- Strelow, J., Dewe, W., Iversen, P.W., Brooks H.B., Radding, J.A., McGee J., & Weidner, J. (2012, May 1) [Updated 2012 Oct 1]. Mechanism of Action Assays for Enzymes. In S. Markossian, A. Grossman, K. Brimacombe, M. Arkin, D. Auld, C.P. Austin, J. Baell, T.D.Y. Chung, N.P. Coussens, J.L. Dahlin, V. Devanarayan, T.L. Foley, M. Glicksman, M.D. Hall, J.V. Haas, S.R.J. Hoare, J. Inglese, P.W. Iversen, S.C. Kales, M. Lal-Nag, Z. Li, J. McGee, O. McManus, T. Riss, P. Saradjian, & Sittampala. (Eds.), *Assay Guidance Manual [Internet]*. Bethesda (MD): Eli Lilly & Company and the National Center for Advancing Translational Sciences; 2004-. Available from: <https://www.ncbi.nlm.nih.gov/books/NBK92001/>
- Takeuchi, N., Wolf, Y. I., Makarova, K. S., & Koonin, E. V. (2012). Nature and intensity of selection pressure on CRISPR-associated genes. *Journal of Bacteriology*, 194(5), 1216–1225. <https://doi.org/10.1128/jb.06521-11>
- Tang, Y., & Fu, Y. (2018). Class 2 CRISPR/Cas: An expanding biotechnology toolbox for and beyond genome editing. *Cell & Bioscience*, 8(1). <https://doi.org/10.1186/s13578-018-0255-x>
- Toledo, C. M., Ding, Y., Hoellerbauer, P., Davis, R. J., Basom, R., Girard, E. J., Lee, E., Corrin, P., Hart, T., Bolouri, H., Davison, J., Zhang, Q., Hardcastle, J., Aronow, B. J., Plaisier, C. L., Baliga, N. S., Moffat, J., Lin, Q., Li, X.-N., ... Paddison, P. J. (2015). Genome-wide CRISPR-Cas9 screens reveal loss of redundancy between PKMYT1 and WEE1 in Glioblastoma stem-like cells. *Cell Reports*, 13(11), 2425–2439. <https://doi.org/10.1016/j.celrep.2015.11.021>
- Wang, Q., Liu, X., Zhou, J., Yang, C., Wang, G., Tan, Y., Wu, Y., Zhang, S., Yi, K., & Kang, C. (2019). The CRISPR-Cas13a gene-editing system induces collateral cleavage of RNA in glioma cells. *Advanced Science*, 6(20), 1901299. <https://doi.org/10.1002/advs.201901299>
- Watters, K. E., Fellmann, C., Bai, H. B., Ren, S. M., & Doudna, J. A. (2018). Systematic discovery of natural CRISPR-Cas12a inhibitors. *Science*, 362(6411), 236–239. <https://doi.org/10.1126/science.aau5138>

- Wright, A. V., Nuñez, J. K., & Doudna, J. A. (2016). Biology and Applications of CRISPR systems: Harnessing Nature's Toolbox for Genome Engineering. *Cell*, *164*(1-2), 29–44. <https://doi.org/10.1016/j.cell.2015.12.035>
- Xu, C., Zhou, Y., Xiao, Q., He, B., Geng, G., Wang, Z., Cao, B., Dong, X., Bai, W., Wang, Y., Wang, X., Zhou, D., Yuan, T., Huo, X., Lai, J., & Yang, H. (2021). Programmable RNA editing with compact CRISPR–Cas13 systems from uncultivated microbes. *Nature Methods*, *18*(5), 499–506. <https://doi.org/10.1038/s41592-021-01124-4>
- Yan, W. X., Chong, S., Zhang, H., Makarova, K. S., Koonin, E. V., Cheng, D. R., & Scott, D. A. (2018). Cas13s is a compact RNA-targeting type VI CRISPR effector positively modulated by a WYL-domain-containing accessory protein. *Molecular Cell*, *70*(2). <https://doi.org/10.1016/j.molcel.2018.02.028>
- Yang, L.-Z., Wang, Y., Li, S.-Q., Yao, R.-W., Luan, P.-F., Wu, H., Carmichael, G. G., & Chen, L.-L. (2019). Dynamic imaging of RNA in living cells by CRISPR-Cas13 Systems. *Molecular Cell*, *76*(6). <https://doi.org/10.1016/j.molcel.2019.10.024>
- Yosef, I., Goren, M. G., & Qimron, U. (2012). Proteins and DNA elements essential for the CRISPR adaptation process in *Escherichia coli*. *Nucleic Acids Research*, *40*(12), 5569–5576. <https://doi.org/10.1093/nar/gks216>
- Zetsche, B., Gootenberg, J. S., Abudayyeh, O. O., Slaymaker, I. M., Makarova, K. S., Essletzbichler, P., Volz, S. E., Joung, J., van der Oost, J., Regev, A., Koonin, E. V., & Zhang, F. (2015). Cpf1 is a single RNA-guided endonuclease of a class 2 CRISPR-Cas System. *Cell*, *163*(3), 759–771. <https://doi.org/10.1016/j.cell.2015.09.038>
- Zhang, B., Ye, W., Ye, Y., Zhou, H., Saeed, A. F., Chen, J., Lin, J., Perčulija, V., Chen, Q., Chen, C.-J., Chang, M.-X., Choudhary, M. I., & Ouyang, S. (2018). Structural insights into Cas13b-guided CRISPR RNA maturation and recognition. *Cell Research*, *28*(12), 1198–1201. <https://doi.org/10.1038/s41422-018-0109-4>
- Zhang, B., Ye, Y., Ye, W., Perčulija, V., Jiang, H., Chen, Y., Li, Y., Chen, J., Lin, J., Wang, S., Chen, Q., Han, Y.-S., & Ouyang, S. (2019). Two HEPN domains dictate CRISPR RNA maturation and target cleavage in Cas13d. *Nature Communications*, *10*(1). <https://doi.org/10.1038/s41467-019-10507-3>
- Zhang, C., Konermann, S., Brideau, N. J., Lotfy, P., Wu, X., Novick, S. J., Strutzenberg, T., Griffin, P. R., Hsu, P. D., & Lyumkis, D. (2018). Structural basis for the RNA-guided ribonuclease activity of CRISPR-Cas13d. *Cell*, *175*(1). <https://doi.org/10.1016/j.cell.2018.09.001>
- Zhang, Z., Sun, W., Shi, T., Lu, P., Zhuang, M., & Liu, J.-L. (2020). Capturing RNA–protein interaction via CRUIS. *Nucleic Acids Research*, *48*(9). <https://doi.org/10.1093/nar/gkaa143>
- Zhou, C., Hu, X., Tang, C., Liu, W., Wang, S., Zhou, Y., Zhao, Q., Bo, Q., Shi, L., Sun, X., Zhou, H., & Yang, H. (2020). CasRx-mediated RNA targeting prevents choroidal neovascularization in a mouse model of age-related macular degeneration. <https://doi.org/10.1101/2020.02.18.955286>

Zhou, H., Su, J., Hu, X., Zhou, C., Li, H., Chen, Z., Xiao, Q., Wang, B., Wu, W., Sun, Y., Zhou, Y., Tang, C., Liu, F., Wang, L., Feng, C., Liu, M., Li, S., Zhang, Y., Xu, H., ... Yang, H. (2020). Glia-to-neuron conversion by CRISPR-CasRx alleviates symptoms of neurological disease in mice. *Cell*, 181(3). <https://doi.org/10.1016/j.cell.2020.03.024>

Zhou, M., Diwu, Z., Panchuk-Voloshina, N., & Haugland, R. P. (1997). A stable nonfluorescent derivative of resorufin for the fluorometric determination of trace hydrogen peroxide: applications in detecting the activity of phagocyte NADPH oxidase and other oxidases. *Analytical Biochemistry*, 253(2), 162–168. <https://doi.org/10.1006/abio.1997.2391>

## Supplementary Figures

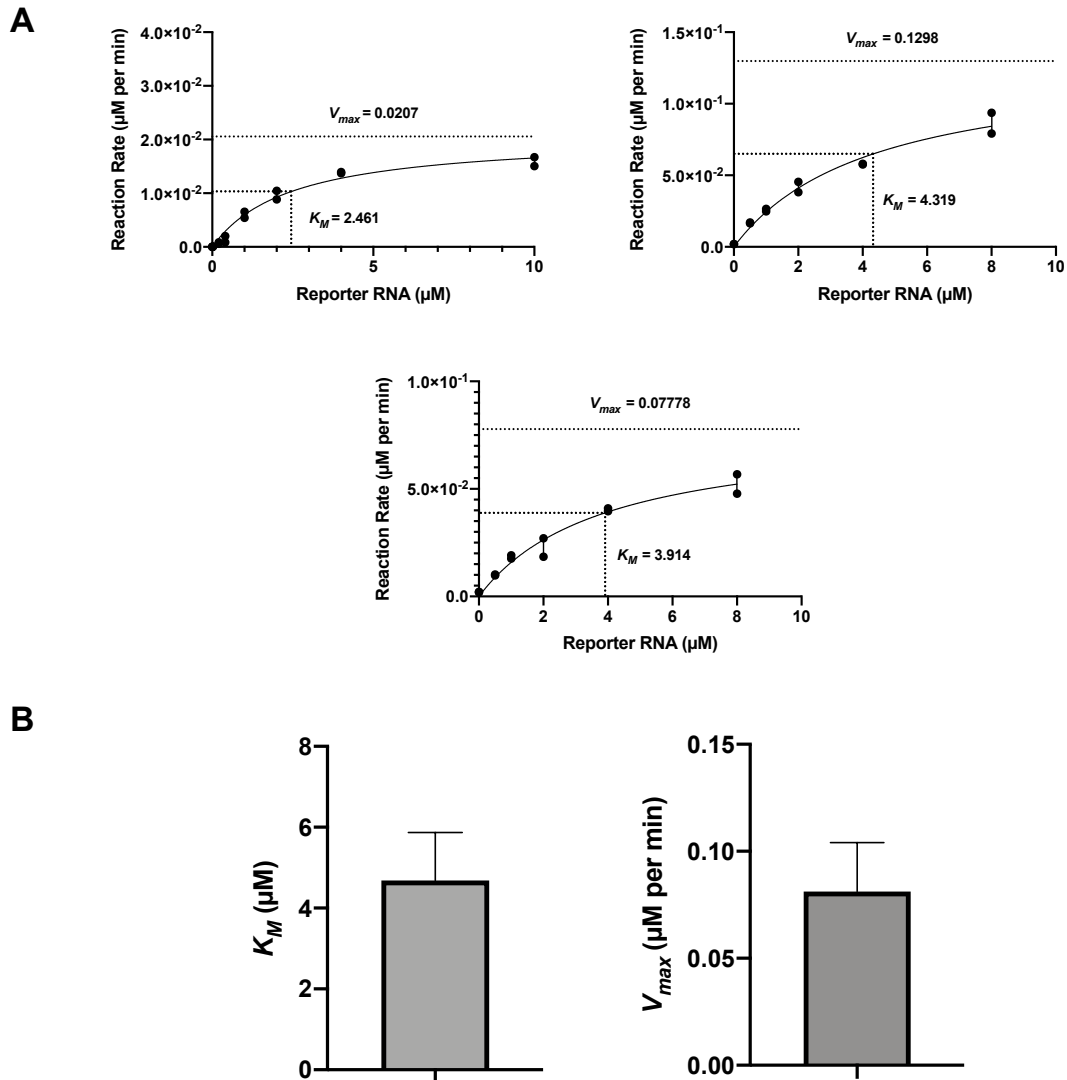
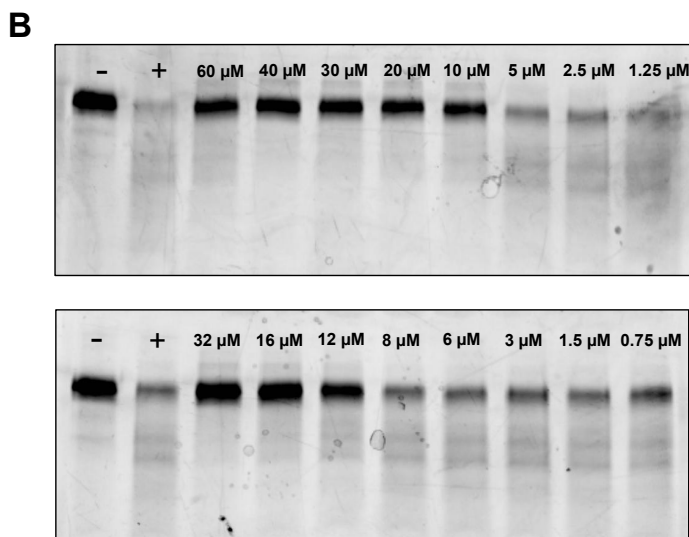
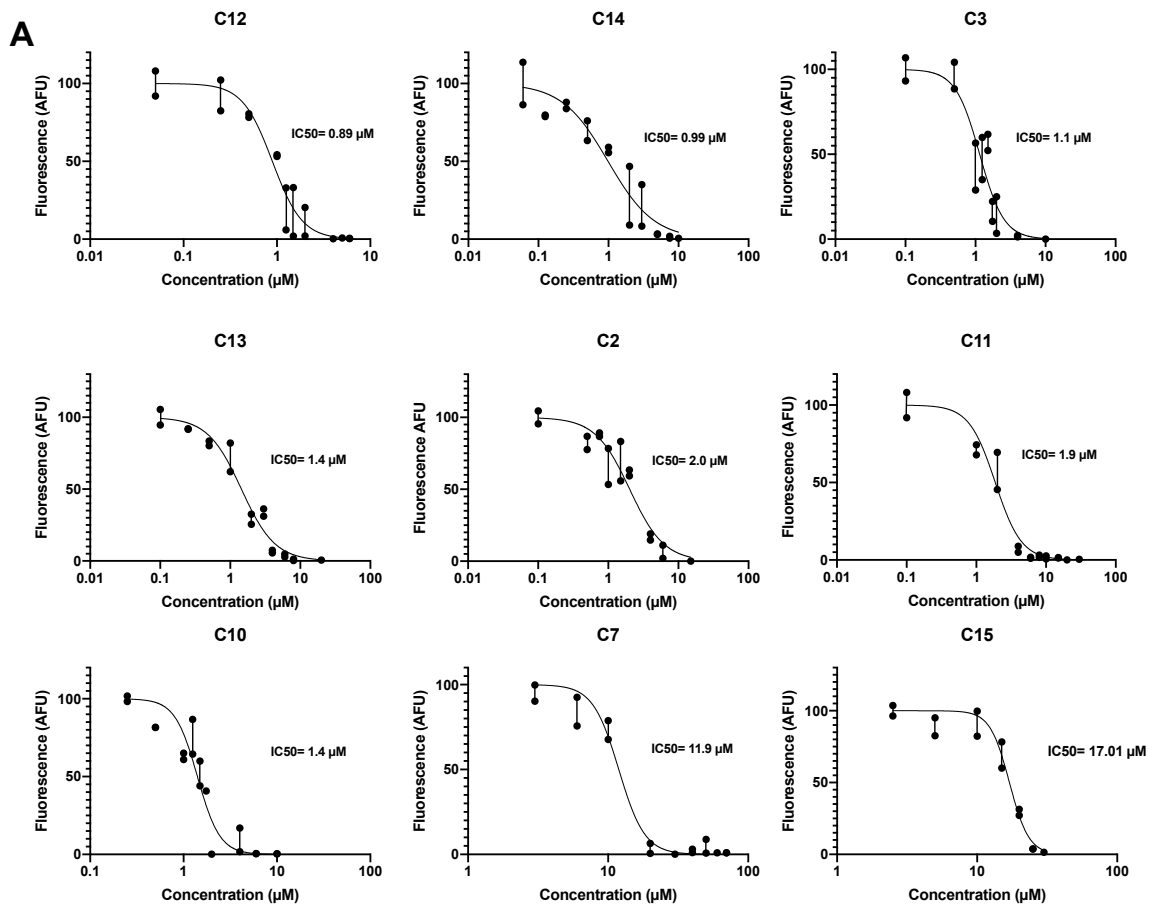


**Figure S1: Additional Michaelis-Menten Curve Replicates and Summary of Results. A)** Additional replicates used to determine the  $K_M$  and  $V_{max}$  of Cas13. Cas13's  $K_M$  ranged from 2  $\mu\text{M}$  to 8  $\mu\text{M}$ , and  $V_{max}$  ranged from 0.02  $\mu\text{M/min}$  to 0.13  $\mu\text{M/min}$  with the PolyU substrate. Both technical replicates are shown on the curve. **B)** Summary of  $K_M$  and  $V_{max}$  values obtained for Cas13a. Average  $K_M$  of 4.68  $\mu\text{M}$ , and average  $V_{max}$  of 0.081  $\mu\text{M/min}$ . Results represented as mean with  $\pm$  SEM (Standard Error of the Mean)  $n=4$ .



**C3 IC50 Comparison:**

Gel Cleavage- around 7.5  $\mu\text{M}$   
 FAM Assay- around 1.2  $\mu\text{M}$

**C13 IC50 Comparison:**

Gel Cleavage- around 10.0  $\mu\text{M}$   
 FAM Assay- around 1.2  $\mu\text{M}$

**Figure S2: Additional  $\text{IC}_{50}$  Replicates and Gel Cleavage  $\text{IC}_{50}$ s.** A) Final  $\text{IC}_{50}$ s are similar to the ones shown in the main figure. Both technical replicates are shown on the curve. B) Gel cleavage  $\text{IC}_{50}$ s for two compounds (C3 and C13) presented. Using this approach yielded higher  $\text{IC}_{50}$ s than with the FAM assay.

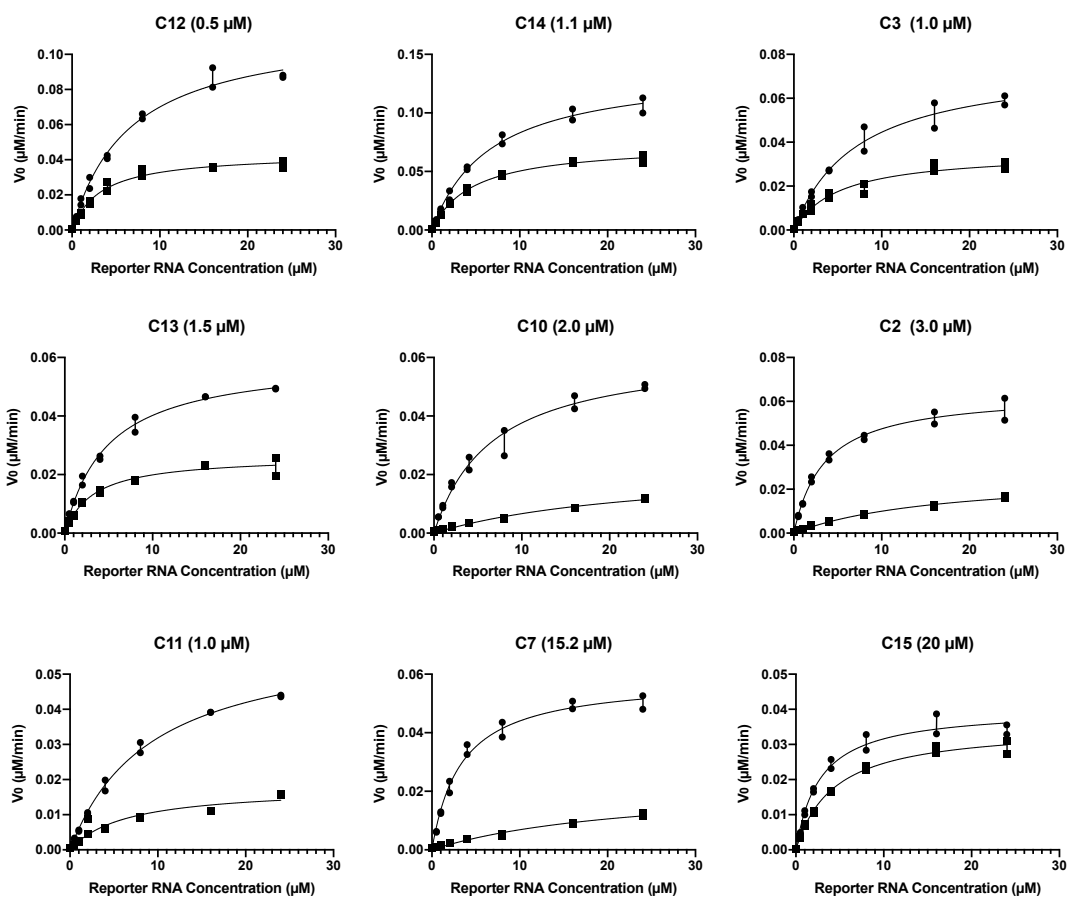


**Figure S3: Additional Mechanism of Inhibition Replicates.** Additional Michaelis-Menten curves used to determine the mechanism of inhibition: graphs are ordered by most effective to least effective. C15 showed minimal inhibition most likely due to poor compound stability at room temperature. Both technical replicates are shown on the curve.

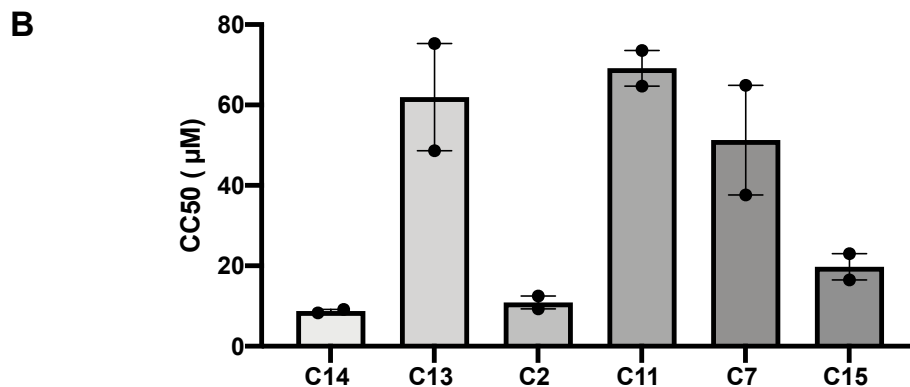
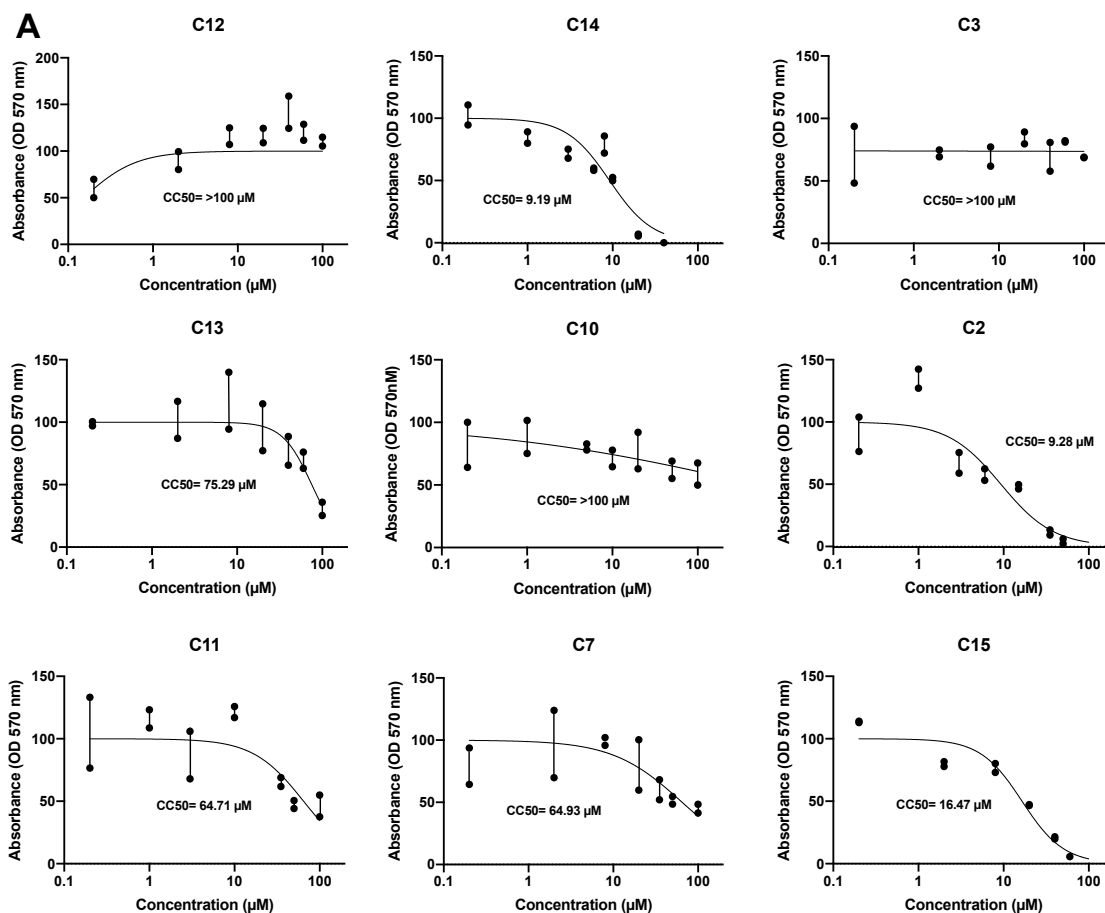


**Figure S4: CC50 Curves and Summary of Results.** A) Compounds C12, C3, and C10 did not demonstrate a typical inhibition curve. Increasing the compound concentration resulted in no or minimal increase in cell death for the aforementioned compounds. Graphs are ordered by most effective to least effective. Both technical replicates are shown on the curve. Future students will perform additional replicates. B) Summary of CC50 values for the Cas13a inhibitors. Compounds C12, C3, and C10 are not shown as CC50 value was greater than 100  $\mu\text{M}$ . Both technical replicates are shown on the graph.

## Tables

**Table S1. DNA Sequences of 6xHis-Cas13a and 6xHis-dCas13a**

Name	Sequence (5' to 3')
Cas13a	catcatcatcatcatcacagcagcggcatgaaagtaccaaggtcgacggcatcagcc acaagaagtacatcgaagagggcaagctcgtgaagtccaccagcgggaaaaccgg accagcgagagactgagcgagctgctgagcatccggctggacatctacatcaagaacc ccgacaacgcctccgaggaagagaaccggatcagaagagagaacctgaagaagttc tttagcaacaaggtgctgcacctgaaggacagcgtgctgtatctgaagaaccggaaaga aaagaacgccgtgcaggacaagaactatagcgaagaggacatcagcgagtacgacc tgaaaaacaagaacagcttctccgtgctgaagaagatcctgctgaacgaggacgtgaa ctctgaggaactggaaatcttccggaaggacgtggaagccaagctgaacaagatcaac agcctgaagtacagcttcaagagaacaaggccaactaccagaagatcaacgagaa caacgtggaaaaagtgggcggaagagcaagcggaaacatcatctacgactactacg agagagcgccaagcgcaacgactacatcaacaacgtgcaggaagccttcgacaagct gtataagaaagaggatcgcgaaactgttttctgatcgagaacagcaagaagcacg agaagtacaagatccgagctactatcacaagatcatcggccggaagaacgacaag agaactcgccaagattatctacgaagagatccagaacgtgaacaacatcaaagagct gattgagaagatccccgacatgtctgagctgaagaaaagccaggtgttctacaagtacta cctggacaaagaggaactgaacgacaagaatattaagtacgccttctgccacttctggtg aatcgagatgtcccagctgctgaaaaactacgtgtacaagcggctgagcaacatcagc aacgataagatcaagcggatcttcgagctaccagaatctgaaaaagctgatcgaaaaca aactgctgaacaagctggacacctacgtgcggaactgcggaagtacaactactatctg caagtgggagatcgccacctccgacttctcgcccggaaccggcagaacgaggcctt cctgagaaacatcatcggcgtgtccagcgtggcctacttcagcctgaggaacatcctgga aaccgagaacgagaacgatcaccggccggatgccccggaagaccgtgaagaac aacaagggcgaagagaaatacgtgtccggcgaggtggacaagatctcaatgagaac aagcagaacgaagtgaagaaaatctgaagatgttctacagctacgactcaacatgga caacaagaacgagatcgaggacttctcgccaacatcgacgaggccatcagcagcatc <b>agacacggcatcgtgcacttcaacctggaactggaaggcaaggacatcttcgccttca</b> agaatatcgccccagcgagatctccaagaagatgttccagaacgaaatcaacgaaaa gaagctgaagctgaaaatctcaagcagctgaacagcgccaacgtgttcaactactacg agaaggatgtgatcatcaagctcctgaagaataccaagttcaacttcgtgaacaaaaac atcccctcgtgccagcttcaccaagctgtacaacaagattgaggacctgcggaatacc ctgaagtttttgagcgtgccaaggacaagaagagaaggacgccagatctacct gctgaagaatactactacggcgagttcctgaacaagttcgtgaaaaactccaaggtgttc ttaagatcaccaatgaagtgatcaagattaacaagcagcgggaaccagaaaaccggcc actacaagatcagaagttcgagaacatcgagaaaaccgtgcccgtggaatacctggcc atcatccagagcagagagatgatcaacaaccaggacaaagaggaaaagaataccta catcgactttattcagcagatttctgaagggttcatcgactacctgaacaagaacaatct gaagtatatcgagagcaacaacaacaatgacaacaacgacatcttccaagatcaag atcaaaaaggataacaagagaagtagcacaagatcctgaagaactatgagaagca caatcggaacaaagaaatccctcacgagatcaatgagttcgtgagcgagatcaagctg ggaagattctgaagtacaccgagaatctgaacatgttttacctgatcctgaagctgctga

accacaaagagctgaccaacctgaagggcagcctggaaaagtaccagtccgccaac  
aaagaagaaccttcagcgacgagctggaactgatcaacctgctgaacctggacaaca  
acagagtaccgaggacttcgagctggaagccaacgagatcggcaagttcctggacttc  
aacgaaaacaaatcaaggaccggaaaagagctgaaaaagttcgacaccaacaagat  
ctatttcgacggcgagaacatcatcaagcaccgggcttctacaatatcaagaatacgg  
catgctgaatctgctggaaaagatcgccgataaggccaagtataagatcagcctgaaag  
aactgaaagagtacagcaacaagaagaatgagattgaaaagaactacaccatgcagc  
agaacctgcaccggaagtacgccagaccaagaaggacgaaaagttcaacgacgag  
gactacaaagagtatgagaaggccatcggcaacatccagaagtacacccacctgaag  
aacaaggtggaattcaatgagctgaacctgctgcagggcctgctgctgaagatcctgcac  
cggctcgtgggctacaccagcatctgggagcgggacctgagattccggctgaagggcg  
agtttcccgagaaccactacatcgaggaaatttcaatttcgacaactccaagaatgtgaa  
gtacaaaagcggccagatcgtgaaaagtatatcaacttctacaagaactgtacaagg  
acaatgtgaaaagcggagcatctactccgacaagaaagtgaagaaactgaagcagg  
aaaaaaaggacctgtacatcc**ggaaactacattgccactt**caactacatccccacgc  
cgagattagcctgctggaagtgtgaaaacctgcggaagctgctgtcctacgaccgga  
agctgaagaacgccatcatgaagtcctcgtggacattctgaaagaatacggcttcgtg  
ccacctcaagatcggcgctgacaagaagatcgaaatccagacctggaatcagagaa  
gatcgtgcacctgaagaatctgaagaaaaagaaactgatgaccgaccggaacagcga  
ggaactgtcgaactcgtgaaagtcatttcgagtagacaaggccctggaa

dCas13a

catcatcatcatcacagcagcggcatgaaagtaccaaggtcgacggcatcagcc  
acaagaagtacatcgaagagggaagctcgtgaagtccaccagcagggaaaaccgg  
accagcgagagactgagcagctgctgagcatccggctggacatctacatcaagaacc  
ccgacaacgcctccgaggaagagaaccggatcagaagagagaacctgaagaagttc  
tttagcaacaaggtgctgcacctgaaggacagcgtgctgtatctgaagaaccggaaaga  
aaagaacgccgtgcaggacaagaactatagcgaagaggacatcagcgagtacgacc  
tgaaaaacaagaacagcttctccgtgctgaagaagatcctgctgaacgaggacgtgaa  
ctctgaggaactggaatcttccggaaggacgtggaagccaagctgaacaagatcaac  
agcctgaagtacagcttcaagagaacaaggccaactaccagaagatcaacgagaa  
caacgtggaaaaagtgggcggcaagagcaagcggaacatcatctacgactactacag  
agagagcgaagcgaacgactacatcaacaacgtgcaggaagccttcgacaagct  
gtataagaaagaggatatcgagaactgttttctgatcgagaacagcaagaagcagc  
agaagtacaagatccgcgagtactatcaaatcatcggccggaagaacgacaaaag  
agaacttcgccaagattatctacgaagagatccagaacgtgaacaacatcaagagct  
gattgagaagatccccgacatgtctgagctgaagaaaagccaggtgttctacaagtacta  
cctggacaaagaggaactgaacgacaagaatattaagtagccttctgccacttcgtgg  
aatcagagatgtcccagctgctgaaaaactacgtgtacaagcggctgagcaacatcagc  
aacgataagatcaagcggatcttcgagtaccagaatctgaaaaagctgatcgaaaaca  
aactgctgaacaagctggacacctacgtgcggaactgcggcaagtacaactactatctg  
caagtgggcgagatcgccacctccgactttatcgcccggaaccggcagaacgaggcctt  
cctgagaaacatcatcggcgtgtccagcgtggcctacttcagcctgaggaacatcctgga  
aaccgagaacgagaacgatcaccggccgatgcggggcaagaccgtgaagaac  
aacaagggcgaagagaaatacgtgtccggcgaggtggacaagatctacaatgagaac  
aagcagaacgaagtgaagaaaaatctgaagatgttctacagctacgactcaacatgga  
caacaagaacgagatcaggacttctcccaacatcgacgaggccatcagcagcatc

**gcccacggcatcgtgcacttcaacctggaactggaaggcaaggacatcttcgcctca**  
agaatatcgccccagcgagatctccaagaagatgttcagaacgaaatcaacgaaa  
gaagctgaagctgaaaatctcaagcagctgaacagcgccaacgtgttcaactactcg  
agaaggatgtgatcatcaagtacctgaagaataccaagttcaacttcgtgaacaaaaac  
atcccctcgtgccagcttcaccaagctgtacaacaagattgaggacctgcggaatacc  
ctgaagtttttggagcgtgcccaaggacaaagaagagaaggacgccagatctacct  
gctgaagaatactactacggcgagttcctgaacaagttcgtgaaaaactccaaggtgttc  
tttaagatcaccaatgaagtgatcaagattaacaagcagcgggaaccagaaaaccggcc  
actacaagtatcagaagttcgagaacatcgagaaaaccgtgcccggtgaataacctggcc  
atcatccagagcagagagatgatcaacaaccaggacaaagaggaaaagaataccta  
catcgactttattcagcagattttcctgaagggttcatcgactacctgaacaagaacaatct  
gaagtatatcgagagcaacaacaacaatgacaacaacgacatcttccaagatcaag  
atcaaaaaggataacaaagagaagtagcacaagatcctgaagaactatgagaagca  
caatcggaacaaagaaatccctcacgagatcaatgagttcgtgcgcgagatcaagctg  
gggaagattcgaagtacaccgagaatctgaacatgtttacctgatcctgaagctgtga  
accacaaagagctgaccaacctgaagggcagcctggaaaagtaccagtccgccaac  
aagaagaaaccttcagcgcgagctggaactgatcaacctgtgaacctggacaaca  
acagagtgaccgaggacttcgagctggaagccaacgagatcggcaagttcctggacttc  
aacgaaaacaaaatcaaggaccggaagagctgaaaagttcgacaccaacaagat  
ctatttcgacggcgagaacatcatcaagcaccggccttctacaatatcaagaatacgg  
catgctgaatctgctggaaaagatcgccgataaggccaagtataagatcagcctgaaag  
aactgaaagagtagcaacaagaagaatgagattgaaaagaactacaccatgcagc  
agaacctgcaccggaagtagccagaccaagaaggacgaaaagttcaacgacgag  
gactacaaagagtagagaaggccatcggcaacatccagaagtagacccacctgaag  
aacaaggtggaattcaatgagctgaacctgtgcagggcctgctgctgaagatcctgcac  
cggctcgtgggctacaccagcatctgggagcgggacctgagattccggctgaagggcg  
agtttcccgagaaccactacatcgaggaaattttcaatttcgacaactccaagaatgtgaa  
gtacaaaagcggccagatcgtggaaaagtatatcaacttctacaaagaactgtacaagg  
acaatgtggaaaagcggagcatctactccgacaagaaagtgaagaaactgaagcagg  
aaaaaaaggacctgtacatc**gccaactacattgcccactt**caactacatccccacgc  
cgagattagcctgctggaagtgtggaacacctgcggaagctgctgtcctacgaccgga  
agctgaagaacgccatcatgaagtccatcgtggacattctgaaagaatacggcttcgtgg  
ccacctcaagatcggcgtgacaagaagatcgaaatccagaccctggaatcagagaa  
gatcgtgcacctgaagaatctgaagaaaaagaaactgatgaccgaccggaacagcga  
ggaactgtgcaactcgtgaaagtcatgttcgagtacaaggccctggaa

**Table S2. RNA Sequences used in Cas13a Inhibitor Project**

Name	Sequence (5' to 3')
crRNA	GGAUUUAGACUACCCCAAAAACGAAGGGGACUAAAA CUAUACCUCCUGACCAGAAGCUGCCUGAA
Scrambled crRNA	GGAUUUAGACUACCCCAAAAACGAAGGGGACUAAAA CUAUCGAAUGAUUAAAGACAUCCGACGAA
Target RNA for FAM assay	GGAUUAGGUCAGGAUCAAGGAGCAAGUAGUGGGGU CUUAAAACACGAUGUUCAGGCAGCUUCUGGUCAGGA GGUAUAAUUAG
Target RNA for gel assay	GGAUUAGGUCAGGAUCAAGGAGCAAGUAGUGGGGU CUUAAAACACGAUGGAGCUUUCAGGCAGCUUCUGGU CAGGAGGUUAAUUAG
Scrambled target RNA for FAM assay	GGAUUAGGCAUGGCAGUCAUUUGAAUCUUGCGGGU CUUAAAACACGAUGUGGCUACAUAGCAAUCAGGCAU CGAGCAAUUAG
Scrambled target RNA for gel assay	GGAUUAGGCAUGGCAGUCAUUUGAAUCUUGCGGGU CUUAAAACACGAUGGAGCUUGGCUACAUAGCAAUCA GGCAUCGAGCAAUUAG
Reporter RNA	6-FAM-UUUUUU-IBFQ
FAM+ RNA	6-FAM-AAAAAAAGU
Fluorescent target RNA for gel assay	AACCAGCGCCUUCAGGCAGCUUCUGGUCAGGAGGU AUACCAC-Cy5
Scrambled fluorescent target RNA for gel assay	AACCAGCGCCUGGCUACAUAGCAAUCAGGCAUCGAG CACCAC-Cy5

**Table S3. DNA oligonucleotides used to produce RNA for Cas13a Inhibitor Project**

Name	Sequence (5' to 3')
5' T7 promoter	TAATACGACTCACTATAGG
3' crRNA sequence	TTCAGGCAGCTTCTGGTCAGGAGGTATAGTTTTAGTC CCCTTCGTTTTTTGGGGTAGTCTAAATCCTATAGTGAGT CGTATTA
3' Scrambled crRNA sequence	TTCGTCGGATGTCTTTAATCATTTCGATAGTTTTAGTCC CCTTCGTTTTTTGGGGTAGTCTAAATCCTATAGTGAGTC GTATTA
3' Target RNA for FAM assay sequence	CTAATTATACCTCCTGACCAGAAGCTGCCTGAACATC GTGTTTTAAGACCCCACTACTTGCTCCTTGATCCTGAC CTAATCCTATAGTGAGTCGTATTA
3' Target RNA for gel assay sequence	CTAATTATACCTCCTGACCAGAAGCTGCCTGAAAGCT CCATCGTGTTTTAAGACCCCACTACTTGCTCCTTGATC CTGACCTAATCCTATAGTGAGTCGTATTAGCCGGCAT CGATAGTCTCAGCTGC
3' Scrambled target RNA for FAM assay sequence	CTAATTGCTCGATGCCTGATTGCTATGTAGCCACATC GTGTTTTAAGACCCGCAAGATTCAAATGACTGCCATG CCTAATCCTATAGTGAGTCGTATTA
3' Scrambled target RNA for gel assay sequence	CTAATTGCTCGATGCCTGATTGCTATGTAGCCAAGCT CCATCGTGTTTTAAGACCCGCAAGATTCAAATGACTG CCATGCCTAATCCTATAGTGAGTCGTATTAGCCGGCA TCGATAGTCTCAGCTGC

**Table S4. Double-stranded DNA Oligonucleotides used to clone crRNA Expression Plasmids**

Name	Sequence (5' to 3')
Insert SIRT1 (1) crRNA sequence	CTTCGAGAAGACTAAAACAACAGAAGGTTATCTCGGT ACCCAATCGTTTTTTGTCTTCGAGAAG
Insert SIRT1 (2) crRNA sequence	CTTCGAGAAGACTAAAACGATACTGATTACCATCAAGC CGCCTACTTTTTTTGTCTTCGAGAAG
Insert CCAR2 (1) crRNA sequence	CTTCGAGAAGACTAAAACGAACACAAAAGCAAGCAGA CAGTCTAAGTTTTTTGTCTTCGAGAAG
Insert CCAR2 (2) crRNA sequence	CTTCGAGAAGACTAAAACCTTCTTGGAGTCATAGTCATC ACTTCGGCTTTTTTTGTCTTCGAGAAG

**Table S5. Full Compound Names**

Code	Compound Name
C1	2,5-dimethyl-1-[(3-methylthiophen-2-yl)methyl]-1H-pyrrole
C2	N-[3-(1,3-benzothiazol-2-yl)-4-methylthiophen-2-yl]-4-chlorobenzene-1-sulfonamide
C3	3-amino-1-(furan-2-yl)-9H-fluorene-2,4-dicarbonitrile
C4	2-(5-methyl-2-phenyl-2H-1,2,3-triazol-4-yl)-5-phenyl-1,3,4-oxadiazole
C5	4-(2,5-dioxo-2,5-dihydro-1H-pyrrol-1-yl)-N-[4-(trifluoromethyl)phenyl]benzene-1-sulfonamide
C6	2,3,5,6-tetrafluoro-4-[[2-(3-nitrophenyl)-2-oxoethyl]sulfanyl]benzoic acid
C7	4,6-bis(furan-2-yl)-2-oxo-1,2-dihydropyridine-3-carbonitrile
C8	N-[(furan-2-yl)methyl]-7-nitro-2,1,3-benzoxadiazol-4-amine
C9	2E)-2-[(E)-cyclopropanecarbonyl]-3-(5-nitrothiophen-2-yl)prop-2-enenitrile
C10	N-[3-cyano-4-(trifluoromethyl)phenyl]-5-ethyl-1H-indole-2-carboxamide
C11	(2E)-3-[4-(2-phenylethynyl)thiophen-2-yl]-2-[(E)-thiophene-2-carbonyl]prop-2-enenitrile
C12	3-(3-ethynylphenyl)-1-[[3-(3-ethynylphenyl)carbamoithioyl]amino]thiourea
C13	(2E,5E)-2,5-bis[(furan-2-yl)methylidene]cyclopentan-1-one
C14	5-[[5-(4-chlorophenyl)furan-2-yl]methylidene]-2-sulfanylidene-1,3-diazinane-4,6-dione
C15	9-(3-methoxybenzoyl)-9-azatricyclo[9.4.0.0 <sup>2,7</sup> ]pentadeca-1(11),2(7),3,5,12,14-hexaen-8-one
C16	N-(pyridin-3-yl)-4H,5H,6H,7H,8H,9H-cycloocta[b]thiophene-2-carboxamide
C17	ethyl 1-[(3-methylphenyl)methyl]piperidine-3-carboxylate
C18	N-(3-propoxyphenyl)furan-2-carboxamide
C19	1-(2-chlorophenyl)-4-[(cyclohex-3-en-1-yl)methyl]piperazine
C20	1-[(3-bromo-4-fluorophenyl)methyl]-4-(pyridin-2-yl)piperazine

# Appendix A: Delivery of Cas9 Ribonucleoprotein Complex via a Hybrid Aptamer/gRNA

## Background

Despite the impressive capabilities of CRISPR proteins, several limitations make it difficult to translate this system into humans (Peng et al., 2015). One of the most significant limitations is delivery (Glass et al., 2018). Current methods of delivering CRISPR/Cas9 include: physical methods- microinjection and electroporation; chemical methods- cell-penetrating peptides and lipid micelles; and viral vectors- adeno-associated virus (AAV) and lentivirus (Glass et al., 2018). In particular, viruses and lipid nanoparticles remain the two best methods of delivering CRISPR to *in vivo* tissue.

The two main types of viral vectors that are used are lentiviral and AAVs. Both these methods have disadvantages: lentiviral vectors integrate into the genome and can lead to prolonged non-specific cleavage of Cas9; while AAVs have a small carrying capacity of around 4.8kb, requiring the coinfection of two viral vectors for Cas9 and its respective gRNA (Liu et al., 2017). Lipid nanoparticles do not suffer from these issues and have been used to deliver Cas9 quite successfully in mice (Zuris et al., 2014). However, their efficiency and immunogenicity still need to be addressed (Mout et al., 2017). Cell-penetrating peptides address these problems but are difficult to engineer, and the mechanism of uptake is still not fully understood (Glass et al., 2018).

To address these issues, we turned to a different class of molecules: cell-internalizing RNA aptamers. Aptamers are short non-coding oligonucleotides that are capable of binding to various proteins and molecules with high affinity. Aptamers possess very little immunogenic behaviour, low batch-to-batch variation, high thermal stability, and low production costs (Sun and Zu, 2015). The primary technique to generate such aptamers is through SELEX: Systematic

Evolution of Ligands Exponential Enrichment (Sun and Zu, 2015). This process involves screening a library of aptamer sequences against a specific target until an individual aptamer sequence is enriched. Aptamers over the past decade have proven to be versatile molecules being able to perform a variety of functions: probing, drug delivery, apoptotic initiation, and simple enzymatic functions (Radom et al., 2013; Gopinath et al., 2016). Several aptamers have been found to penetrate a large variety of cell types (Burke, 2012). These aptamers internalize into cells by binding to a specific cell receptor and then becoming internalized via clathrin-mediated endocytosis (Gopinath et al., 2016).

Aptamers provide an attractive, discreet, and viable option for transporting CRISPR into cells. Unlike nanoparticles and viruses, aptamers seem to have minimal impact on cellular functions and, unlike cell-penetrating peptides, can be engineering to be very specific.

## **Methodology**

### ***Cloning and Synthesis of Aptamer/gRNA Hybrids***

The hybrid aptamer/gRNA sequences were ordered as gBlocks from IDT. The gBlocks were digested at 37°C for 3 hours with restriction enzymes BsaI and PspOMI (NEB), and ligated into the plasmid pUC57-sgRNA (Addgene- item #51132) using Quick Ligase from NEB. Ligated plasmids were transformed into Subcloning Efficiency™ DH5α cells (Invitrogen), and the plasmids were isolated and purified using the Miniprep kit (Qiagen). Plasmids were Sanger sequenced and verified using the SnapGene alignment tool. RNA was transcribed using the HiScribe Quick T7 RNA (NEB) synthesis kit. The hybrid aptamer/gRNA plasmids were linearized with DraI (NEB) and purified with QIAquick PCR Purification Kit (Qiagen). The linearized plasmids were incubated with T7 RNA polymerase at 37°C for 16 hours, as per the kits' instructions. The final transcribed guide RNAs were treated with DNaseI (Invitrogen) for 10 minutes at 37°C to remove the DNA template and purified using Guide-it™ IVT RNA Clean-Up Kit (Takara). Final RNAs were denatured for 10 minutes at 70°C with 2x RNA loading dye and run

on 5% TBE Urea Gels (Biorad) for visualization. For a complete list of all RNA sequences used, see **Table A1**, and for a complete list of all gBlock oligonucleotides, see **Table A2**.

### ***Expression and Purification of Cas9***

To express and purify Cas9, the plasmid pET-NLS-Cas9-6\*His (Addgene-item #62934) was transformed into BL21 DE3 competent *E. coli* cells (NEB). Competent cells were grown in LB media with carbenicillin (100 µg/mL) at 37°C. Once an OD<sub>600</sub> of 0.6 was reached, expression was induced with IPTG and grown at 18°C at 200 rpm for 16 hours. Cells were centrifuged, resuspended in lysis buffer (20 mM Tris-Cl, pH 8.0, 250 mM NaCl, 5 mM imidazole, pH 8.0, cOmplete™, Mini, EDTA-free Protease Inhibitor Cocktail (Roche) and 1 mM DTT) and lysed via sonication. The lysate was applied to Ni-NTA Agarose beads (Qiagen) and incubated at 4°C for 1 hour. After, the column was washed twice with 10ml of wash buffer (20 mM Tris-Cl, pH 8.0, 250 mM NaCl, 10 mM imidazole, pH 8.0, 1 mM DTT) and incubated for 30 minutes at 4°C with elution buffer (20 mM Tris-Cl, pH 8.0, 250 mM NaCl, 250 mM imidazole, pH 8.0, 1 mM DTT) and eluted. The protein was further purified with the HiTrap SP FF cation exchange column (Cytiva). The column was washed with IEX buffer A (20 mM HEPES, pH 7.5, 100 mM NaCl, 1 mM DTT) and eluted with IEX buffer B (20 mM HEPES, pH 7.5, 1 M NaCl, 1 mM DTT). The protein was concentrated down with 50 kDa concentrator (Pierce) and buffer exchanged with storage buffer (20 mM HEPES, pH 7.5, 500 mM NaCl, and 1 mM DTT). Protein was analyzed on an SDS-page gel for visualization, and the final concentration was determined with a BCA assay (Pierce). Protein was aliquoted and stored in the -80°C.

### ***In Vitro Activity Assay***

*In vitro* activity assay was performed by incubating 15 nM of Cas9 protein with 15 nM of hybrid gRNA at 37°C for 15 minutes to allow for the formation of the RNP complex. After, CRISPR/Cas9 was incubated with 100 ng of EMX1

target DNA (GAGTCCGAGCAGAAGAAGAAGGG) at 37°C for 1 hour. Lastly, the reaction was purified using the QIAquick PCR Purification Kit (Qiagen) and run on a 1% agarose gel for visualization.

## **Results**

Five aptamers were chosen from the literature as candidates for creating our cell-internalizing CRISPR molecule: C1. min, Otter. min, CD133- A15, CD133- B19, and C2. min (**Figure A1A**). Aptamers, C1. min and Otter. min, have been shown to internalize in many different cell types (Magalhães et al., 2012). However, the mechanism by which they internalize is not known. Aptamers, CD133- A15 and CD133- B19, are the shortest cell-internalizing aptamers ever generated (Shigdar et al., 2013). They internalize by binding to the receptor PROM, a ubiquitous protein thought to help organize cell membrane topology (Shigdar et al., 2013). The final aptamer is C2. min that internalizes through binding to CD71, a transferrin receptor also found in many cell types (Wilner et al., 2012). These aptamers were appended to three locations on the gRNA sequence: tetraloop, stem-loop 2, and the 3' end. A crystal structure of the Cas9 RNP shows these locations (Nishimasu et al., 2014) (**Figure A1B**). All three of the locations can tolerate modifications without affecting Cas9 activity.

A total of 16 sequences were synthesized: 5 aptamers in 3 different gRNA locations plus a positive control (**Figure A2A**). An *in vitro* cleavage assay was performed with all 16 sequences at 15 nM concentration of RNP. All sequences successfully cleaved EMX1 target DNA at a similar efficiency as the positive control (**Figure A2B**). Some initial cell work was conducted to test these aptamer/gRNA hybrids. However, after trying several different approaches – multiple cell lines, different DNA targets, and adding chloroquine – the obtained results were inconclusive. It was decided to move onto another project. Future work could aim to explore the reasons why our initial experiments failed.

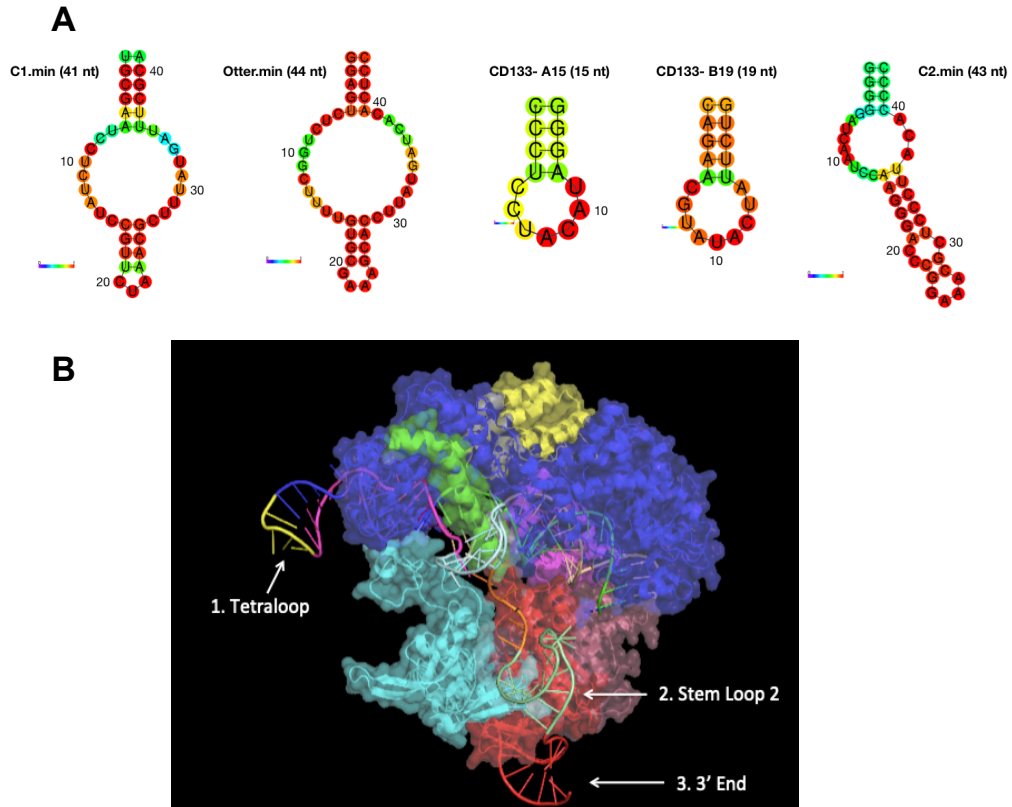


**Figure A1. Selected Cell- Internalizing Aptamers and Locations for Attachment. A)** Five aptamers were chosen from the literature as candidates for creating our cell-internalizing CRISPR molecule: C1. Min, Otter. min, CD133- A15, CD133- B19, and C2. Min. The colour of each nucleotide represents the probability of existing in this conformation. These aptamers have been generated using the RNAfold program from the website <http://rna.tbi.univie.ac.at/cgi-bin/RNAWebSuite/RNAfold.cgi>. **B)** Crystal structure of SpCas9 showing the three possible locations for appending the aptamer: tetraloop, stem-loop 2, and the 3' end. Crystal structure was downloaded from RCSB PDB and color-coded using PyMOI software.

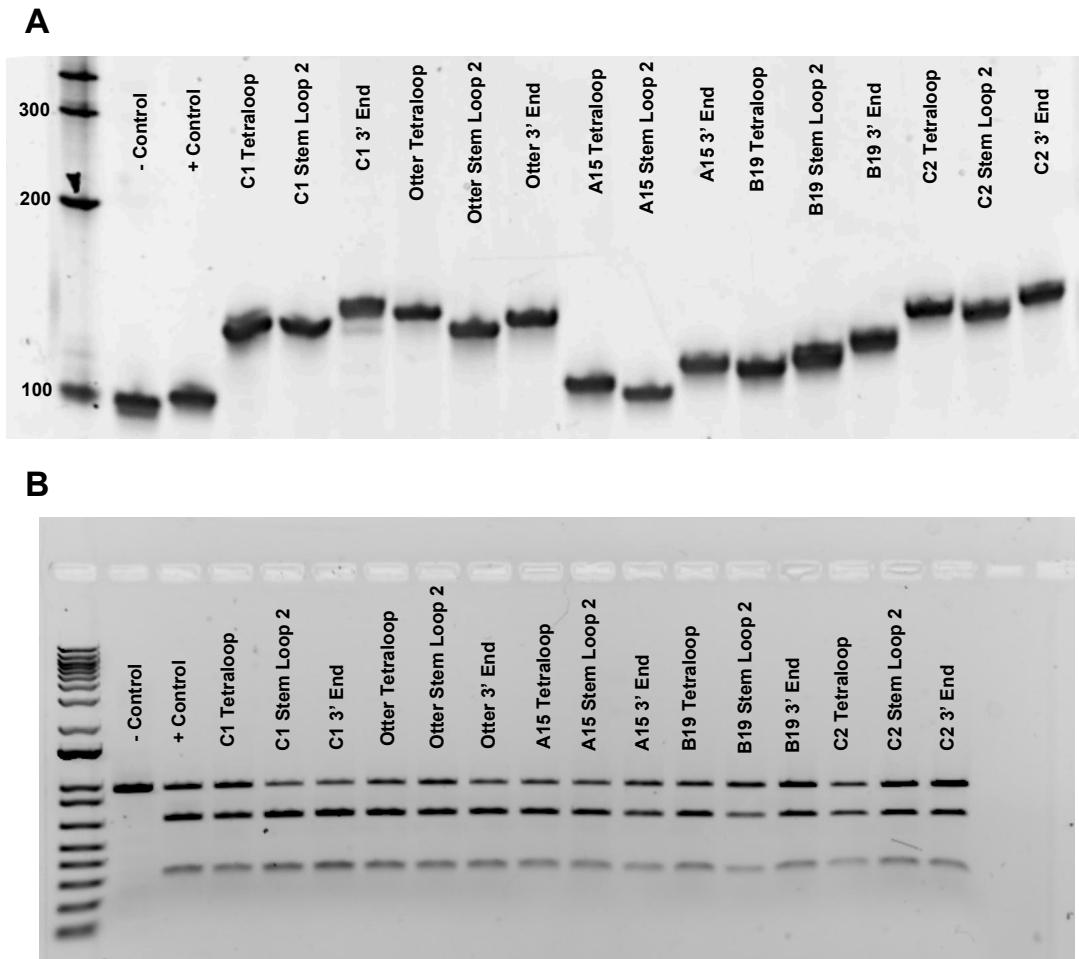


**Figure A2: 16 Aptamer/gRNA Sequences and *In Vitro* Cleavage Assay.** **A)** All 16 aptamer/gRNA sequences synthesized *in vitro* and ran on 5% TBE-Urea gel. **B)** *In vitro* cleavage assay reveal that the appended aptamer sequences do not affect Cas9 nuclease activity.

## Discussion

Effective and cytotoxic-free delivery remains a complex problem that all CRISPR systems have to contend with and overcome if CRISPR is to be used on humans. We attempted to address this problem by using cell-penetrating aptamers. A literature survey was performed to identify and select aptamers that have been shown to penetrate various cell types or penetrate a cell by binding to a ubiquitous cell receptor. Care was taken to ensure the selected aptamers do not cause any adverse effects (such as apoptosis), contain no peculiar bases

and have a reasonable length (smaller than 60 nucleotides). Five aptamers were selected: C1. Min, Otter. min, CD133- A15, CD133- B19, and C2. Min.

Next, we determined where precisely the aptamers should be appended to the sgRNA sequence. The location should be in a position where the aptamer is not interfering with the CRISPR complex, does not impact the stability and structure of the CRISPR RNP, and does not impact the nuclease activity of Cas9. Based on the literature review, we have found examples of how and where RNA sequences/aptamers have been added to a guide RNA sequence without impacting activity (Shechner et al., 2015, Shao et al., 2016). The three possible locations for appending the aptamer were the tetraloop, stem-loop 2, and the 3' end.

The selected aptamers were appended to these regions and did not impact Cas9 activity as was seen with the *in vitro* cleavage assays. Delivery of the Cas9 RNP with the hybrid gRNA/aptamer sequences was tried in a few cell lines, but initial results showed no cleavage and little promise. The aptamers most likely can be applied in addressing the problem of delivery, but would have to be implemented via a different method.

### **Limitations**

The most significant limitation of this project is the reliance on a single aptamer to deliver Cas9. The large size of the Cas9 protein (163 kDA) may prevent it from entering the cell. A possible explanation was that the Cas9/gRNA aptamer hybrids could not reach the nucleus: perhaps due to clumping on the cell's surface or an inability to escape vesicles. Another issue is whether or not the cell types used in the experiments express the appropriate receptors for these RNA ligands.

## **Future Direction**

In pursuing this project further, alternative approaches could be applied, such as adding aptamer sequences to all three locations on the gRNA, extending the length of the aptamer sequences, or simply choosing an aptamer sequence with higher efficacy from the literature. Interestingly, aptamers have been used to deliver CRISPR/Cas9. However, it was via nanoparticle delivery where nanoparticles were coated with the aptamers (Zhen et al., 2016).

In conclusion, the project did show that the insertion of these aptamers into the gRNA sequence led to no decrease in Cas9 activity. While we could not achieve delivery, this information could be helpful in future projects involving amendments of gRNAs.

## **References**

- Burke, D. H. (2012). Cell-penetrating RNAs: New keys to the castle. *Molecular Therapy*, *20*(2), 251–253. <https://doi.org/10.1038/mt.2011.306>
- Glass, Z., Lee, M., Li, Y., & Xu, Q. (2018). Engineering the delivery system for CRISPR-based genome editing. *Trends in Biotechnology*, *36*(2), 173–185. <https://doi.org/10.1016/j.tibtech.2017.11.006>
- Gopinath, S. C., Lakshmipriya, T., Chen, Y., Arshad, M. K., Kerishnan, J. P., Ruslinda, A. R., Al-Douri, Y., Voon, C. H., & Hashim, U. (2016). Cell-targeting aptamers act as intracellular delivery vehicles. *Applied Microbiology and Biotechnology*, *100*(16), 6955–6969. <https://doi.org/10.1007/s00253-016-7686-2>
- Liu, C., Zhang, L., Liu, H., & Cheng, K. (2017). Delivery strategies of the CRISPR-Cas9 gene-editing system for therapeutic applications. *Journal of Controlled Release*, *266*, 17–26. <https://doi.org/10.1016/j.jconrel.2017.09.012>
- Magalhães, M. L. B., Byrom, M., Yan, A., Kelly, L., Li, N., Furtado, R., Palliser, D., Ellington, A. D., & Levy, M. (2012). A general RNA motif for cellular transfection. *Molecular Therapy*, *20*(3), 616–624. <https://doi.org/10.1038/mt.2011.277>
- Mout, R., Ray, M., Lee, Y.-W., Scaletti, F., & Rotello, V. M. (2017). *In vivo* delivery of CRISPR/Cas9 for therapeutic gene editing: progress and challenges. *Bioconjugate Chemistry*, *28*(4), 880–884. <https://doi.org/10.1021/acs.bioconjchem.7b00057>
- Nishimasu, H., Ishitani, R., & Nureki, O. (2014). Crystal structure of *Streptococcus pyogenes* Cas9 in complex with guide RNA and target DNA. <https://doi.org/10.2210/pdb4oo8/pdb>

- Peng, R., Lin, G., & Li, J. (2015). Potential pitfalls of CRISPR/Cas9-mediated genome editing. *The FEBS Journal*, 283(7), 1218–1231. <https://doi.org/10.1111/febs.13586>
- Radom, F., Jurek, P. M., Mazurek, M. P., Otlewski, J., & Jeleń, F. (2013). Aptamers: molecules of great potential. *Biotechnology Advances*, 31(8), 1260–1274. <https://doi.org/10.1016/j.biotechadv.2013.04.007>
- Shao, S., Zhang, W., Hu, H., Xue, B., Qin, J., Sun, C., Sun, Y., Wei, W., & Sun, Y. (2016). Long-term dual-color tracking of genomic loci by modified sgRNAs of the CRISPR/Cas9 system. *Nucleic Acids Research*, 44(9). <https://doi.org/10.1093/nar/gkw066>
- Shechner, D. M., Hacısuleyman, E., Younger, S. T., & Rinn, J. L. (2015). Multiplexable, locus-specific targeting of long RNAs with CRISPR-display. *Nature Methods*, 12(7), 664–670. <https://doi.org/10.1038/nmeth.3433>
- Shigdar, S., Qiao, L., Zhou, S.-F., Xiang, D., Wang, T., Li, Y., Lim, L. Y., Kong, L., Li, L., & Duan, W. (2013). RNA aptamers targeting cancer stem cell marker CD133. *Cancer Letters*, 330(1), 84–95. <https://doi.org/10.1016/j.canlet.2012.11.032>
- Sun, H., & Zu, Y. (2015). A highlight of recent advances in Aptamer technology and its application. *Molecules*, 20(7), 11959–11980. <https://doi.org/10.3390/molecules200711959>
- Wilner, S. E., Wengerter, B., Maier, K., de Lourdes Borba Magalhães, M., Del Amo, D. S., Pai, S., Opazo, F., Rizzoli, S. O., Yan, A., & Levy, M. (2012). An RNA alternative to human transferrin: a new tool for targeting human cells. *Molecular Therapy - Nucleic Acids*, 1. <https://doi.org/10.1038/mtna.2012.14>
- Zhen, S., Takahashi, Y., Narita, S., Yang, Y.-C., & Li, X. (2016). Targeted delivery of CRISPR/Cas9 to prostate cancer by modified gRNA using a flexible aptamer-cationic liposome. *Oncotarget*, 8(6), 9375–9387. <https://doi.org/10.18632/oncotarget.14072>
- Zuris, J. A., Thompson, D. B., Shu, Y., Guilinger, J. P., Bessen, J. L., Hu, J. H., Maeder, M. L., Joung, J. K., Chen, Z.-Y., & Liu, D. R. (2014). Cationic lipid-mediated delivery of proteins enables efficient protein-based genome editing *in vitro* and *in vivo*. *Nature Biotechnology*, 33(1), 73–80. <https://doi.org/10.1038/nbt.3081>

## Tables

**Table A1. Hybrid Aptamer/gRNA Sequences**

Name	Sequence (5' to 3')
Control	GAGUCCGAGCAGAAGAAGAAGUUUUAGAGCUAGAAAUAGCA AGUUAAAUAAGGCUAGUCCGUUAUCAACUUGAAAAGUGG CACCGAGUCGGUGC
C1 tetraloop	GAGUCCGAGCAGAAGAAGAAGUUUUAGAGCUAUGCGAAUCC UCUAUCCGUUCUAAACGCUUUUAUGAUUUCGCAUAGCAAGUU AAAUAAGGCUAGUCCGUUAUCAACUUGAAAAGUGGCACC GAGUCGGUGC
C1 stem loop 2	GAGUCCGAGCAGAAGAAGAAGUUUUAGAGCUAGAAAUAGCA AGUUAAAUAAGGCUAGUCCGUUAUCAACUUGCGAAUCCU CUAUCCGUUCUAAACGCUUUUAUGAUUUCGCAAAGUGGCACC GAGUCGGUGC
C1 3' end	GAGUCCGAGCAGAAGAAGAAGUUUUAGAGCUAGAAAUAGCA AGUUAAAUAAGGCUAGUCCGUUAUCAACUUGAAAAGUGG CACCGAGUCGGUGCUGCUGGAAUCCUCUAUCCGUUCUAAA CGCUUUUAUGAUUUCGCAGC
Otter tetraloop	GAGUCCGAGCAGAAGAAGAAGUUUUAGAGCUAAUGGAGUCU CUGGCUUUUGUGCGAAAGCACCUUAUGAUCACACUCCAUA GCAAGUUAAAUAAGGCUAGUCCGUUAUCAACUUGAAAAG UGGCACCGAGUCGGUGC
Otter stem loop 2	GAGUCCGAGCAGAAGAAGAAGUUUUAGAGCUAGAAAUAGCA AGUUAAAUAAGGCUAGUCCGUUAUCAACUUGCGGAGUCUC UGGCUUUUGUGCGAAAGCACCUUAUGAUCACACUCCGCAAG UGGCACCGAGUCGGUGC
Otter 3' end	GAGUCCGAGCAGAAGAAGAAGUUUUAGAGCUAGAAAUAGCA AGUUAAAUAAGGCUAGUCCGUUAUCAACUUGAAAAGUGG CACCGAGUCGGUGCUGGCCGAGUCUCUGGCUUUUGUGCGA AAGCACCUUAUGAUCACACUCCGGCC
A15 tetraloop	GAGUCCGAGCAGAAGAAGAAGUUUUAGAGCUACCCUCCUAC AUAGGGUAGCAAGUUAAAUAAGGCUAGUCCGUUAUCAACU UGAAAAGUGGCACCGAGUCGGUGC
A15 stem loop 2	GAGUCCGAGCAGAAGAAGAAGUUUUAGAGCUAGAAAUAGCA AGUUAAAUAAGGCUAGUCCGUUAUCAACUUCCUCCUACA UAGGGAAGUGGCACCGAGUCGGUGC
A15 3' end	GAGUCCGAGCAGAAGAAGAAGUUUUAGAGCUAGAAAUAGCA AGUUAAAUAAGGCUAGUCCGUUAUCAACUUGAAAAGUGG CACCGAGUCGGUGC GCCCUCCUACA UAGGGGC

B19 tetraloop	GAGUCCGAGCAGAAGAAGAAGUUUUAGAGCUACAGAACGUA UACU AUUCUGUAGCAAGUUAAAAUAAGGCUAGUCCGUUAUC AAUUGAAAAAGUGGCACCGAGUCGGUGC
B19 stem loop 2	GAGUCCGAGCAGAAGAAGAAGUUUUAGAGCUAGAAAUAGCA AGUUAAAAUAAGGCUAGUCCGUUAUCAACUUCAGAACGUAU ACU AUUCUGAAGUGGCACCGAGUCGGUGC
B19 3' end	GAGUCCGAGCAGAAGAAGAAGUUUUAGAGCUAGAAAUAGCA AGUUAAAAUAAGGCUAGUCCGUUAUCAACUUGAAAAAGUGG CACCGAGUCGGUGC GCCAGAACGUAUACU AUUCUGGC
C2 tetraloop	GAGUCCGAGCAGAAGAAGAAGUUUUAGAGCUAGGGGGAUC AAUCCAAGGGACCCGAAACGCUCCCUACACCCCUAGCAA GUUAAAAUAAGGCUAGUCCGUUAUCAACUUGAAAAAGUGGC ACCGAGUCGGUGC
C2 stem loop 2	GAGUCCGAGCAGAAGAAGAAGUUUUAGAGCUAGAAAUAGCA AGUUAAAAUAAGGCUAGUCCGUUAUCAACUUGGGGGAUCAA UCCAAGGGACCCGAAACGCUCCCUACACCCAAGUGGCA CCGAGUCGGUGC
C2 3' end	GAGUCCGAGCAGAAGAAGAAGUUUUAGAGCUAGAAAUAGCA AGUUAAAAUAAGGCUAGUCCGUUAUCAACUUGAAAAAGUGG CACCGAGUCGGUGC GCGGGGGAUCAAUCCAAGGGACCCGG AAACGCUCCCUACACCCCGC

**Table A2. DNA Oligonucleotides to produce Hybrid Sequences**

Name	Sequence (5' to 3')
Control	GCCGGGTCTCATAGGTGAGACCGAGAGAGGATTACAGAGTC CGAGCAGAAGAAGAAGTTTTAGAGCTAGAAATAGCAAGTTAA AATAAGGCTAGTCCGTTATCAACTTGAAAAAGTGGCACCGAG TCGGTGCTTTTTTTAAAGGGCCCGCCG
C1 tetraloop	GCCGGGTCTCATAGGTGAGACCGAGAGAGGATTACAGAGTC CGAGCAGAAGAAGAAGTTTTAGAGCTATGCGAATCCTCTATC CGTTCTAAACGCTTTATGATTTTCGCATAGCAAGTTAAAATAAG GCTAGTCCGTTATCAACTTGAAAAAGTGGCACCGAGTCGGTG CTTTTTTTAAAGGGCCCGCCG
C1 stem loop 2	GCCGGGTCTCATAGGTGAGACCGAGAGAGGATTACAGAGTC CGAGCAGAAGAAGAAGTTTTAGAGCTAGAAATAGCAAGTTAA AATAAGGCTAGTCCGTTATCAACTTTGCGAATCCTCTATCCGT TCTAAACGCTTTATGATTTTCGCAAAGTGGCACCGAGTCGGTG CTTTTTTTAAAGGGCCCGCCG
C1 3' end	GCCGGGTCTCATAGGTGAGACCGAGAGAGGATTACAGAGTC CGAGCAGAAGAAGAAGTTTTAGAGCTAGAAATAGCAAGTTAA AATAAGGCTAGTCCGTTATCAACTTGAAAAAGTGGCACCGAG TCGGTGCGCTGCGAATCCTCTATCCGTTCTAAACGCTTTATG ATTCGCAGCTTTTTTTAAAGGGCCCGCCG
Otter tetraloop	GCCGGGTCTCATAGGTGAGACCGAGAGAGGATTACAGAGTC CGAGCAGAAGAAGAAGTTTTAGAGCTAATGGAGTCTCTGGCT TTTGTGCGAAAGCACCTTATGATCACACTCCATTAGCAAGTTA AAATAAGGCTAGTCCGTTATCAACTTGAAAAAGTGGCACCGA GTCGGTGCTTTTTTTAAAGGGCCCGCCG
Otter stem loop 2	GCCGGGTCTCATAGGTGAGACCGAGAGAGGATTACAGAGTC CGAGCAGAAGAAGAAGTTTTAGAGCTAGAAATAGCAAGTTAA AATAAGGCTAGTCCGTTATCAACTTGCGGAGTCTCTGGCTTT TGTGCGAAAGCACCTTATGATCACACTCCGCAAGTGGCACC GAGTCGGTGCTTTTTTTAAAGGGCCCGCCG
Otter 3' end	GCCGGGTCTCATAGGTGAGACCGAGAGAGGATTACAGAGTC CGAGCAGAAGAAGAAGTTTTAGAGCTAGAAATAGCAAGTTAA AATAAGGCTAGTCCGTTATCAACTTGAAAAAGTGGCACCGAG TCGGTGCGGCCGGAGTCTCTGGCTTTTGTGCGAAAGCACCT TATGATCACACTCCGGCCTTTTTTTAAAGGGCCCGCCG
A15 tetraloop	GCCGGGTCTCATAGGTGAGACCGAGAGAGGATTACAGAGTC CGAGCAGAAGAAGAAGTTTTAGAGCTACCCTCCTACATAGGG TAGCAAGTTAAAATAAGGCTAGTCCGTTATCAACTTGAAAAAG TGGCACCGAGTCGGTGCTTTTTTTAAAGGGCCCGCCG

A15 stem loop 2	GCCGGGTCTCATAGGTGAGACCGAGAGAGGATTACAGAGTC CGAGCAGAAGAAGAAGTTTTAGAGCTAGAAATAGCAAGTTAA AATAAGGCTAGTCCGTTATCAACTTCCCTCCTACATAGGGAA GTGGCACCGAGTCGGTGCTTTTTTTAAAGGGCCCGCCG
A15 3' end	GCCGGGTCTCATAGGTGAGACCGAGAGAGGATTACAGAGTC CGAGCAGAAGAAGAAGTTTTAGAGCTAGAAATAGCAAGTTAA AATAAGGCTAGTCCGTTATCAACTTGAAAAAGTGGCACCGAG TCGGTGCGCCCCCTCCTACATAGGGGCTTTTTTTAAAGGGCCC GCCG
B19 tetraloop	GCCGGGTCTCATAGGTGAGACCGAGAGAGGATTACAGAGTC CGAGCAGAAGAAGAAGTTTTAGAGCTACAGAACGTATACTAT TCTGTAGCAAGTAAAATAAGGCTAGTCCGTTATCAACTTGAA AAAGTGGCACCGAGTCGGTGCTTTTTTTAAAGGGCCCGCCG
B19 stem loop 2	GCCGGGTCTCATAGGTGAGACCGAGAGAGGATTACAGAGTC CGAGCAGAAGAAGAAGTTTTAGAGCTAGAAATAGCAAGTTAA AATAAGGCTAGTCCGTTATCAACTTCAGAACGTATACTATTCT GAAGTGGCACCGAGTCGGTGCTTTTTTTAAAGGGCCCGCCG
B19 3' end	GCCGGGTCTCATAGGTGAGACCGAGAGAGGATTACAGAGTC CGAGCAGAAGAAGAAGTTTTAGAGCTAGAAATAGCAAGTTAA AATAAGGCTAGTCCGTTATCAACTTGAAAAAGTGGCACCGAG TCGGTGCGCCAGAACGTATACTATTCTGGCTTTTTTTAAAGG GCCCGCCG
C2 tetraloop	GCCGGGTCTCATAGGTGAGACCGAGAGAGGATTACAGAGTC CGAGCAGAAGAAGAAGTTTTAGAGCTAGGGGGATCAATCCA AGGGACCCGGAACGCTCCCTTACACCCCTAGCAAGTTAAA ATAAGGCTAGTCCGTTATCAACTTGAAAAAGTGGCACCGAGT CGGTGCTTTTTTTAAAGGGCCCGCCG
C2 stem loop 2	GCCGGGTCTCATAGGTGAGACCGAGAGAGGATTACAGAGTC CGAGCAGAAGAAGAAGTTTTAGAGCTAGAAATAGCAAGTTAA AATAAGGCTAGTCCGTTATCAACTTGGGGGATCAATCCAAGG GACCCGGAACGCTCCCTTACACCCCAAGTGGCACCGAGTC GGTGCTTTTTTTAAAGGGCCCGCCG
C2 3' end	GCCGGGTCTCATAGGTGAGACCGAGAGAGGATTACAGAGTC CGAGCAGAAGAAGAAGTTTTAGAGCTAGAAATAGCAAGTTAA AATAAGGCTAGTCCGTTATCAACTTGAAAAAGTGGCACCGAG TCGGTGCGCGGGGGATCAATCCAAGGGACCCGGAACGCT CCCTTACACCCCGCTTTTTTTAAAGGGCCCGCCG

# Appendix B: Targeting and Eliminating Specific Cells via RNA Identification using Tandem dCas13-PE3 Toxin System

## Background

The specific and powerful RNA knockdown capabilities of Cas13 have led to the creation of multiple Cas13-based tools. In this collaborative project, we attempted to make a Cas13 complementation system. Such an approach has been tried with Cas9, where two dCas9 fused with FokI nuclease would bind to a DNA strand in close proximity leading to FokI dimerization and cleavage: this greatly improved CRISPR/Cas9 specificity (Guilinger et al., 2014). Our idea was to fuse two dCas13 with two complementary fragments of domain III of *Pseudomonas* exotoxin A, i.e., PE3 (Boland et al., 2014).

*Pseudomonas aeruginosa* is a gram-negative bacterium that is found to cause pathogenic effects in humans due to exotoxin A's effect on eukaryotic elongation factor 2 (eEF2) (Yates and Merrill, 2004). eEF2 is a translation factor that contains a highly modified histidine residue at position 699 called diphthamide (Yates and Merrill, 2004). This highly conserved residue is targeted by exotoxin A (Yates and Merrill 2004; Boland et al., 2014). Exotoxin A uses NAD<sup>+</sup> as a substrate and transfers the ADP-ribose group from NAD<sup>+</sup> to this residue: a process referred to as ribosylation. This prevents eEF2 from transferring peptidyl t-RNA to different sites in the ribosome leading to the cessation of protein elongation and eventual cell death (Yates and Merrill, 2004).

Exotoxin A has been used to target and kill and cells infected with hepatitis B and cancer cells. However, results have been limited due to off-target toxicity (Hafkmeyer et al., 2008; Stuckey et al., 2015). In 2014, Boland and collaborators took *Pseudomonas* exotoxin A domain III (PE3) – the active domain – and split it

into two components: PE3 $\alpha$  and PE3 $\beta$  (Boland et al., 2014). These two components were unable to ribosylate eEF2 individually, but were able to do so when brought together (Boland et al., 2014). We believe that a dual dCas13-PE3 system can address the issues of specificity and toxicity. By only having the toxin become activated in the presence of a specific cancer or viral RNA transcript, we believe that it would allow the usage of the PE3 toxin with minimal off-site toxicity.

## **Methodology**

### ***Cloning of dCas13-PE3 Constructs***

Cloning of the dCas13d-PE3 hybrid expression plasmids was performed using the NEBuilder® HiFi DNA assembly method and was designed using the NEBuilder tool. The dRfxCas13d sequence was taken from the Konnerman et al., 2018 paper, was optimized for bacterial protein expression using the IDT Codon Optimization Tool, and was ordered as a bacterial plasmid. The nucleotide sequences of the PE3 $\alpha$  and PE3 $\beta$  toxins from the Boland et al., 2014 paper were ordered as gBlocks (oligonucleotides) from IDT: 354 bp (118 aa) and 462 bp (154 aa) long, respectively. The fragments were all cloned into the pET His6 TEV LIC cloning vector (1B) (Addgene- item #29653) to make the final plasmid.

Additionally, an MBP tag with a TEV cut site was added to the dCas13d-PE3 constructs to increase solubility and stability (Lebendiker & Danieli, 2010). The NEBuilder tool generated pairs of primers with overlapping regions to make the final dCas13d-PE3 construct of choice. These primers were ordered, and the respective sequence was PCR amplified using Q5® High-Fidelity 2x Master Mix (NEB). The amplified sequences were run on a 1% agarose gel, and were gel extracted using the QIAquick Gel Extraction Kit (Qiagen) according to the kit's instructions. The amount of vector and insert was quantified using a NanoDrop spectrophotometer. 0.1:0.2 pmol insert to vector ratio was used to assemble the dCas13d-PE3 expression plasmid. The appropriate amount of purified DNA was added along with 2x HiFi DNA Assembly Master Mix (NEB); this was incubated at 50°C for 1 hour per kit instructions. NEB® 5 $\alpha$  Competent *E. coli* (High Efficiency) were transformed with the plasmid and plated on carbenicillin plates (100  $\mu$ g/mL).

The plasmid was isolated and purified using QIAprep Spin Miniprep Kit (Qiagen). It was Sanger sequenced and verified using the SnapGene alignment tool. An array of dCas13d permutations was designed with either PE3 $\alpha$  or PE3 $\beta$  toxin being placed on either the N-terminal or C-terminal with one of three different lengths of linkers (short, medium, long).

For cloning dCas13a-PE3 hybrids, a similar approach was taken. The dLwCas13a sequence was acquired from pC013 - Twinstrep-SUMO-huLwCas13a plasmid (Addgene- item #90097); the same PE3 $\alpha$  and PE3 $\beta$  gBlocks were used, and all components were cloned into the empty pC013 vector from the aforementioned plasmid to make our final construct. The rest of the protocol was as described previously. For a complete list of all dCas13-PE3 hybrids made, see **Table B1**. For a list of all the primers used to make the dCas13a-PE3 hybrids, see **Table B2**.

### ***Expression and Purification of dCas13d-PE3 hybrids***

The protocol from Konermann 2018 was adapted and modified to express and produce dCas13d-PE3 proteins. The respective plasmids were transfected into BL21 DE3 competent *E. coli* cells (NEB) and plated onto carbenicillin plates (100  $\mu$ g/mL). Cells were grown in LB broth at 37°C and were induced at an OD of 0.6 with 1 mM of IPTG, and incubated at 18°C overnight at 200 rpm. The bacteria was pelleted, and resuspended with lysis buffer (50 mM HEPES, 500 mM NaCl, 20 mM Imidazole, 1% Triton X100, 1 mM DTT, 0.5 mM PMSF, and cComplete™, Mini, EDTA-free Protease Inhibitor Cocktail (Roche)). The suspension was incubated for 20 minutes at 4°C and lysed via sonication. The lysate was ultracentrifuged at 18 000 g for 1 hour. The supernatant was applied to Ni-NTA Agarose beads (Qiagen) and incubated at 4°C for 1 hour. After, the column was washed twice with 10 ml of wash buffer (50 mM Tris HCl pH 7, 500 mM NaCl, 20 mM Imidazole, 0.1% Triton X100, 10% glycerol, 1 mM DTT, 0.2 mM PMSF). Elution buffer (50 mM Tris HCl pH 7, 500 mM NaCl, 300 mM Imidazole, 0.1% Triton X100, 10% glycerol, 1 mM DTT, 0.2 mM PMSF) was added to the beads

and incubated for 30 minutes at 4°C and eluted. To remove the MBP tag, 200 µL of 1 mg/ml of TEV protease was added to the eluted sample. The sample was placed in dialysis tubing, and the tubing was placed in 400 mL of dialysis buffer (50 mM Tris-HCL pH 7, 0.1 M KCl, 300 mM Imidazole, 0.2 mM TCEP, 0.8 mM DTT, 7.5% Glycerol) overnight at 4°C.

The next day, the dialysed protein was buffer exchanged to IEX wash buffer (20 mM Tris-HCl pH 8.0, 1 mM DTT, 5% glycerol, 0.01 M NaCl) using a 50 kDa concentrator (Pierce). The protein was then further purified with the HiTrap SP FF cation exchange column (Cytiva). The column was washed with IEX buffer A (20 mM Tris pH 8.0, 5% glycerol, 20 mM NaCl, 1 mM DTT, and 0.2 mM PMSF) and eluted with a gradient concentration of 0.01 to 1 M NaCl using IEX buffer B (20 mM Tris pH 8.0, 5% glycerol, 1 M NaCl, 1 mM DTT, and 0.2 mM PMSF). Appropriate fractions were collected, and the protein was concentrated down with 50 kDa concentrator (Pierce) and buffer exchanged into storage buffer (50 mM Tris pH 8.0, 30% glycerol, 1 M NaCl, 1 mM DTT, and 0.1 mM PMSF). Protein was run on an SDS-page gel for visualization. The final concentration was determined with a BCA assay (Pierce). Protein was aliquoted and stored in the -80°C freezer.

### ***Expression and Purification of standalone PE3 $\alpha$ and PE3 $\beta$ Toxins***

To express and purify the standalone PE3 $\alpha$  and PE3 $\beta$  toxins, a similar protocol was followed as described for the dCas13d-PE3 hybrids. The differences were: after dialysis, the protein was once again applied to Ni-NTA Agarose beads (Qiagen) at 4°C for 1 hour to remove the His-tagged MBP, and the protein was buffer exchanged into PE3 storage buffer (PBS, glycerol 30%, DTT 2 mM). Quantification and storage were the same as for the dCas13d-PE3 hybrids.

### ***Expression and Purification of dCas13a-PE3 hybrids***

To synthesize dCas13a-PE3 proteins, the respective plasmids were transfected into BL21 DE3 competent *E. coli* cells (NEB) and plated onto carbenicillin plates (100 µg/mL). Cells were grown in LB broth at 37°C, and were induced at an OD of 0.6 with 1 mM of IPTG, and incubated at 18°C overnight at 200 rpm. The bacteria was pelleted and resuspended with lysis buffer (50 mM HEPES, 500 mM NaCl, 20 mM Imidazole, 1% Triton X100, 1 mM DTT, 0.5 mM PMSF, and cOmplete™, Mini, EDTA-free Protease Inhibitor Cocktail (Roche)). The suspension was incubated for 20 minutes at 4°C and lysed via sonication. Lysate was ultracentrifuges at 18 000 g for 1 hour. The supernatant was applied to Ni-NTA Agarose beads (Qiagen) and incubated at 4°C for 1 hour. After, the column was washed twice with 10 ml of wash buffer (50 mM Tris HCl pH 7, 500 mM NaCl, 20 mM Imidazole, 0.1% Triton X-100, 10% glycerol, 1 mM DTT, 0.2 mM PMSF), elution buffer (50 mM Tris HCl pH 7, 500 mM NaCl, 300 mM Imidazole, 0.1% Triton X100, 10% glycerol, 1 mM DTT, 0.2 mM PMSF) was added to the beads and incubated for 30 minutes at 4°C and eluted.

The eluted protein was diluted with IEX wash buffer without salt (20 mM Tris pH 8.0, 5% glycerol, 1 mM DTT, and 0.2 mM PMSF) to reduce the salt concentration to 125 mM NaCl. The protein was then further purified with the HiTrap SP FF cation exchange column (Cytiva). The column was washed with IEX buffer A (20 mM Tris pH 8.0, 5% glycerol, 20 mM NaCl, 1 mM DTT, and 0.2 mM PMSF) and eluted with a gradient concentration of 0.01 to 1M NaCl using IEX buffer B (20mM Tris pH 8.0, 5% glycerol, 1 M NaCl, 1 mM DTT, and 0.2 mM PMSF). Appropriate fractions were collected, and the protein was concentrated down with a 50 kDA concentrator (Pierce) and buffer exchanged into storage buffer (50 mM Tris pH 8.0, 30% glycerol, 1 M NaCl, 1 mM DTT, and 0.1 mM PMSF). Protein was run on an SDS-page gel for visualization. The final concentration was determined with a BCA assay (Pierce). Protein was aliquoted and stored at -80°C.

### ***Expression and Purification of eEF2***

To express and purify eEF2, we employed a His-eEF2 overexpressing yeast strain called TKY675 (Jørgensen et al., 2002). The protocol to express and purify eEF2 was adapted from Jørgensen et al., 2002. The yeast strain was grown to an OD<sub>600</sub> of 2.0 at 30°C, pelleted, and resuspended in lysis buffer (50 mM potassium phosphate, pH 7.6, 300 mM KCl, 10 mM imidazole, cOmplete™, Mini, EDTA-free Protease Inhibitor Cocktail (Roche), and 1 mM DTT). After, the cells were lysed with an emulsiflex homogenizer. The lysate pH was adjusted to pH 7 with 1 M Tris and spun at 18 000 g for 1 hour. The lysate was applied to Ni-NTA Agarose beads (Qiagen) and incubated for 1 hour at 4°C. The column was then washed twice with 10 ml of wash buffer (50 mM potassium phosphate, pH 7.6, 300 mM KCl, 20 mM imidazole, 1 mM DTT). Elution buffer (50 mM potassium phosphate, pH 7.6, 300 mM KCl, 250 mM imidazole, 1 mM DTT) was added to the beads and incubated for 30 minutes at 4°C and eluted. The protein was concentrated down with a 50 kDA concentrator (Pierce) and buffer exchanged with storage buffer (20 mM Tris, pH 6.8, 100 mM NaCl, and 1 mM DTT). Protein was run on an SDS-page gel for visualization. The final concentration was determined with a BCA assay (Pierce). Protein was aliquoted and stored in the -80°C.

### ***Cloning and Synthesis of crRNAs and Target RNA***

We selected crRNA and target RNA that have been used in the literature: the crRNA that targets the B4GALNT1 transcript (Koneremann et al., 2018). To synthesize the crRNAs and target RNAs, the sequences were ordered as DNA oligonucleotide primers: the 5' sequence for the T7 promoter and the 3' sequence for the reverse complement T7 promoter and the respective crRNA or target RNA sequence. These two oligonucleotide sequences were annealed together using a thermocycler and then *in vitro* transcribed (IVT) using the HiScribe™ T7 Quick High Yield RNA Synthesis Kit from NEB. The mixture was incubated at 37°C for 14 hours to produce our RNA. The final transcribed RNA was treated with DNaseI (Invitrogen) for 10 minutes at 37°C to remove the DNA template and

purified using Guide-it™ IVT RNA Clean-Up Kit (Takara). Final RNAs were denatured for 10 minutes at 70°C with 2x RNA loading dye and ran on 5% TBE Urea Gels (Biorad) for visualization. A series of target RNAs were made with a variable distance between two crRNA binding regions for testing of PE3 hybridization. For complete lists of all RNA sequences and DNA oligonucleotide sequences, see **Tables B3-B6**.

### ***Collateral Cleavage Assay***

The Cas13a Cleavage Buffer 5x is composed of the following: 100 mM HEPES pH 6.8, 250 mM KCl, 25 mM MgCl<sub>2</sub>, 25% Glycerol (East-Seletsky 2016). The reporter RNA used for this experiment was the IDT Reporter RNA. This RNA came in tubes with 50 pmol of RNA per tube. This RNA was dissolved in 10uL of water for a final concentration of 5 µM.

#### **Mixture 1:** 40 µL

Cas13a: 25 nM  
crRNA: 12.5 nM  
Cas13a cleavage buffer 5x: 10 µl  
Water: to 37 µl

#### **Mixture 2:** 10 µL

Reporter RNA (RNase Alert): 250 nM  
Target RNA: 10 nM

Mixture 1 was incubated at 37°C for 10 minutes to hybridize the Cas13a and crRNA. After, mixture 2 was added and mixed. The reaction was incubated at 37°C for 60 minutes and read with the SpectraMax® i3x spectrophotometer at an excitation of 490 nm and an emission at 510 nm.

### ***Gel Cleavage Assay***

The Cas13a Cleavage Buffer 5x is composed of the following: 100 mM HEPES pH 6.8, 250 mM KCl, 25 mM MgCl<sub>2</sub>, 25% Glycerol. Total reaction volume is 20 µL

**Mixture 1:**

Cas13a: 250 nM  
crRNA: 125 nM  
Cas13a cleavage buffer 5x: 4  $\mu$ l  
Water: to 19.5  $\mu$ l

**Mixture 2:**

Cy5 Target RNA: 50 nM

Mixture 1 was incubated at 37°C for 10 minutes to hybridize the Cas13a and crRNA. After, mixture 2 was added, mixed, and incubated at 37°C for 45 minutes. After, the reaction was purified using Guide-it™ IVT RNA Clean-Up Kit (Takara) – final elution volume of 30  $\mu$ L. 4x RNA loading dye (95% Formamide and 5% glycerol) was added and boiled at 85°C for 10 minutes. Homemade 10% TBE-Urea PAGE gels were pre-ran at 200V for 15 minutes, followed by flushing the wells with 1x TBE buffer to remove residual urea and APS. 30  $\mu$ L of samples were loaded and the gel was run at 200 V for 60 minutes. The gel was imaged using Cy5 excitation/emission wavelengths, 650 nm and 670 nm respectively, using the Amersham Imager 600.

***In vitro ADP-Ribosylation Assay***

For negative controls dCas13-PE3 protein was not included. For positive control standalone PE3 $\alpha$  and PE3 $\beta$  toxin was used. The 10x Ribosylation Buffer is composed of the following: 250 mM Tris pH 7.5, 150 mM Tris pH 7.0, 10 mM DTT, 60 mM MgCl<sub>2</sub>. Total volume of reaction is 20  $\mu$ L:

**Mixture 1:**

dCas13- PE3 $\alpha$  (or PE3 $\alpha$ ): 1  $\mu$ M  
dCas13- PE3 $\beta$  (or PE3 $\beta$ ): 1  $\mu$ M  
10x ribosylation buffer: 2  $\mu$ l  
Water: adjust to volume

**Mixture 2:**

Target RNA: 0.25  $\mu$ M

eEF2: 0.2  $\mu$ M

Biotin NAD<sup>+</sup> (R&D Systems): 37.5  $\mu$ M

Mixture 1 and mixture 2 were made independently. They were mixed and incubated at 30°C for 60 minutes. After, Laemmli 4x buffer (Biorad) with  $\beta$ -mercaptoethanol were added to the samples and boiled at 95°C for 5 minutes. Samples were loaded on a 4-20% MINI-PROTEAN TGX gel (Biorad) and ran at 140 V for 60 minutes. The contents of the gel were transferred to a PVDF membrane at 0.4 A for 60 minutes. The membrane was blocked with TBST 5% milk solution for 1 hour (or alternatively overnight at 4°C). Steptavidin-HRP solution (Cytiva) was prepared by adding 2  $\mu$ L of stock (5000x) to 10 mL of TBST 5% milk solution and placed on the membrane for 1 hour. The membrane was washed for 10 minutes with 10 mL of TBST solution 4 times. ECL prime (GE) was added to the membrane and incubated for 1 min. The membrane was imaged using the chemiluminescent channel of the Amersham Imager 600.

## **Results**

Initially, we decided to focus on the Cas13d subtype for several reasons: it is the smallest of Cas13s, which would make it easier for viral delivery; there is literature evidence that 5' or 3' protein additions are possible; and it has high knockdown efficiency (Konnerman et al., 2018). In particular, we decided to try RfxCas13d that has been shown to be able to achieve robust knockdown in cells (Konnerman et al., 2018). We tested three different sized linkers (**Figure B1**) and initially placed all the PE3 $\alpha$  toxins on the C-terminal end and the PE3 $\beta$  toxins on the N-terminal end: a fellow Ph.D. graduate student Chris Cromwell conducted the cloning. Schematic diagrams of several of the dCas13d-PE3 proteins are demonstrated in (**Figure B3A**).

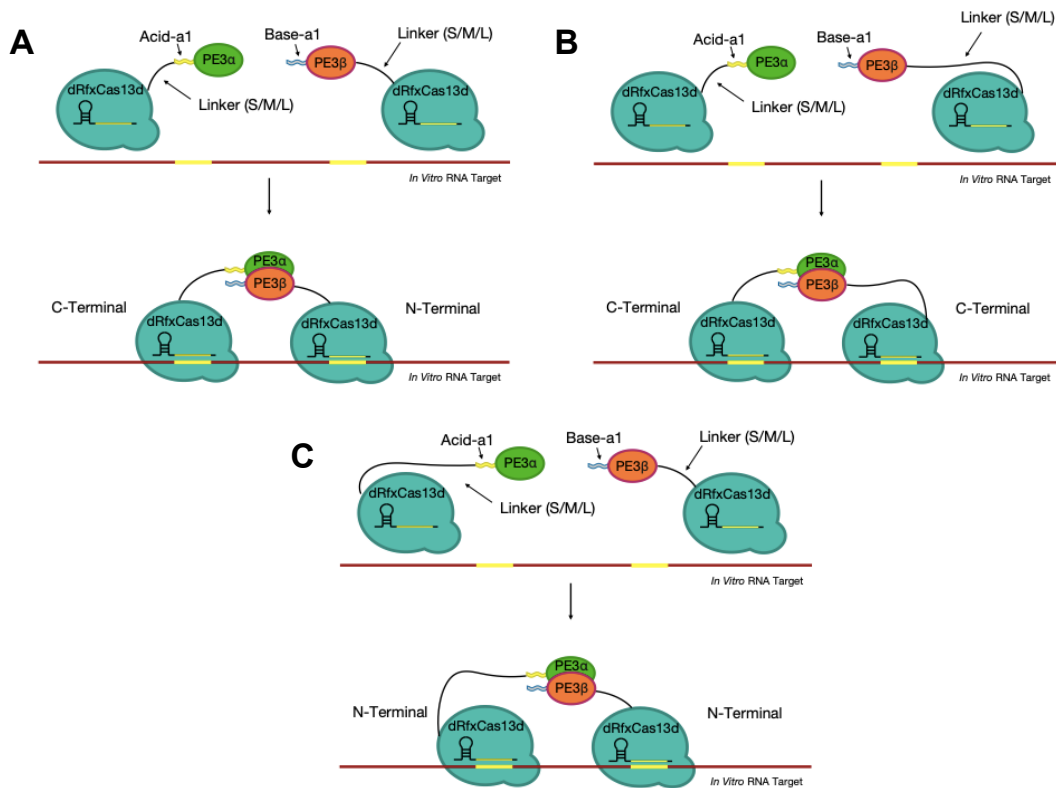


**Figure B1: Diagram of dCas13d-PE3 System and Protein Permutations.** An overview of the dCas13-PE3 system with several protein configurations demonstrated. **A)** PE3 $\alpha$  fused to the C-terminal and PE3 $\beta$  fused to the N-terminal. **B)** PE3 $\alpha$  fused to the C-terminal and PE3 $\beta$  fused to the C-terminal. This protein configuration was never tested. **C)** PE3 $\alpha$  fused to the N-terminal and PE3 $\beta$  fused to the N-terminal.

It took a few months to optimize the hybrid protein production, but we could produce enough protein to test its ribosylation properties (for most productions, the protein was about 50-60% pure). To test ribosylation, we used biotin-NAD<sup>+</sup>. This assay tests whether the combined PE3 toxin can transfer the ADP-ribose moiety from NAD<sup>+</sup> and place it on the diphthamide residue of eEF2. In this case, the biotin tag was attached to the ADP-ribose and was transferred to eEF2 (**Figure B2**). This results in biotin-labeled eEF2 that can be probed for using streptavidin-HRP. Streptavidin and biotin form one of the strongest non-covalent bonds in nature, with a dissociation constant ( $K_D$ ) on the order of  $\approx 10-14$  mol/L (Green, 1975). Biotin, also called vitamin B7, is involved in a wide range of metabolic processes (Pacheco-Alvarez et al., 2002). Streptavidin is found in raw

eggs and is thought to function as an anti-bacterial agent by tightly sequestering biotin to prevent bacterial growth (Hendrickson et al., 1989).

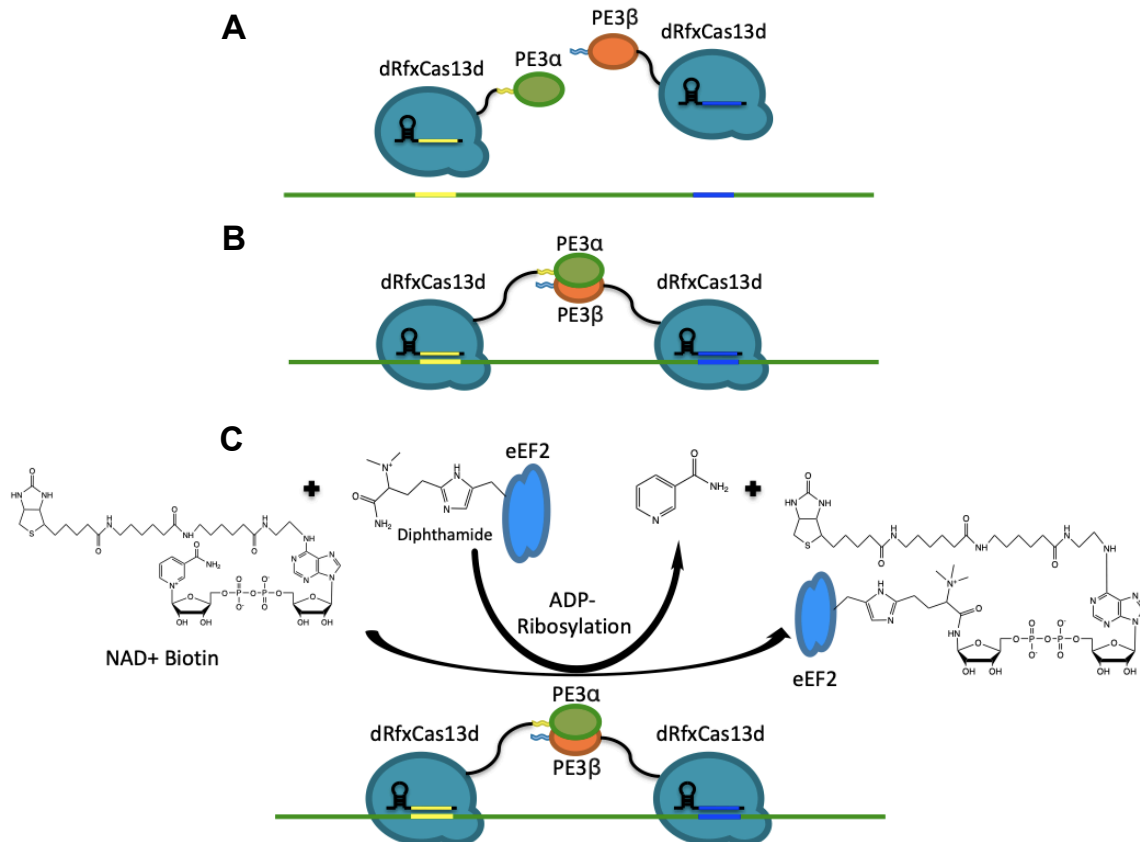


**Figure B2: *In Vitro* ADP- Ribosylation Assay.** **A)** dCas13d- PE3 $\alpha$  and dCas13d- PE3 $\beta$  are hybridized with their respective crRNA and added to target RNA. **B)** The dCas13d binds to the RNA, and the toxin components combine. **C)** In the presence of eEF2 and biotin-NAD<sup>+</sup>, the hybridized toxin transfers the biotin ADP-ribose to the diphthamide residue in eEF2. This can be probed for using streptavidin-HRP.

The ribosylation assay showed that all the PE3 $\beta$  mutants were able to ribosylate with standalone PE3 $\alpha$  toxin, but none of the PE3 $\alpha$  mutants could ribosylate with standalone PE3 $\beta$  toxin (**Figure B3B**). Moving the PE3 $\alpha$  mutant to the N-terminal resolved the issue. Additionally, dCas13d- PE3 $\alpha$  and dCas13d- PE3 $\beta$  could also ribosylate together.

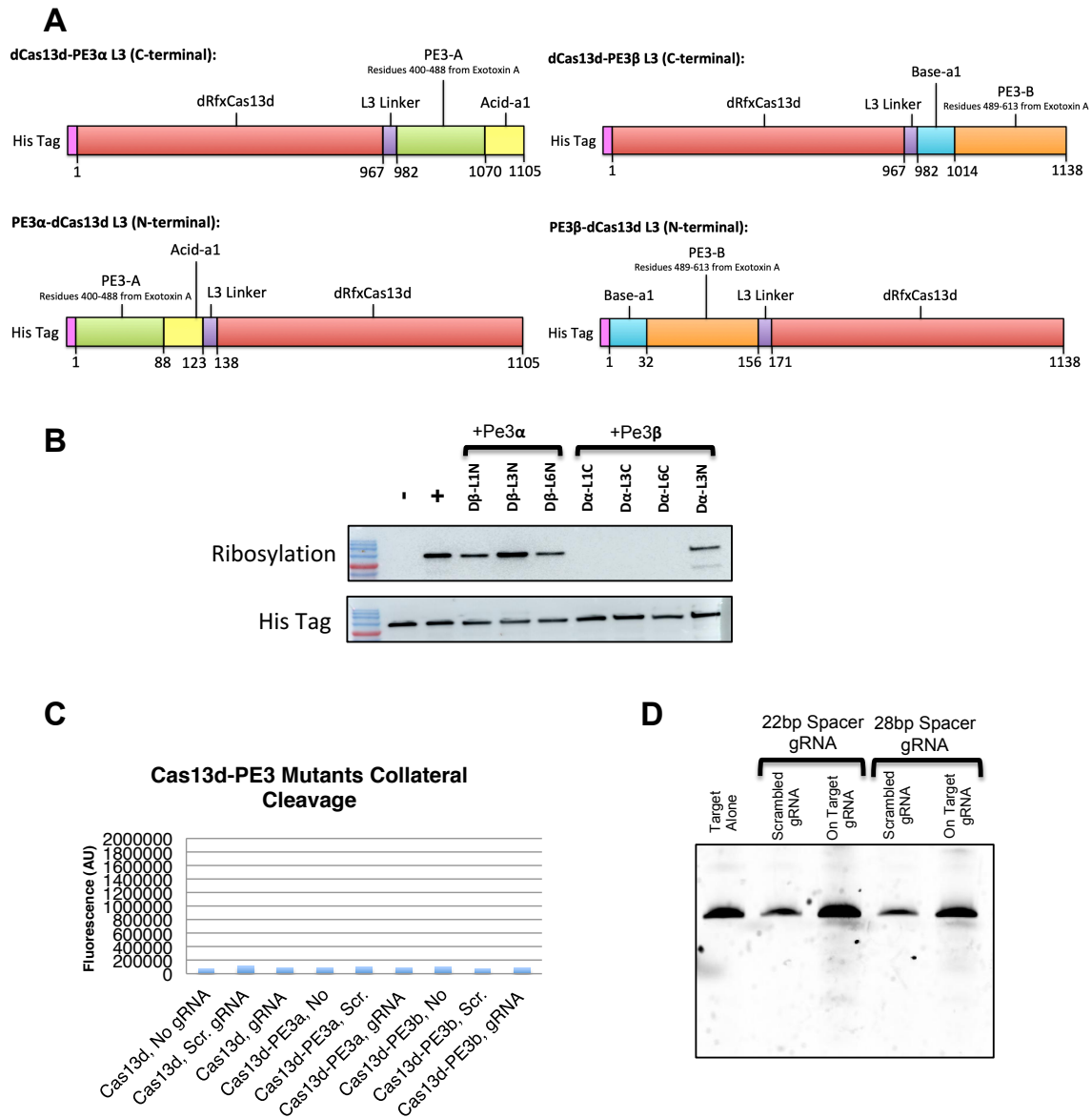


**Figure B3: Schematics, Ribosylation, and Cleavage Data for dCas13d-PE3 Hybrids. A)** A schematic diagram for the L3 mutants of dCas13d-PE3. **B)** Ribosylation assay testing the ability of each dCas13d-PE3 hybrid to ribosylate. All N-terminal mutants can ribosylate. His-tagged eEF2 is shown as a loading control below. **C)** Graph showing the fluorescent values of the collateral cleavage assay for different Cas13d-PE3 mutants and wild type Cas13d. No cleavage was seen in any circumstance. **D)** Wild type Cas13d subjected to standard cleavage assay, further confirming that Cas13d cannot cleave *in vitro*.

Next, we wanted to determine if these hybrids could hybridize with crRNA and bind to the target RNA. Our initial approach consisted of trying electrophoretic mobility shift assays (EMSA). However, after several attempts, the results were too difficult to interpret, and we decided to take an indirect approach. Active versions of our hybrid recombinant proteins were made; if they were able to cleave that would indicate that they were able to bind. We tried two approaches: a collateral cleavage assay and a gel cleavage assay. Unfortunately, there was no cleavage with the RfxCas13d mutants (**Figure B3C**). Even with the wild-type RfxCas13d, there was no cleavage. Different conditions were tried with an extended crRNA, but no cleavage was detected for both collateral and gel assays (**Figure B.3D**).

To mitigate this problem, we decided to switch to LwaCas13a. LwaCas13a is often used in Cas13 papers, and there is evidence of both *in vitro* and cellular cleavage activity (Abudayyeh et al., 2016; Abudayyeh et al., 2017). The cloning was performed to make dCas13a- PE3 $\alpha$  and dCas13a- PE3 $\beta$ . This time, the majority of the mutant proteins produced had their toxin on the N-terminal: schematic representations of dCas13a-PE3 proteins shown in (**Figure B4A**). The ribosylation assay worked with most of the mutants, particularly the protein hybrids with L1 and L3 linkers (**Figure B4B**). Active versions were made, Cas13a- PE3 $\alpha$  L3 and Cas13a- PE3 $\beta$  L3; both mutants were able to conduct collateral cleavage. However, the fluorescent signal was not as high as with the wild-type (**Figure B4C**). A gel cleavage assay further confirmed successful cleavage by both proteins (**Figure B4D**).

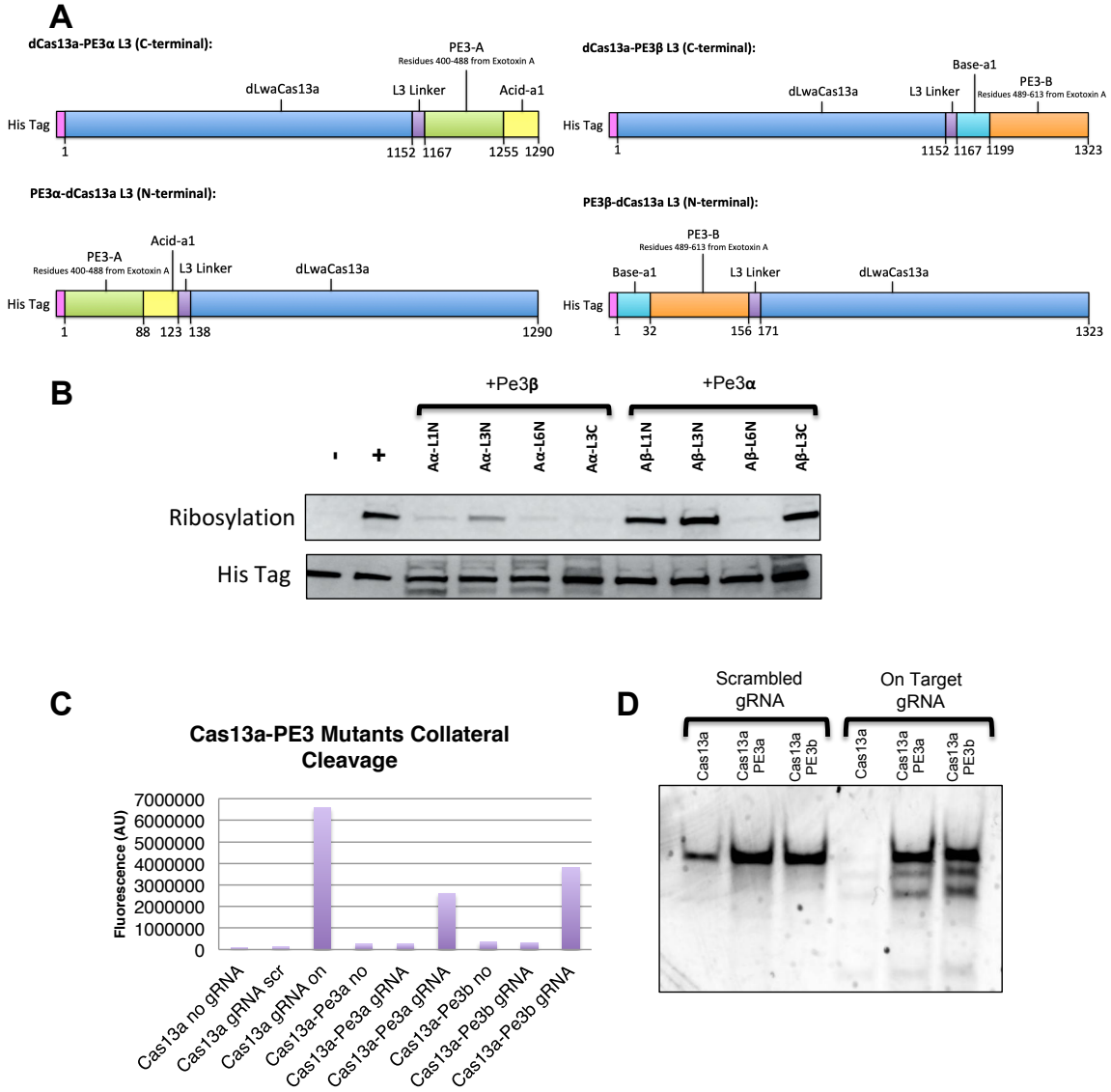


**Figure B4: Schematics, Ribosylation, and Cleavage Data for dCas13a-PE3 Hybrids. A)** A schematic diagram for the L3 mutants of dCas13a-PE3. **B)** Ribosylation assay testing the ability of each dCas13a-PE3 hybrid to ribosylate. All mutants can ribosylate at varying degrees, with L1 and L3 mutants being the most effective. His tagged eEF2 is shown as a loading control below. **C)** Graph showing the fluorescent values of the collateral cleavage assay for different Cas13a-PE3 mutants and wild type Cas13a: collateral cleavage seen with all proteins. However, both mutants did not cleave as well as wild type. **D)** Cleavage capabilities further confirmed with standard cleavage assay.

## Discussion

To expand the arsenal of CRISPR/Cas13a tools we wanted to design a tandem dCas13-PE3 complementation tool. Inspired by the dCas9-FokI system, we adapted the PE3 toxin to dCas13. This tool would be used to target cancerous cells or viral cells with an abundance of a certain RNA transcript.

We initially selected RfxCas13d for its robust ability to knockdown RNA in cells and small size. The ribosylation assay was very reproducible and there was excellent ribosylation activity with the N-terminal PE3 $\beta$  mutants, and good activity with the N-terminal PE3 $\alpha$  mutant. However, there was no cleavage for the RfxCas13d or RfxCas13d-PE3 mutants *in vitro*. This was quite strange and puzzling. There are quite a few examples of the RfxCas13d working in cells (Koner mann et al., 2018, Mahas et al., 2019) and one example *in vitro* (Xu et al., 2021). A possible explanation is that our production of RfxCas13d led to a misfolded protein, or it was difficult for RfxCas13d to cleave the chosen RNA target sequence and length.

LwaCas13a proved to be a better Cas13 to work with. LwaCas13a-PE3 proteins expressed more efficiently, and both wild type and mutant LwaCas13a-PE3 were able to cleave *in vitro*. For the ribosylation assay, all the mutants worked at varying degrees of efficiency. The most effective ones were the L1 and L3 mutants: both N-terminal and C-terminal mutants. Some initial work was performed testing the dCas13a-PE3 complexes with RNA, but unfortunately, we could not replicate these experiments effectively. Often, the signal was quite weak, and it was difficult to discern whether there was an increase in signal with RNA. Believing that the problem may be due to kinetics – and elucidating this is a large project on its own – it was decided that a future student would continue working on this project.

## **Limitations**

A major limitation of the project is the production of these hybrid proteins. In general, producing the dCas13-PE3 mutants has been difficult, with low expression and quick degradation. Even though the Cas13a mutants were easier to work with, we encountered many of the same problems. In particular, the dCas13-PE3a hybrids were hard to produce and quick to degrade. These proteins had to be remade on a bimonthly basis: as seen by the gradual loss of ribosylation activity. Purity was also an issue: the gels showed that after proteins were purified through affinity and ion-exchange columns they were still only about 50-70% pure. These impurities may be due to contaminant proteins, but are most likely degradation products. In continuing this project, it would be wise to review the expression and purification procedure and make changes. Perhaps instead of relying on ion exchange, size exclusion could be implemented instead.

Another significant limitation was the stability of these proteins. As previously mentioned, experiments with RNA could not be replicated due to weak signal from the hybrid proteins. This problem may also be due to protein kinetics, where there was a disruption in Cas13 binding to the crRNA or PE3 toxin activation. This issue could be addressed by implementing changes in protein spacing or architecture. This limitation could also stem from technical factors such as contaminant RNA that causes off-target RNA binding of the hybrid complexes or contaminant proteins that destroy the target RNA or bind to the complex itself.

## **Future Directions**

We need to improve the purification of the various components and study the system's kinetics. Perhaps an alternative Cas13 ortholog that binds RNA more strongly might be more appropriate. Alternative designs might also be tested, using both fluorescence and gel-based cleavage assay. Once this issue has been rectified, the dCas13a-PE3 complexes can be tested in the presence of target RNA to see if there is an increase in ribosylation.

If the system works *in vitro*, the next phase would be translating this system into cells. Delivering this system as an RNP may prove difficult due to stability and toxicity issues. Instead, a most likely delivery method will be via inducible plasmids to allow only a limited amount of time to express this protein. LwaCas13a does work in cells and can be used for such purposes.

## **References**

- Abudayyeh, O. O., Gootenberg, J. S., Konermann, S., Joung, J., Slaymaker, I. M., Cox, D. B., Shmakov, S., Makarova, K. S., Semenova, E., Minakhin, L., Severinov, K., Regev, A., Lander, E. S., Koonin, E. V., & Zhang, F. (2016). C2c2 is a single-component programmable RNA-guided RNA-targeting CRISPR effector. *Science*, 353(6299). <https://doi.org/10.1126/science.aaf5573>
- Abudayyeh, O. O., Gootenberg, J. S., Essletzbichler, P., Han, S., Joung, J., Belanto, J. J., Verdine, V., Cox, D. B., Kellner, M. J., Regev, A., Lander, E. S., Voytas, D. F., Ting, A. Y., & Zhang, F. (2017). RNA targeting with CRISPR–Cas13. *Nature*, 550(7675), 280–284. <https://doi.org/10.1038/nature24049>
- Boland, E. L., Van Dyken, C. M., Duckett, R. M., McCluskey, A. J., & Poon, G. M. (2014). Structural complementation of the catalytic domain of *Pseudomonas* exotoxin A. *Biophysical Journal*, 106(2). <https://doi.org/10.1016/j.bpj.2013.11.3398>
- East-Seletsky, A., O'Connell, M. R., Knight, S. C., Burstein, D., Cate, J. H., Tjian, R., & Doudna, J. A. (2016). Two distinct RNase activities of CRISPR-C2c2 enable guide-RNA processing and RNA detection. *Nature*, 538(7624), 270–273. <https://doi.org/10.1038/nature19802>
- Green, N. M. (1975). Avidin. *Advances in Protein Chemistry*, 85–133. [https://doi.org/10.1016/s0065-3233\(08\)60411-8](https://doi.org/10.1016/s0065-3233(08)60411-8)
- Guillinger, J. P., Thompson, D. B., & Liu, D. R. (2014). Fusion of catalytically inactive Cas9 to FokI nuclease improves the specificity of genome modification. *Nature Biotechnology*, 32(6), 577–582. <https://doi.org/10.1038/nbt.2909>
- Hafkemeyer, P., Brinkmann, U., Brinkmann, E., Pastan, I., Blum, H. E., & Baumert, T. F. (2008). *Pseudomonas* exotoxin antisense RNA selectively kills hepatitis B virus infected cells. *World Journal of Gastroenterology*, 14(18), 2810. <https://doi.org/10.3748/wjg.14.2810>
- Hendrickson, W. A., Pahler, A., Smith, J. L., Satow, Y., Merritt, E. A., & Phizackerley, R. P. (1989). Crystal structure of core streptavidin determined from multiwavelength anomalous diffraction of synchrotron radiation. *Proceedings of the National Academy of Sciences*, 86(7), 2190–2194. <https://doi.org/10.1073/pnas.86.7.2190>
- Jørgensen, R., Carr-Schmid, A., Ortiz, P. A., Kinzy, T. G., & Andersen, G. R. (2002). Purification and crystallization of the yeast elongation factor eEF2. *Acta Crystallographica Section D Biological Crystallography*, 58(4), 712–715. <https://doi.org/10.1107/s0907444902003001>

- Konermann, S., Lotfy, P., Brideau, N. J., Oki, J., Shokhirev, M. N., & Hsu, P. D. (2018). Transcriptome engineering with RNA-targeting type VI-D CRISPR effectors. *Cell*, 173(3). <https://doi.org/10.1016/j.cell.2018.02.033>
- Lebendiker, M., & Danieli, T. (2010). Purification of proteins fused to maltose-binding protein. *Methods in Molecular Biology*, 281–293. [https://doi.org/10.1007/978-1-60761-913-0\\_15](https://doi.org/10.1007/978-1-60761-913-0_15)
- Mahas, A., Aman, R., & Mahfouz, M. (2019). CRISPR-Cas13d mediates robust RNA virus interference in plants. *Genome Biology*, 20(1). <https://doi.org/10.1186/s13059-019-1881-2>
- Pacheco-Alvarez, D., Solórzano-Vargas, R. S., & Del Río Alfonso León. (2002). Biotin in metabolism and its relationship to human disease. *Archives of Medical Research*, 33(5), 439–447. [https://doi.org/10.1016/s0188-4409\(02\)00399-5](https://doi.org/10.1016/s0188-4409(02)00399-5)
- Stuckey, D. W., Hingtgen, S. D., Karakas, N., Rich, B. E., & Shah, K. (2015). Engineering toxin-resistant therapeutic stem cells to treat brain tumors. *STEM CELLS*, 33(2), 589–600. <https://doi.org/10.1002/stem.1874>
- Xu, C., Zhou, Y., Xiao, Q., He, B., Geng, G., Wang, Z., Cao, B., Dong, X., Bai, W., Wang, Y., Wang, X., Zhou, D., Yuan, T., Huo, X., Lai, J., & Yang, H. (2021). Programmable RNA editing with compact CRISPR–Cas13 systems from uncultivated microbes. *Nature Methods*, 18(5), 499–506. <https://doi.org/10.1038/s41592-021-01124-4>
- Yates, S. P., & Merrill, A. R. (2004). Elucidation of eukaryotic elongation factor-2 contact sites within the catalytic domain of *Pseudomonas aeruginosa* exotoxin A. *Biochemical Journal*, 379(3), 563–572. <https://doi.org/10.1042/bj20031731>

## Tables

**Table B1. Cas13-PE3 Hybrids cloned and produced**

<b>Abbreviation</b>	<b>Full Cas13-PE3 Hybrid Name</b>
D $\alpha$ -L1C	dCas13d-PE3 $\alpha$ L1 (C-terminal)
D $\alpha$ -L3C	dCas13d-PE3 $\alpha$ L3 (C-terminal)
D $\alpha$ -L6C	dCas13d-PE3 $\alpha$ L6 (C-terminal)
D $\alpha$ -L3N	dCas13d-PE3 $\alpha$ L3 (N-terminal)
Active D $\alpha$ -L3N	Cas13d-PE3 $\alpha$ L3 (N-terminal)
D $\beta$ -L1N	dCas13d-PE3 $\beta$ L1 (N-terminal)
D $\beta$ -L3N	dCas13d-PE3 $\beta$ L3 (N-terminal)
D $\beta$ -L6N	dCas13d-PE3 $\beta$ L6 (N-terminal)
Active D $\beta$ -L3N	Cas13d-PE3 $\beta$ L3 (N-terminal)
A $\alpha$ -L1N	dCas13a-PE3 $\alpha$ L1 (N-terminal)
A $\alpha$ -L3N	dCas13a-PE3 $\alpha$ L3 (N-terminal)
A $\alpha$ -L6N	dCas13a-PE3 $\alpha$ L6 (N-terminal)
A $\alpha$ -L3C	dCas13a-PE3 $\alpha$ L3 (C-terminal)
Active A $\alpha$ -L3N	Cas13a-PE3 $\alpha$ L3 (N-terminal)
A $\beta$ -L1N	dCas13a-PE3 $\beta$ L1 (N-terminal)
A $\beta$ -L3N	dCas13a-PE3 $\beta$ L3 (N-terminal)
A $\beta$ -L6N	dCas13a-PE3 $\beta$ L6 (N-terminal)
A $\beta$ -L3C	dCas13a-PE3 $\beta$ L3 (C-terminal)
Active A $\beta$ -L3N	Cas13a-PE3 $\beta$ L3 (N-terminal)

**Table B2. Primers used to clone dLwCas13a-PE3 Plasmids**

Name	Sequence (5' to 3')
pC013_fwd	TAAGCGGCCGCACTCGAG
pC013_rev	GCCGCTGCTGTGATGATG
dLwCas13a_fwd (C-ter)	ATCATCATCACAGCAGCGGCATGAAAGTGAC CAAGGTCG
dLwCas13a_rev PE3A (C-ter)	CACCACCGCCTTCCAGGGCCTTGTACTC
dLwCas13a_rev PE3B (C-ter)	TTCCAGGGCCTTGTACTC
L3-PE3A_fwd (C-ter)	GGCCCTGGAAGGCGGTGGTGG AAGCGGC
L3-PE3A_rev (C-ter)	GCCTCGAGTGCGGCCGCTTATTACTGTGCCA GCTCTTTCTCTAATGCCTG
L3-PE3B_fwd (C-ter)	TCGAGTACAAGGCCCTGGAAGGCGGTGGTG GAAGCGGCGGAGGAGGGTCCGGCGGCGGT GGTTCAGCACAGCTGAAAAAAAAAG
L3-PE3B_rev (C-ter)	GCCTCGAGTGCGGCCGCTTATTATTTTCAGAT CTTCACGAG
dLwCas13a_fwd PE3A-L1 (N-ter)	GGCGGCGAAAATGAAAGTGACCAAGGTC
dLwCas13a_fwd PE3A-L3 (N-ter)	CGGTGGTTCAATGAAAGTGACCAAGGTC
dLwCas13a_fwd PE3A-L6 (N-ter)	GGGCGGAAGTATGAAAGTGACCAAGGTC
dLwCas13a_fwd PE3B-L1 (N-ter)	GGCGGCGAAAATGAAAGTGACCAAGGTC
dLwCas13a_fwd PE3B-L3 (N-ter)	CGGTGGTTCAATGAAAGTGACCAAGGTC
dLwCas13a_fwd PE3B-L6 (N-ter)	GGGCGGAAGTATGAAAGTGACCAAGGTC

dLwCas13a_rev (N-ter)	GCCTCGAGTGCGGCCGCTTATTATTCCAGGG CCTTGATAC
PE3A-L1_fwd	ATCATCATCACAGCAGCGGGCGCCGAAGAGGC ATTTTTAGGTGATG
PE3A-L1_rev	TCACTTTCATTTTCGCCGCCGCTTCCTG
PE3A-L3_fwd	ATCATCATCACAGCAGCGGGCGCCGAAGAGGC ATTTTTAGGTGATGGTG
PE3A-L3_rev	TCACTTTCATTGAACCACCGCCGCCGGA
PE3A-L6_fwd	ATCATCATCACAGCAGCGGGCGCCGAAGAGGC ATTTTTAGGTG
PE3A-L6_rev	TCACTTTCATACTTCCGCCCGATCCACC
PE3B-L1_fwd	ATCATCATCACAGCAGCGGGCGCACAGCTGAA AAAAAAGCTGC
PE3B-L1_rev	TCACTTTCATTTTCGCCGCCGCTTCTTTC
PE3B-L3_fwd	ATCATCATCACAGCAGCGGGCGCACAGCTGAA AAAAAAGCTGCAGGC
PE3B-L3_rev	TCACTTTCATTGAACCACCGCCGCCGGA
PE3B-L6_fwd	ATCATCATCACAGCAGCGGGCGCACAGCTGAA AAAAAAGCTGC
PE3B-L6_rev	TCACTTTCATACTTCCGCCCGATCCACC

**Table B3. crRNA Sequences for Cas13- PE3 Tandem Project**

Name	Sequence (5' to 3')
Cas13a crRNA 1	GGAUUUAGACUACCCCAAAAACGAAGGGGACUAAAAC UAUACCUCUGACCAGAAGCUGCCUGAA
Cas13d crRNA 1	GGAACCCCUACCAACUGGUCGGGGUUUGAAACCCUCC UGACCAGAAGCUGCCUG
Cas13a crRNA 3 (Scrambled crRNA 1)	GGAUUUAGACUACCCCAAAAACGAAGGGGACUAAAAC UAUCGAAUGAUUAAAGACAUCCGACGAA
Cas13d crRNA 3 (Scrambled crRNA 1)	GGAACCCCUACCAACUGGUCGGGGUUUGAAACCCUGA AUCUCAGUCCA AUAGCU
Cas13a crRNA 2	GGAUUUAGACUACCCCAAAAACGAAGGGGACUAAAAC CCCACUACUUGCUCUUGAUCCUGACC
Cas13d crRNA 2	GGAACCCCUACCAACUGGUCGGGGUUUGAAACCACUA CUUGCUCUUGAUCCUG
Cas13a crRNA 4 (Scrambled crRNA 2)	GGAUUUAGACUACCCCAAAAACGAAGGGGACUAAAAC CACGCTAGGACA ACTCTTATAGACTACC
Cas13d crRNA 4 (Scrambled crRNA 2)	GGAACCCCUACCAACUGGUCGGGGUUUGAAACCACUU AGGGCAGAGACCAUGCU

**Table B4. DNA Oligonucleotides to produce crRNA**

Name	Sequence (5' to 3')
5' T7 Promoter	TAATACGACTCACTATAGG
Cas13a crRNA 1	TTCAGGCAGCTTCTGGTCAGGAGGTATAGTTTTAGTCC CCTTCGTTTTTGGGGTAGTCTAAATCCTATAGTGAGTC GTATTA
Cas13d crRNA 1	CAGGCAGCTTCTGGTCAGGAGGGTTTCAAACCCCGAC CAGTTGGTAGGGGTTCCCTATAGTGAGTCGTATTA
Cas13a crRNA 3 (Scrambled crRNA 1)	TTCGTCGGATGTCTTTAATCATTCGATAGTTTTAGTCC CCTTCGTTTTTGGGGTAGTCTAAATCCTATAGTGAGTC GTATTA
Cas13d crRNA 3 (Scrambled crRNA 1)	AGCTATTGGACTGAGATTCAGGGTTTCAAACCCCGAC CAGTTGGTAGGGGTTCCCTATAGTGAGTCGTATTA
Cas13a crRNA 2	GGTCAGGATCAAGGAGCAAGTAGTGGGGTTTTAGTCC CCCTTCGTTTTTGGGGTAGTCTAAATCCTATAGTGAGT CGTATTA
Cas13d crRNA 2	CAGGATCAAGGAGCAAGTAGTGGTTTCAAACCCCGAC CAGTTGGTAGGGGTTCCCTATAGTGAGTCGTATTA
Cas13a crRNA 4 (Scrambled crRNA 2)	GGTAGTCTATAAGAGTTGTCCTAGCGTGGTTTTAGTCC CCTTCGTTTTTGGGGTAGTCTAAATCCTATAGTGAGTC GTATTA
Cas13d crRNA 4 (Scrambled crRNA 2)	AGCATGGTCTCTGCCCTAAGTGGTTTCAAACCCCGAC CAGTTGGTAGGGGTTCCCTATAGTGAGTCGTATTA

**Table B5. Target RNA Sequences for Cas13- PE3 Tandem Project**

Name	Sequence (5' to 3')
Target RNA 1 Cas13d(5bp) Cas13a(0bp)	GGAUUAGGUCAGGAUCAAGGAGCAAGUAGUGG GGUUCAGGCAGCUUCUGGUCAGGAGGUUAAA UUAG
Target RNA 2 Cas13d(10bp) Cas13a(5bp)	GGAUUAGGUCAGGAUCAAGGAGCAAGUAGUGG GGUCCAGUUCAGGCAGCUUCUGGUCAGGAGG UAUAAUUAG
Target RNA 3 Cas13d(15bp) Cas13a(10bp)	GGAUUAGGUCAGGAUCAAGGAGCAAGUAGUGG GGUCCAGCGACAUUCAGGCAGCUUCUGGUCA GGAGGUUAAUUAG
Target RNA 4 Cas13d(20bp) Cas13a(15bp)	GGAUUAGGUCAGGAUCAAGGAGCAAGUAGUGG GGUCUAAAACACGAUGUUCAGGCAGCUUCUG GUCAGGAGGUUAAUUAG
Target RNA 5 Cas13d(25bp) Cas13a(20bp)	GGAUUAGGUCAGGAUCAAGGAGCAAGUAGUGG GGUCUAAAACACGAUGGAGCUUUCAGGCAGC UUCUGGUCAGGAGGUUAAUUAG
Target RNA 6 Cas13d(30bp) Cas13a(25bp)	GGAUUAGGUCAGGAUCAAGGAGCAAGUAGUGG GGUCUAAAACACGAUGGAGCUAUUGAUUCAG GCAGCUUCUGGUCAGGAGGUUAAUUAG
Target RNA 7 Cas13d(35bp) Cas13a(30bp)	GGAUUAGGUCAGGAUCAAGGAGCAAGUAGUGG GGUCUAAAACACGAUGGAGCUAUGGCGAACA UUCAGGCAGCUUCUGGUCAGGAGGUUAAUUA G
Target RNA 8 Cas13d(50bp) Cas13a(45bp)	GGAUUAGGUCAGGAUCAAGGAGCAAGUAGUGG GGUCUAAAACACGAUGGAGCUAUGGCGAACG CAAAGGCAGUUGAAGUUCAGGCAGCUUCUGGU CAGGAGGUUAAUUAG
Scrambled crRNA 1 Target RNA 4 Cas13d(20bp) Cas13a(15bp)	GGAUUAGGCAUGGCAGUCAUUUGAAUCUUGCG GGUCUAAAACACGAUGUUCAGGCAGCUUCUG GUCAGGAGGUUAAUUAG
Scrambled crRNA 2 Target RNA 4 Cas13d(20bp) Cas13a(15bp)	GGAUUAGGUCAGGAUCAAGGAGCAAGUAGUGG GGUCUAAAACACGAUGUGGCUACAUAAGCAAU CAGGCAUCGAGCAAUUAG

Scrambled crRNA 1 & 2 Target RNA 4 Cas13d(20bp) Cas13a(15bp)	GGAUUAGGCAUGGCAGUCAUUUGAAUCUUGCG GGUCUUAAAACACGAUGUGGCUACAUAAGCAAU CAGGCAUCGAGCAAUUAG
Fluorescent Target RNA	AACCAGCGCCUUCAGGCAGCUUCUGGUCAGGA GGUAUACCAC-Cy5

**Table B6. DNA Oligonucleotides to produce Target RNAs**

Name	Sequence (5' to 3')
5' T7 Promoter Price: Bought	TAATACGACTCACTATAGG
Target RNA 1 Cas13d(5bp) Cas13a(0bp)	CTAATTATACCTCCTGACCAGAAGCTGCCTGAA CCCCACTACTTGCTCCTTGATCCTGACCTAATC CTATAGTGAGTCGTATTA
Target RNA 2 Cas13d(10bp) Cas13a(5bp)	CTAATTATACCTCCTGACCAGAAGCTGCCTGAA CTGGACCCCACTACTTGCTCCTTGATCCTGACC TAATCCTATAGTGAGTCGTATTA
Target RNA 3 Cas13d(15bp) Cas13a(10bp)	CTAATTATACCTCCTGACCAGAAGCTGCCTGAAT GTCGCTGGACCCCACTACTTGCTCCTTGATCCT GACCTAATCCTATAGTGAGTCGTATTA
Target RNA 4 Cas13d(20bp) Cas13a(15bp)	CTAATTATACCTCCTGACCAGAAGCTGCCTGAA CATCGTGTTTTAAGACCCCACTACTTGCTCCTTG ATCCTGACCTAATCCTATAGTGAGTCGTATTA
Target RNA 5 Cas13d(25bp) Cas13a(20bp)	CTAATTATACCTCCTGACCAGAAGCTGCCTGAA AGCTCCATCGTGTTTTAAGACCCCACTACTTGC TCCTTGATCCTGACCTAATCCTATAGTGAGTCGT ATTAGCCGGCATCGATAGTCTCAGCTGC
Target RNA 6 Cas13d(30bp) Cas13a(25bp)	CTAATTATACCTCCTGACCAGAAGCTGCCTGAAT CAATAGCTCCATCGTGTTTTAAGACCCCACTACT TGCTCCTTGATCCTGACCTAATCCTATAGTGAGT CGTATTAGCCGGCATCGATAGTCTCAGCTGC
Target RNA 7 Cas13d(35bp) Cas13a(30bp)	CTAATTATACCTCCTGACCAGAAGCTGCCTGAAT GTTCCGCATAGCTCCATCGTGTTTTAAGACCCC ACTACTTGCTCCTTGATCCTGACCTAATCCTATA GTGAGTCGTATTAGCCGGCATCGATAGTCTCAG CTGC

Target RNA 8 Cas13d(50bp) Cas13a(45bp)	CTAATTATACCTCCTGACCAGAAGCTGCCTGAA CTTCAACTGCCTTTGCGTTCGCCATAGCTCCAT CGTGTTTTAAGACCCCACTACTTGCTCCTTGATC CTGACCTAATCCTATAGTGAGTCGTATTA
Scrambled crRNA 1 Target RNA 4 Cas13d(20bp) Cas13a(15bp)	CTAATTATACCTCCTGACCAGAAGCTGCCTGAA CATCGTGTTTTAAGACCCGCAAGATTCAAATGA CTGCCATGCCTAATCCTATAGTGAGTCGTATTA
Scrambled crRNA 2 Target RNA 4 Cas13d(20bp) Cas13a(15bp)	CTAATTGCTCGATGCCTGATTGCTATGTAGCCA CATCGTGTTTTAAGACCCCACTACTTGCTCCTTG ATCCTGACCTAATCCTATAGTGAGTCGTATTA
Scrambled crRNA 1 & 2 Target RNA 4 Cas13d(20bp) Cas13a(15bp)	CTAATTGCTCGATGCCTGATTGCTATGTAGCCA CATCGTGTTTTAAGACCCGCAAGATTCAAATGA CTGCCATGCCTAATCCTATAGTGAGTCGTATTA

## Appendix C: Identification and Characterizations of Compounds that Inhibit Nsp15 of SARS-CoV-2

### Background

Severe acute respiratory syndrome coronavirus 2 (SARS-CoV-2) is a type of coronavirus responsible for causing the ongoing COVID-19 pandemic (Fauci et al., 2020). As of writing this dissertation, the virus has infected over 213 million people and led to the deaths of over 4.6 million<sup>1</sup>. In addition to the cost of human life, the pandemic has caused significant societal, political, and economic disruptions that have led to the largest global recession since the Great Recession of the 1930s (Gopinath, 2020). Several vaccines have been developed, including mRNA vaccines that have shown great efficacy (Wang, 2021). Despite this, the worry about other variants of SARS-CoV-2, other coronaviruses, the inability to vaccinate the entire population quickly, and the hesitancy to receive a vaccine in some populations has heightened the importance of drug development against this virus.

SARS-CoV-2 encodes for 16 different non-structural proteins (Nsp), where the name is derived from the fact that they do not contribute to the final structure of the virus. Of particular interest is the protein Nsp15. Following the 2003 SARS outbreak, the coronavirus genome was examined, and the unknown function of Nsp15 was predicted to have endonuclease activity due to its similarity to the sequence of XendoU: a polyU manganese-dependent endonuclease that performs snoRNA processing in *Xenopus laevis* (Snijder et al., 2003). Nsp15 endonuclease activity was first confirmed in 2004 (Bhardwaj et al., 2004; Ivanov et al., 2004). Nsp15 was found to cleave ssRNA and dsRNA, and just like XendoU, Nsp15 required manganese for effective cleavage (Bhardwaj et al.,

---

<sup>1</sup> <https://covid19.who.int> (retrieved August 23, 2021)

2004). Later studies reveal that Nsp15 adopts a hexameric form to cleave RNA (Guarino et al., 2005, Joseph et al., 2007). In addition, Nsp15 cleaves specifically at the 3' end of uridylate, with minor cleavage at 3'cytidylate (Bhardwaj et al., 2006). The culmination of this work has led to Nsp15 being characterized as an RNA uridylate specific endoribonuclease.

The Coronavirus family is very effective at evading innate immune responses, resulting in low levels of type-I interferon expression (Channappanavar et al., 2016; Kindler et al., 2017). In 2017, it was found that NSP15 plays a crucial role in preventing the activation of dsRNA immune response by dsRNA sensors: PKR, OAS, and Mda5 (Kindler et al., 2017). Replication of Nsp15-deficient coronaviruses was severely restricted in primary cells and greatly attenuated *in vivo*: NSP15 deficient strains could not replicate and spread in C57BL/6 mice (Kindler et al., 2017). Furthermore, these Nsp15 deficient viruses could only effectively replicate in cells lacking RNase L and PKR proteins that could not induce IFN-1 expression (Kindler et al., 2017). Due to the conserved nature of the Nsp15 in all coronaviruses (Snijder et al., 2003) and the importance in immune evasion (Kindler et al., 2017), Nsp15 was chosen as our target to find chemical compounds that could inhibit SARS-CoV-2.

## **Methodology**

### ***Cloning of Nsp15 and Catalytically Deficient Mutants***

Cloning of Nsp15 expression plasmid was initiated using the NEBuilder® HiFi DNA assembly method. Initially, the expression plasmid was designed using the NEBuilder tool. The sequence of the backbone vector, pC013 from Cas13a plasmid (Addgene- item #90097), was entered into the program along with the sequence of the bacterial optimized Nsp15 insert. The program gave two pairs of primers that have overlapping regions to make the Nsp15 plasmid. These primers were ordered, and the plasmid was PCR amplified using Q5® High-Fidelity 2x Master Mix (NEB). The amplified sequences were run on a 1% agarose gel and gel extracted using the QIAquick Gel Extraction Kit (Qiagen)

according to the kit's instructions. The amount of vector and insert was quantified using a NanoDrop spectrophotometer. 0.03:0.06 pmol insert to vector ratio was used to assemble the Nsp15 expression plasmid. The appropriate amount of purified DNA was added along with 2x HiFi DNA Assembly Master Mix (NEB); this was incubated at 50°C for 1 hour. NEB® 5α Competent E. coli (High Efficiency) were transformed with the plasmid and plated on carbenicillin plates (100 µg/mL). The plasmid was isolated and purified using QIAprep Spin Miniprep Kit (Qiagen). The plasmid was Sanger sequenced and verified using the SnapGene alignment tool. Same procedure was followed for the truncated mutants. To generate the H250A Nsp15 mutant, the Q5® Site-Directed Mutagenesis Kit from NEB was used. The kit instructions were followed, and plasmid isolation and verification were conducted as previously described. For the complete list of primers used, see **Table C1**.

### ***Nsp15 Cleavage Assay***

The components in the assay are as follows: NSP15 concentration of 1 ng/µl, RNA concentration of 0.5 µM, and Nsp15 cleavage buffer consisting of final a concentration of 25 mM HEPES, 50 mM NaCl, 5 mM MnCl, and 1 mM DTT (Bhardwaj et al., 2006). The total reaction volume was 60 µl, and compounds were added before RNA addition at <1% final constant DMSO concentration. Reactions were incubated at 37°C and read at 490/520 nm for FAM with 6 flashes per reading for a total time of 12 minutes. The fluorescence values were uploaded into the PRISM program for analysis. For a complete list of all RNA sequences used, see **Table C2**.

### ***Cas13a Cleavage Assay for 1280 Compound Nsp15 Secondary Screen***

The amount of reagents and protocol used for the 1280 compound screen at University of Alberta. Reagents and protocol parameters were adapted from the SHERLOCKv2 paper (Gootenberg et al., 2018). The Cas13a Cleavage Buffer 10x is composed of the following: (200 mM HEPES, 600 mM NaCl, 60 mM MgCl<sub>2</sub>, pH 6.8).

**Mixture 1:** 10  $\mu$ L

Cas13a 45 nM

crRNA 22.5 nM

Cas13a Cleavage Buffer 10x 2.5  $\mu$ lWater to 10  $\mu$ l**Mixture 2:** 10  $\mu$ L

Reporter RNA 125 nM

Target RNA 12.5 nM

Water to 10  $\mu$ L

DMSO in place of a chemical compound was added to the reaction for the positive control. Two negative controls were utilized: one with scrambled crRNA and the other with scrambled target RNA. Mixture 1 was incubated at 37°C for 15 minutes to hybridize the Cas13a and crRNA. Next, mixture 1 was added to the plates with 10  $\mu$ M of drugs. The background fluorescence was determined with a spectrophotometer (excitation of 490 nm and an emission of 525 nm). After, mixture 2 was added to begin the reaction, and the plate was incubated at 37°C for 15 minutes. The reaction was stopped with 20 mM of EDTA. The final fluorescence was determined with a spectrophotometer (excitation of 490 nm and an emission of 525 nm). Dr. Joaquin Lopez-Orozco at the University of Alberta performed analysis of results.

***Nsp15 Gel Cleavage Assay***

For the gel cleavage assay, a 31 nucleotide ssRNA oligonucleotide (IDT and Biosynthesis) was used. The oligonucleotide consists of a single “U” surrounded by “A” whose cleavage at the “U” results in a 21 and 10 nucleotide fragment. The reaction volume was 10  $\mu$ l with a final concentration of 7.5 ng/ $\mu$ l NSP15, 250 ng of RNA, and the final DMSO concentration was 1%. The reaction proceeded for 1 hour at 37°C. After the incubation, samples were mixed with 2x RNA Loading Dye and boiled at 95°C for 5 minutes. 15% Criterion™ TBE-Urea Precast Gel 18-well (30  $\mu$ L) (Biorad) were pre-ran at 175 V for 10 minutes, followed by flushing the wells with 1x TBE buffer to remove residual urea and APS. Next, 20  $\mu$ L of

samples were loaded, and the gel was run at 175V for 45 minutes. SYBR gold (Invitrogen) staining solution was prepared by adding 5  $\mu$ L of 10000x stock to 50 mL of TBE buffer. Staining was performed for 15 minutes, followed by visualization using the Fluorescence Cy5 channel of the Amersham Imager 600.

## **Results**

The DNA sequence of Nsp15 was taken from the protein data bank (PDB) and optimized for bacterial protein expression by using the IDT Codon Optimization Tool. In addition to the recombinant Nsp15, three non-catalytically active mutants were generated. The first mutant had an H250A mutation, which removed one of the residues responsible for RNA cleavage (Guarino et al., 2005). The second mutant was a shortened Nsp15 that lacks 28 amino acids from the N-terminal and 11 amino acids from the C-terminal. This prevents Nsp15 oligomerization into a hexamer, which is required for cleavage (Joseph 2007). The third mutant was a 'super-truncation' that removed 28 amino acids from the N-terminal and 112 amino acids from the C-terminal to remove all the active residues (**Figure C1A**). Nsp15 and the first two non-catalytically active mutants were expressed and purified, while the third mutant could not be expressed.

For the assay itself, we opted for a fluorophore-quencher reporter system (**Figure C2A**). Nsp15 cleaves the reporter RNA leading to the separation of the fluorophore and quencher: this results in fluorescent signal. If a chemical compound inhibits Nsp15, there will be no cleavage, and no fluorescent signal will be detected. A literature search was conducted to determine which RNA sequence Nsp15 can cleave effectively. Two different RNAs were chosen and tested. The first sequence (RNA1): AAAAAAAGUAAAAA (Nedialkova et al., 2009). The second sequence (RNA2): CAACUAAACGAAC (Kang et al., 2007). Additionally, an RNA sequence that contained no uracils was ordered as a negative control: the full list of RNA sequences can be seen in **Table C2**. For each of these sequences a 6-Carboxyfluorescein (6-FAM) fluorophore was

added to the 5' end and a Black Hole Quencher®-1 (BHQ1) quencher was added to the 3' end. Once both the RNA and Nsp15 were made, an assay was performed as illustrated in the paper (Bhardwaj et al., 2006). Nsp15 was able to cleave RNA2 and was used for all subsequent assays (**Figure C1B**). No cleavage was seen with RNA1 and non-catalytically active mutants. The optimization of the assay and the determination of the  $K_M$  of Nsp15 were performed by my MSc colleague Jerry Chen. He produced and bought enough components to test several different libraries: LOPAC® 1280, TimTec, and an assortment of compound libraries from the Canadian Chemical Biology Network (CCBN) collection that totalled over 100000 compounds.

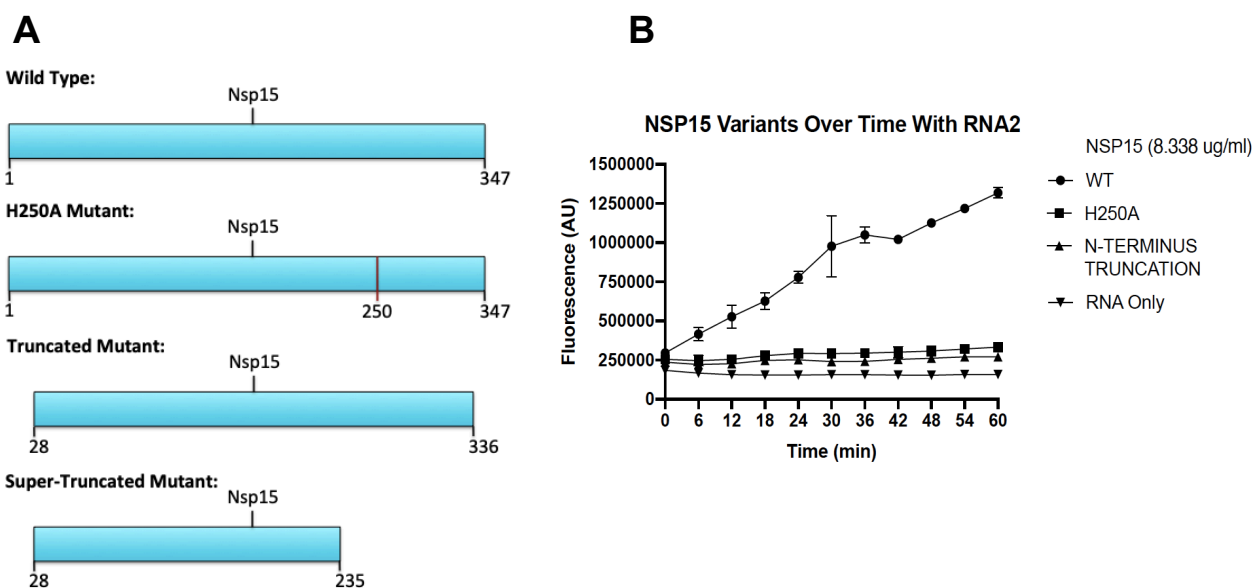


**Figure C1: Nsp15 and Non-Catalytically Active Mutants.** **A)** The schematics of all Nsp15s made: H250A mutant, truncated mutant, and super-truncated mutant. **B)** An assay with the Nsp15 variants shows ablation of cleavage with H250A and truncated mutant. The super-truncated mutant was unable to be expressed. Results expressed as the mean  $\pm$  SD n=3.

From these libraries, there were 1280 compounds above two standard deviations from the mean that were selected for the secondary Nsp15 screen. This secondary screen tested the compounds effect on Cas13a in order to remove any compounds that were general RNase inhibitors: this narrowed the hits that were specific to Nsp15. The assay was inspired by the aforementioned SHERLOCK assay, where activation of Cas13 would lead to the collateral

cleavage of fluorophore/quencher reporter RNA and subsequent fluorescent signal (Gootenberg 2018). The same reporter RNA (6-FAM-UUUUU-IBFQ), the same concentration of reagents, and the same assay parameters were utilized as described in the paper. An illustration of the secondary screen is shown in (Figure C2B).

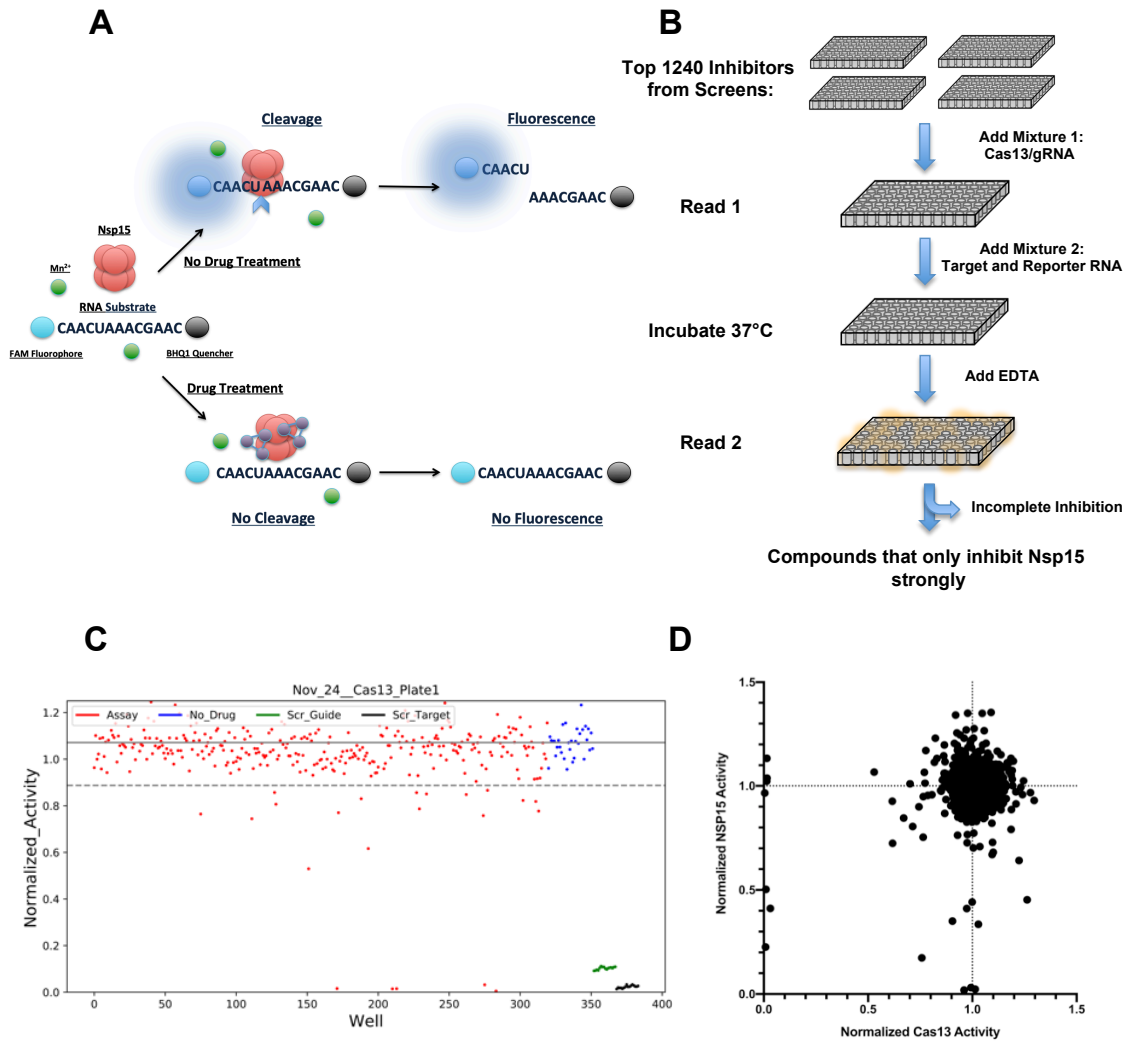


**Figure C2: Nsp15 Cleavage Assay, Nsp15 Secondary Screening Workflow, and Screening Results.** **A)** A schematic of the Nsp15 cleavage assay. **B)** The workflow of the secondary Nsp15 screen using Cas13a. **C)** The result of the 1280 compound screen. For the positive control, DMSO was added in place of compound. There were two negative controls: one with scrambled target RNA and one with scrambled crRNA. **D)** A graph showing the distribution of compounds that inhibit Nsp15 and Cas13a. 9 compounds inhibited Nsp15 exclusively. In contrast, 7 compounds exclusively or predominantly inhibited Cas13a.

The screen revealed that 9 compounds specifically inhibited Nsp15: the result of the screen is seen in (**Figure C2C**). Interestingly, 7 compounds fully or predominantly inhibited Cas13 without inhibiting, or only slightly inhibiting, Nsp15 (**Figure C2D**). The top inhibitors were ordered and their inhibitory effect was validated. Assistance was provided for the final gel cleavage assay, where a non-fluorophore RNA substrate was used to verify genuine inhibition. The final gel showed 6 compounds that could inhibit Nsp15. My colleague characterized these compounds by finding their IC<sub>50</sub> and method of inhibition.

## **Discussion**

This project was started in response to the SARS-CoV-2 pandemic that began during our MSc studies. To assist in combating this virus, we decided to take on a COVID-19 project that involved finding and characterizing chemical compounds that inhibit SARS-CoV-2. Nsp15 proved to be an optimal target for two reasons: it is crucial for early immune evasion allowing the virus to propagate undetected, and is highly conserved in all coronaviruses. A fluorophore/quencher reporter system was adapted and tested with recombinant Nsp15. Once this system was optimized, it was applied to screen over 100000 chemical compounds. We confirmed six highly promising compounds that reliably inhibit this enzyme. These compounds have IC<sub>50</sub>s ranging from 5  $\mu$ M to 100  $\mu$ M and are primarily non-competitive inhibitors. We continue to evaluate these compounds in cell models of COVID-19 and characterize their pharmacological and biophysical properties (i.e., surface plasmon resonance binding studies).

## **Limitations**

The Nsp15 project had several limitations. One limitation is that the fluorescent assays can give false positive results due to compounds having similar excitation/emission profiles, and false negatives due to quenching caused by the compounds. For this reason, we validated all final compounds using a non-fluorophore based assay. Another possible limitation is the permeability and toxicity of the compounds – they have to enter cells to effectively inhibit the

coronavirus without causing cytotoxic effects. This will be fully determined once these compounds will be tried in cells.

### **Future Directions**

The next direction of this project is to test its efficacy in COVID-19 cell culture models. Collaborative work is underway in biosafety level 3 labs to test these compounds in cell lines that express SARS-CoV-2 virus.

### **References**

- Bhardwaj, K., Guarino, L., & Kao, C. C. (2004). The severe acute respiratory syndrome coronavirus Nsp15 protein is an endoribonuclease that prefers manganese as a cofactor. *Journal of Virology*, *78*(22), 12218–12224. <https://doi.org/10.1128/jvi.78.22.12218-12224.2004>
- Bhardwaj, K., Sun, J., Holzenburg, A., Guarino, L. A., & Kao, C. C. (2006). RNA recognition and cleavage by the SARS coronavirus endoribonuclease. *Journal of Molecular Biology*, *361*(2), 243–256. <https://doi.org/10.1016/j.jmb.2006.06.021>
- Channappanavar, R., Fehr, A. R., Vijay, R., Mack, M., Zhao, J., Meyerholz, D. K., & Perlman, S. (2016). Dysregulated type I interferon and inflammatory monocyte-macrophage responses cause lethal pneumonia in SARS-CoV-infected mice. *Cell Host & Microbe*, *19*(2), 181–193. <https://doi.org/10.1016/j.chom.2016.01.007>
- Fauci, A. S., Lane, H. C., & Redfield, R. R. (2020). Covid-19 — navigating the uncharted. *New England Journal of Medicine*, *382*(13), 1268–1269. <https://doi.org/10.1056/nejme2002387>
- Gootenberg, J. S., Abudayyeh, O. O., Kellner, M. J., Joung, J., Collins, J. J., & Zhang, F. (2018). Multiplexed and portable nucleic acid detection platform with Cas13, Cas12a, and Csm6. *Science*, *360*(6387), 439–444. <https://doi.org/10.1126/science.aaq0179>
- Gopinath, G. (2020, April 14). The Great Lockdown: Worst Economic Downturn Since the Great Depression. *IMFBlog*. <https://blogs.imf.org/2020/04/14/the-great-lockdown-worst-economic-downturn-since-the-great-depression/>.
- Guarino, L. A., Bhardwaj, K., Dong, W., Sun, J., Holzenburg, A., & Kao, C. (2005). Mutational analysis of the SARS virus Nsp15 endoribonuclease: Identification of residues affecting hexamer formation. *Journal of Molecular Biology*, *353*(5), 1106–1117. <https://doi.org/10.1016/j.jmb.2005.09.007>
- Ivanov, K. A., Hertzog, T., Rozanov, M., Bayer, S., Thiel, V., Gorbalenya, A. E., & Ziebuhr, J. (2004). Major genetic marker of nidoviruses encodes a replicative endoribonuclease. *Proceedings of the National Academy of Sciences*, *101*(34), 12694–12699. <https://doi.org/10.1073/pnas.0403127101>

- Joseph, J. S., Saikatendu, K. S., Subramanian, V., Neuman, B. W., Buchmeier, M. J., Stevens, R. C., & Kuhn, P. (2007). Crystal structure of a monomeric form of severe acute respiratory syndrome coronavirus endonuclease Nsp15 suggests a role for hexamerization as an allosteric switch. *Journal of Virology*, *81*(12), 6700–6708. <https://doi.org/10.1128/jvi.02817-06>
- Kang, H., Bhardwaj, K., Li, Y., Palaninathan, S., Sacchettini, J., Guarino, L., Leibowitz, J. L., & Kao, C. C. (2007). Biochemical and genetic analyses of murine hepatitis virus Nsp15 endoribonuclease. *Journal of Virology*, *81*(24), 13587–13597. <https://doi.org/10.1128/jvi.00547-07>
- Kindler, E., Gil-Cruz, C., Spanier, J., Li, Y., Wilhelm, J., Rabouw, H. H., Züst, R., Hwang, M., V'kovski, P., Stalder, H., Marti, S., Habjan, M., Cervantes-Barragan, L., Elliot, R., Karl, N., Gaughan, C., van Kuppeveld, F. J., Silverman, R. H., Keller, M., ... Thiel, V. (2017). Early endonuclease-mediated evasion of RNA sensing ensures efficient coronavirus replication. *PLOS Pathogens*, *13*(2). <https://doi.org/10.1371/journal.ppat.1006195>
- Nedialkova, D. D., Ulferts, R., van den Born, E., Lauber, C., Gorbalenya, A. E., Ziebuhr, J., & Snijder, E. J. (2009). Biochemical characterization of arterivirus nonstructural protein 11 reveals the nidovirus-wide conservation of a replicative endoribonuclease. *Journal of Virology*, *83*(11), 5671–5682. <https://doi.org/10.1128/jvi.00261-09>
- Snijder, E. J., Bredenbeek, P. J., Dobbe, J. C., Thiel, V., Ziebuhr, J., Poon, L. L. M., Guan, Y., Rozanov, M., Spaan, W. J. M., & Gorbalenya, A. E. (2003). Unique and conserved features of genome and proteome of SARS-coronavirus, an early split-off from the coronavirus group 2 lineage. *Journal of Molecular Biology*, *331*(5), 991–1004. [https://doi.org/10.1016/s0022-2836\(03\)00865-9](https://doi.org/10.1016/s0022-2836(03)00865-9)
- Wang, X. (2021). Safety and efficacy of the BNT162B2 mRNA Covid-19 vaccine. *New England Journal of Medicine*, *384*(16), 1576–1578. <https://doi.org/10.1056/nejmc2036242>

## Tables

**Table C1. Primers used to clone Nsp15 & Inactive Mutants**

Name	Sequence (5' to 3')
pC013_fwd (WT)	TAAGCGGCCGCACTCGAG
pC013_rev (WT)	GCCGCTGCTGTGATGATG
Nsp15_fwd (WT)	ATCATCATCACAGCAGCGGCGTGGATCTTGGTAC GGAAAATC
Nsp15_rev (WT)	GCCTCGAGTGCGGCCGCTTACTGCAGCTTGGGA TAAAATG
pC013_fwd	TTATGCTTTGGTGCAAGGATTAAGCGGCCGCACT CGAG
pC013_rev	GGCATTGGATTGAAAGTACAGATTTTCC
Nsp15 Truncated_fwd	TGTACTTTCAATCCAATGCCAACAATACGGTATAC ACCAAAG
Nsp15 Truncated_rev	ATCCTTGCACCAAAGCATAAAG
pC013_fwd	TGGAAGGATATGCTTTCGAATAAGCGGCCGCACT CGAG
pC013_rev	GGCATTGGATTGAAAGTACAGATTTTCC
Nsp15 Super Truncated_fwd	TGTACTTTCAATCCAATGCC ACAATACGGTATACACCAAAG
Nsp15 Super Truncated_rev	TTCGAAAGCATATCCTTC
Nsp15_SDM_F	GGGTGGCCTTGCTCTTTTAATAGG
Nsp15_SDM_R	AGTTGCGAATGAGAAAATC

**Table C2. RNA Sequences used in Nsp15 Inhibitor Project**

Name	Sequence (5' to 3')
Cas13a crRNA	GGAUUUAGACUACCCCAAAAACGAAGGGGACUA AAACUAUACCUCCUGACCAGAAGCUGCCUGAA
Cas13a Scrambled crRNA	GGAUUUAGACUACCCCAAAAACGAAGGGGACUA AAACUAUCGAAUGAUUAAAGACAUCGACGAA
Cas13a Target RNA	CTAATTATACCTCCTGACCAGAAGCTGCCTGAAC ATCGTGTTTTAAGACCCCACTACTTGCTCCTTGAT CCTGACCTAATCCTATAGTGAGTCGTATTA
Cas13a Scrambled Target RNA	CTAATTGCTCGATGCCTGATTGCTATGTAGCCAC ATCGTGTTTTAAGACCCGCAAGATTCAAATGACT GCCATGCCTAATCCTATAGTGAGTCGTATTA
Reporter RNA	6-FAM-UUUUU-IBFQ
Nsp15 RNA 1	6-FAM-AAAAAAGUAAAA-BHQ1
Nsp15 RNA 2	6-FAM-CAACUAAACGAAC-BHQ1
Nsp15 Negative Control RNA	6-FAM-AAAAAAGAAAAA-BHQ1
Nsp15 Gel Target RNA	AA